UNIVERSIDAD DE MURCIA

FACULTAD DE QUÍMICA

Electrochemical Catalytic Decomposition of NO_x with a *NiO/YSZ* Catalyst

Descomposición Electrocatalítica del NO_x con el Catalizador *NiO/YSZ*

Dña. María Pilar Alfonso Martínez
2012

UNIVERSIDAD DE
MURCIA
DEPARTAMENTO DE INGENIERÍA QUÍMICA

Dª. Maria Gloria Víllora Cano, Catedrática de Universidad del Área de Ingeniería Química en el Departamento de Ingeniería Química de la Universidad de Murcia.

AUTORIZA:

La presentación de la Tesis Doctoral titulada "*Electrochemical catalytic decomposition of NOx with a NiO/YSZ catalyst*" realizada por Dª. Pilar Alfonso Martínez, bajo mi inmediata dirección y supervisión, en el Departamento de Ingeniería Química, y que presenta para la obtención del Grado de Doctor por la Universidad de Murcia.

Murcia, a 1 de Septiembre de 2012

Facultad de Química
Departamento de Ingeniería Química

Campus Universitario de Espinardo. 30071 Murcia
Teléfono Centralita: 868 88 30 00. Teléfono Secretaría Departamento: 868 88 73 59. Fax: 868 88 41 48 - **www.um.es**

Karlsruher Institut für Technologie

KIT-Campus Süd | TCP| Engesserstr. 20| 76131 Karlsruhe

Karlsruher Institut für Technologie
Institut für Technische Chemie und Polymerchemie
Leiter/in: Prof. Dr. Olaf Deutschmann

Engesserstraße 20
76131 Karlsruhe

Prof. Dr.-Ing. Henning Bockhorn

Telefon: 0721 608-42570
Fax: 0721 608-47770
E-Mail: Henning.Bockhorn@kit.edu
Web: www.vbt.uni-karlsruhe.de

Bearbeiter/in:
Unser Zeichen:
Datum: 8. August 2012

Confirmation

I confirm that the experimental part of the PhD Thesis “Electrochemical catalytic decomposition of NOx with a NiO/YSZ catalyst“, submitted by Ms. Pilar Alfonso Martinez has been accomplished under my supervision at the Institute for Chemical Technology and Polymer Chemistry at the Karlsruhe Institute of Technology, KIT. It meets the requirements of the Faculty of Chemistry and Bio-Sciences and can be submitted to be evaluated by the responsible commission at the University of Murcia, Spain.

Prof. Dr.-Ing. Henning Bockhorn

Karlsruher Institut für Technologie (KIT)
Großforschungsbereich
Kaiserstraße 12
76131 Karlsruhe

Präsidenten: Prof. Dr. Horst Hippler, Prof. Dr. Eberhard Umbach
Vizepräsidenten: Dr. Elke Luise Barnstedt, Dr. Ulrich Breuer, Dr.-Ing. Peter Fritz, Prof. Dr.-Ing. Detlef Löhe

Baden-Württembergische Bank, Stuttgart
BLZ 600 501 01 | Kto. 7495501296
BIC: SOLADEST
IBAN: DE18 6005 0101 7495 5012 96
USt-IdNr. DE266749428

KIT – Universität des Landes Baden-Württemberg und nationales Forschungszentrum in der Helmholtz-Gemeinschaft

www.kit.edu

UNIVERSIDAD DE
MURCIA
DEPARTAMENTO DE INGENIERÍA QUÍMICA

D. Demetrio Gómez Pérez, Profesor Titular del Área de Ingeniería Química y Director del Departamento de Ingeniería Química de la Universidad de Murcia.

INFORMA:

Que la Tesis Doctoral titulada "*Electrochemical catalytic decomposition of NOx with a NiO/YSZ catalyst*" ha sido realizada por Dª. Pilar Alfonso Martínez, bajo la inmediata dirección y supervisión de Dª. Maria Gloria Víllora Cano y del Prof. Dr.-Ing Henning Bockhorn, y que el Departamento ha dado su conformidad para que sea presentada ante la Comisión de Doctorado.

Murcia, a 1 de Septiembre de 2012

POLITECNICO DI MILANO

Dipartimento di Energia
Prof. Isabella Nova
Laboratory of Catalysis and Catalytic Processes
www.lccp.polimi.it
Dipartimento di Energia, Politecnico di Milano
Piazza Leonardo da Vinci 32
20133 Milano, Italia
tel +39 02 2399 3228
fax +39 02 2399 3318
e-mail isabella.nova@polimi.it

25th October 2012

Professor G. Víllora
Department of Chemical Engineering
University of Murcia
Campus di Espinardo
30071 Murcia
Spain

Object: Review of 'Electrochemical catalytic decomposition of NOx with a NiO/Y SZ catalyst' presented for a PhD degree by Ms. Pilar Alfonso Martinez

Dear Professor Víllora,
I have reviewed the thesis you sent to me have concluded that it is suitable for the award of the above degree.

My reasons are as follows:

The thesis describes original scientific investigations, focused on the regeneration of the active centers of NiO=Y SZ catalysts by chemical reduction and electro-chemical elimination of O2. It is very well known that Ni-based catalysts show good activity in the decomposition of nitrogen oxides but thir use at commercial scale is still hindered due to the strong inhibition played by oxygen that adsorbs on the Ni active centers giving rise to the catalyst deactivation. This is a topic of actual great interest, due to new regulations aiming at control of NOx pollutant in the atmosphere.

There is breadth to the work, which covers several aspects dealing with both catalytic and electrochemical processes. In particulars, the thesis analyses the experimental working conditions of the catalysts, looking at both the gas and surface species involved in the catalytic processes; the chemical and electro-chemical regeneration of the catalysts; the NOx decomposition activity and selectivity of the NiO=Y SZ catalyst with and without electrochemical support.

The experimental work has been carried out with evident care and competence.

The thesis is well organized, experiments logically performed, results clearly presented and discussed, also in comparison to literature results. Indeed, relevant and updated previous work published in the open literature is properly referenced.

The thesis is clearly written and laid out, setting out in individual chapters the background of the work done, the experimental data obtained and sensible conclusions derived from them.

The thesis is reasonably free of typographical and other errors.

On balance, I have no hesitation in concluding that the work meets the required standard.

Yours sincerely

Isabella Nova

STU
FCHPT

SLOVAK UNIVERSITY OF TECHNOLOGY IN BRATISLAVA
FACULTY OF CHEMICAL AND FOOD TECHNOLOGY
DEPARTMENT OF CHEMICAL AND ENVIRONMENTAL ENGINEERING

To whom it may concern

This is a review of the PhD thesis of **Pilar Alfonso Martínez** entitled "**Electrochemical catalytic decomposition of NO_x with a NiO/YSZ catalyst**" that was elaborated at the Karlsruhe Institute of Technology, Germany and the University of Murcia, Spain.

Formally, the thesis presented is composed of nine chapters, including Appendix with the results of catalyst characterization. Chapters 1–4 contain introduction, thesis objectives, and relatively short overview of the literature information. The following chapters (5 and 6) show the experimental data on the catalytic system design, catalytic and electro-catalytic NO_x decomposition, and the catalyst characterization by several experimental techniques. Discussion of experimental data and conclusions based on this information are given in chapters 7 and 8.

Motivation of this thesis is the atmosphere and ozone layer protection against persistent greenhouse gases produced by fuel combustion. During fuel combustion in compression-ignition engines, a non-negligible amount of nitrogen oxides is formed. Due to the use of excess amount of oxidant (air), three-way catalysts based on noble metals that are active only in oxygen-lean conditions are of limited use. In order to meet the EURO exhaust-gas legislation regarding nitrogen oxides emissions, different catalytic system should be used.

In the present thesis, NiO supported on yttria-stabilized zirconia (NiO-YSZ) was tested as a catalyst for NO_x abatement in the presence of oxygen. Two types of heterogeneous catalytic reactors were tested, namely tubular fixed bed reactor and a reactor with inserted catalyst bed in the form of a flat plate. In order to overcome the catalyst deactivation by adsorbed species, regeneration of the catalyst active centers was carried out by connecting the catalyst layer to the direct-current electrical circuit.

High NiO-YSZ catalyst selectivity and activity was observed using the model mixture containing 0.1 mole % of NO and 1 mole % O_2. It was found that under electric current-free conditions, a fast catalyst poisoning by the adsorbed oxygenates was observed. The catalytic activity, however, could be restored by supplying current to the catalytic system.

Catalyst activity was correlated to the catalyst physical–chemical properties. Based on the results of these characterization experiments, the author derived several conclusions. Firstly, it was confirmed that the active component of this catalyst is NiO regarding both, adsorption of NO_x species and their (electro-)catalytic reduction. DRIFT experiment results allowed distinguishing the forms in which the nitrogen-containing species are stored at the catalyst surface in the presence or absence of oxygen. Furthermore, the mechanism of electro-catalytic decomposition of NO_x was proposed.

Altogether 70 pages of experimental results and additional 14 pages of characterization data form a solid base of this thesis. The dissertant showed her theoretical and practical skills in the field of catalytic NO_x abatement and also heterogeneous catalyst characterization. On the other hand, further experiments are necessary to examine the NiO-YSZ catalyst activity under more realistic conditions (gas phase composition similar to that of the diesel engine exhaust gases). Moreover, it is expected that the presented results are published in peer reviewed journals to undergo a formal scrutiny by the scientific community.

To conclude, the dissertant presented an extensive amount of new data regarding the NO_x decomposition in the presence of oxygen and showed detailed knowledge of the catalyst characterization. These original scientific results serve as more than sufficient base to confer the European Doctorate degree to Pilar Alfonso Martínez.

Bratislava, November 12, 2012

assoc. prof. Dr. Pavol Steltenpohl

This work is presented in order to obtain the PhD in Chemistry from the University of Murcia with the mention of *European doctorate*

Murcia, November 11th, 2012

Pilar Alfonso Martínez

Acknowledgments

The present work was developed between June 2007 and December 2010 at the Karlsruhe Institute of Technology (KIT) and subsequently between January 2011 and October 2011 at the University of Murcia.

Firstly, I would like to thank my advisor Professor María Gloria Víllora Cano for her support without which I would not have finished my PhD.

Furthermore, I would like to thank my co-advisor Professor Henning Bockhorn for the opportunity to work on this exciting topic and for his support during the entire time of writing this thesis.

In particular, I would like to thank Professor Sven Kureti for his continuous support during my work and the many discussions that we had during the entire PhD time.

I would like to thank all my colleagues for the enjoyable working atmosphere and their helpfulness. Specially I would like to thank Peter Balle, Bastian Geiger, Dr. Florian Schott and Hans Herberger.

For the economical support I would like to thank Robert Bosch GmbH Stuttgart.

I would also like to thank Dr. Wolfgang Menesklou for providing me the platinum paste and Dr. Boris Reznik for his help with the *SEM* analysis.

Above all, I would like to thank my parents for giving me the opportunity of completing my studies in chemistry.

Contents

Preface

In order to adhere to the *EURO* exhaust-gas limit value legislation, an exhaust after-treatment has to be utilized in diesel engine vehicles with the purpose of reducing the nitrogen oxide emissions. It is already known that Ni-based catalysts present a good activity in the decomposition of nitrogen oxides but they are strongly inhibited by oxygen since it adsorbs on the Ni active centers giving rise to the catalyst deactivation. In the present work, the regeneration of the active centers of a NiO/YSZ catalyst by means of chemical reduction and the electro-chemical elimination of O_2 were studied. The electro-chemical regeneration presents a big advantage if it is compared with the chemical reduction since a continuous regeneration of the catalyst could be achieved. An improvement of the cell selectivity in the decomposition of NO_x in oxygen excess with the cell operating time was also observed. In the literature such an improvement of similar cells was also reported and related to a change in the catalyst structure. In the present work, a catalyst color change with the operating time was observed. However more detailed studies aimed to elucidate the reason and mechanism of that selectivity improvement could not lead to a definitive conclusion since problems with the reproducible preparation of the electro-chemical cell appeared. In order to increase the reproducibility of the cell preparation and the catalyst performance, different electro-catalytic cell preparation procedures and two different reactor configuration (tubular and planar) were tested. The planar reactor gave the most reproducible results but the NO_x decomposition activity of the tubular reactor was higher. Moreover, no improvement of the cell selectivity with the operating time was achieved with the planar reactor. The NiO/YSZ NO_x decomposition activity was also compared with the one achieved by another Ni-containing catalyst ($LaNiO_3$ and La_2NiO_4) and the best results were obtained with the NiO/YSZ catalyst. The capacity of the NiO/YSZ catalyst of storing NO_x as nitrates and nitrites was studied and a storage mechanism which would explain the formation of the surface nitrates and nitrites observed in the *DRIFT* experiments was proposed. As a consequence of the experimental results achieved in the present work, a mechanism for the NO_x decomposition was proposed in which the dissociative chemisorption of the nitrogen oxides on the catalyst surface first occurs and a subsequent recombination of the adsorbed nitrogen atoms leads to the N_2 formation.

CHAPTER 1

Resumen

Con el fin de cumplir la legislación EURO para el control de valores límite de emisión de gases procedentes de motores diesel, es necesario someter a dichos gases a un post-tratamiento de purificación enfocado a reducir las emisiones de óxidos de nitrógeno. Los catalizadores basados en níquel son conocidos por presentar una buena actividad en la descomposición de los óxidos de nitrógeno pero presentan el inconveniente de ser fuertemente inhibidos por el oxígeno debido a que éste e adsorbe fuertemente a los centros activos del catalizador dando lugar a su desactivación. En este trabajo se estudió la regeneración de los centros activos del catalizador haciendo uso tanto de una reducción química como de una eliminación electro-química del oxígeno adsorbido. Es posible conseguir una regeneración continua de los centros activos del catalizador haciendo uso de la regeneración electro-química lo cuál implica una ventaja importante frente a la reducción química. En este trabajó también se observó un aumento en la selectividad de la celda electroquímica respecto a la descomposición de los óxidos de nitrógeno con el tiempo de operación de la celda. En la literatura se pueden encontrar trabajos que afirman observar un aumento en la selectividad, dicho umento es relacionados con cambios en la estructura del catalizador. En el presente trabajo, un cambio de color del catalizador fue relacionado con un cambio en su estructura, sin embargo, es necesario llevar a cabo estudios mas detallados con el fin de elucidar el mecanismo de mejora de la selectividad del catalizador. Con el fin de aumentar la reproducibilidad de la celda electro-química, se hizo uso en este trabajo de dos tipos de reactores, uno tubular y uno plano. Los resultados más reproducibles se obtuvieron con el reactor plano mientras que los valores mas altos de actividad catalítica en la descomposición de los óxidos de nitrógeno fueron observados con el reactor tubular. Sin embargo no se encontró mejora en la selectividad de la celda con el tiempo en el caso del reactor plano. La actividad catalítica del catalizador NiO/YSZ fue también comparada con la actividad catalítica presentada por otro tipo de catalizadores de níquel como La_2NiO_4 y $LaNiO_3$, siendo el catalizador NiO/YSZ el que dio mejores resultados. La capacidad del catalizador NiO/YSZ de almacenar compuestos de nitrógeno en forma de nitratos y nitritos también fue estudiada en este trabajo y se propuso un mecanismo de almacenamiento coherente con los resultados obtenidos mediante los experimentos TPD y DRIFT. En este trabajo también se ha propuesto un mecanismo de descomposición de los óxidos de nitrógeno según el cuál, la quimiadsorción disociativa de las moléculas de óxido de nitrógeno en la superficie del catalizador es seguida de la recombinación de los átomos de nitrógeno dando de esta forma lugar a la formación de moléculas de nitrógeno.

CHAPTER 2

Introduction

The efficiency of diesel engines is higher than the one presented by gasoline engines. Hence a decrease in the fuel consumption can be achieved which lead to a decrease in the CO_2 emissions if we compare it with the CO_2 emissions produced by gasoline engines. That fact makes the diesel engines more economic and environmental friendly. Due to the advantages presented by the diesel engines, its importance and presence in the market has been increasing among the years [**1**] [**2**]

The fossil materials combustion in order to obtain energy destined to the industry, transport and house maintenance gives rise to gas emissions which can be damaging to the health. They can also contain gases which have other harmful effects like the depletion of the ozone layer, the greenhouse effect and the acid rain. CO, CO_2, hydrocarbons (HC), volatile organic compounds ($VOCs$), aldehydes, SO_2, NO, NO_2, N_2O and particulate matter (PM) are considered to be among these gases.

The elimination of CO, HC and aldehydes in oxidant rich conditions by using diesel oxidation catalysts is possible with typical conversion efficiencies between 70 and 95% [**3**]. However, there is no effective method for the elimination of NO_x in oxidant rich conditions. The present work aims to contribute to finding an effective method for the reduction of NO_x in oxidant rich conditions.

2.1. Description and chemistry of the nitrogen oxides

The references utilized for that section are [**4**]-[**8**].

2.1.1. Nitrous Oxide (N_2O).

Nitrous oxide (N_2O) is an important atmospheric gas that is emitted predominantly by biological sources in soils and water. Although N_2O has a far lower concentration than CO_2 and H_2O, it is an extremely influential greenhouse gas since its residence time is long and its infrared energy (8.610^{-6}-7.810^{-6}) absorption capacity per molecule is relatively large . Per unit mass the global warming potential of $N_2O$is about 300 times that of CO_2. Nitrous oxide is inert in the troposphere. Its major atmospheric sink is photo-dissociation in the stratosphere (about 90 %). The other 10 % of the N_2O atmospheric elimination process consist in the reaction with excited oxygen atoms, $O(1D)$ in order to yield NO. That oxidation reaction provides the major input of NO to the stratosphere.

2.1.2. Nitrogen oxides (NO_2 and NO).

The oxides of nitrogen, NO and NO_2 (referred together as NO_x), are among the most important molecules in atmospheric chemistry.

The nitrogen monoxide (NO) is a toxic and colorless gas and the nitrogen dioxide (NO_2) is a non-toxic brown-red gas which possesses a characteristic smell. The most important nitrogen containing compounds sources are the combustion of fossil matter. The nitrogen monoxide emission which is originated during the combustion in engines can be classified in three types; thermal NO, fuel NO and prompt NO. Although the nitrogen molecule is not chemically reactive at low temperature due to the strength of its triple bound, the high temperature found in combustion engines permit that the N_2 molecule reacts with the present O-atoms in order to form metastable NO which is referred as thermal NO. A requirement for that reaction to occur is the decomposition of the oxygen molecule into its atoms which can occur due to the high temperatures found in the combustion engines (2.1). Then, the oxygen atoms react with the nitrogen molecules to form NO and nitrogen atoms (2.2). M represents any molecule which can absorbs the extra energy produced during the reactions.

$$O_2 + M \leftrightarrow 2\,O + M \tag{2.1}$$

$$N_2 + O \leftrightarrow NO + N \tag{2.2}$$

The nitrogen and oxygen atoms formed in the reactions (2.1) and (2.2) respectively reacts then to form NO as shown in equation (2.3). The global reaction is presented in equation (2.4)

$$2\,N + 2\,O \leftrightarrow 2\,NO \tag{2.3}$$

$$N_2 + O_2 \leftrightarrow 2\,NO \tag{2.4}$$

The fuel NO is produced by the oxidation of organic nitrogen compounds contained in the fuel. The oxidation reaction occurs relatively fast and it can be influenced by the combustion temperature.

The prompt NO is formed as a result of a sequence of complicated reactions between the atmospheric nitrogen and activated fuel molecules mainly in processes which occur in poor oxygen conditions.

When the NO is exposed to air, it combines with the oxygen molecules in order to produce nitrogen dioxide (2.5)

$$2\,NO\ +\ O_2\ \leftrightarrow\ 2\,NO_2\ \ slow\ oxidation \tag{2.5}$$

The oxidation of NO as indicated in equation (2.5) is a third-order reaction and its rate depends on the square of the very low NO concentration. Hence, the formation of NO_2 could not have resulted from the direct oxidation of NO. A most important NO_2 formation mechanism is the one which involves the reaction of ozone with the nitrogen monoxide radicals as shown in (2.6).

$$NO\ +\ O_3\ \leftrightarrow\ NO_2 +\ O_2\ \ fast\ oxidation \tag{2.6}$$

That reaction is fast but the ozone is a sub-product of the NO_2 formation and is not present in significant amount until a certain amount of NO_2 is already formed. Another NO_2 formation mechanism in air actually involves free radical oxidation of HC (or more slowly with CO), and one of the more important series of free radical reaction leading to NO_2 is described by equations (2.8)-(2.11) with the global equation indicated in formula (2.12)

$$OH\ +\ RCH_3\ \rightarrow\ H_2O\ +\ RCH_2 \tag{2.7}$$

$$RCH_2\ +\ O_2\ \rightarrow\ RCH_2O_2 \tag{2.8}$$

$$RCH_2O_2\ +\ NO\ \rightarrow\ RCH_2O\ +\ NO_2 \tag{2.9}$$

$$RCH_2O\ +\ O_2\ \rightarrow\ RCHO\ +\ HO_2 \tag{2.10}$$

$$HO_2\ +\ NO\ \rightarrow\ NO_2\ +\ OH \tag{2.11}$$

The global reaction is then

$$RCH_3 \,+\, 2\,NO \,+\, 2\,O_2 \,\rightarrow\, RCHO \,+\, 2\,NO_2 \,+\, H_2O \tag{2.12}$$

The nitrogen dioxide absorbs solar radiation in the visible and near UV ($\lambda \leq 420nm$) which leads to its dissociation resulting in the production of oxygen atoms and nitrogen oxide radicals (2.13)

$$NO_2 \overset{\lambda \leq 420nm}{\rightarrow} NO \,+\, O \tag{2.13}$$

The oxygen atoms can then react very fast with the oxygen molecules in order to produce ozone (2.14) and then ozone can react with NO according to the equation (2.6) giving rise to nitrogen dioxide.

$$O \,+\, O_2 \,+\, M \,\rightarrow\, O_3 \,+\, M \tag{2.14}$$

2.1.3. Chemistry of the nitrogen oxides.

At very low temperatures, the NO_2 molecules can dimerize giving rise to colorless N_2O_4.

$$2\,NO_2 \,\leftrightarrow\, N_2O_4 \tag{2.15}$$

The NO indirectly causes the acid rain since the NO_2, which is a product of the NO oxidation which take place in the air, can rapidly dissolve in water. As NO_2 comes in contact with the air humidity, it disproportionates giving rise to nitrous acid and nitric acid as shown in equation (2.16).

$$2\,NO_2(g) \,+\, H_2O(l) \,\leftrightarrow\, HNO_3(aq) \,+\, HNO_2(g) \tag{2.16}$$

The N_2O produced in the troposphere can reach the stratosphere where it is rapidly converted by the solar radiation with $\lambda \leq 250nm$ mainly in N_2 (95 %) and also in NO (5 %)

$$N_2O \overset{h\nu}{\rightarrow} NO + N \tag{2.17}$$

$$N_2O \overset{h\nu}{\rightarrow} N_2 + O \tag{2.18}$$

Another consequence derived from the formation of nitrogen oxides in the troposphere is the smog. The smog, consisting of a mixture of partially oxidized hydrocarbons, ozone and other oxidants, is observable from midday to late afternoon. In addition to producing a visible haze, it also causes eyes and other membrane irritations, can adversely affect plant growth, and is implicated in other serious eco-toxicological problems. The main pollutants that cause photochemical smog are NO, NO_2, hydrocarbons (RH), PAN, ozone and the aldehyde. The chemical reactions that lead to smog formation center on the hydroxyl radical.

The nitrogen oxides can make their way from the troposphere where they are produced to the stratosphere and then they can react with the ozone as shown in equation (2.6) giving rise to its depletion. That contributes to the ozone hole formation.

CHAPTER 3

Objectives

The objectives of the present Ph.d Thesis are listed below.

- Determination of the experimental conditions in which storage of nitrogen-containing species take place.
- Identification of the nitrogen-containing species stored on the catalyst surface and study of the storage mechanism.
- Study of the chemical and electro-chemical regeneration of the catalyst.
- Study of the NO_x decomposition activity of the NiO/YSZ catalys with and without electrochemical support.
- Study of the selectivity of the NO_x decomposition reaction on the NiO/YSZ catalyst.
- Comparison of the catalytic activity presented by different systems.
- Comparison of the convenience of using a tubular or a planar reactor for the electro-catalytic experiments.

CHAPTER 4

Bibliographic review

In order to reduce the nitrogen-containing emissions to the levels established by the EURO legislation [**9**], the automotive exhaust can be subjected to a purification treatment. However, the technology used since the 80s in Otto engines, the three way catalyst (TWC), which uses the novel metal combinations Pt/Rh and Pd/Rh as active components has been proved not to be a good method for purification applications of automotive exhaust which come from diesel engines [**10**] due to the high oxygen concentration present in the gas mixture.

The lambda value is a parameter used to indicate the ratio between the amount of oxygen present in the combustion gas mixture and the amount of oxygen needed for a complete combustion of the fuel. In Otto engines coupled with a TWC gas purification system, the lambda value is approximately 1, and therefore the gases CO, HC and CO_2 can be oxidized and the reduction of NO_x to N_2 is also possible. Therefore those harmful gases can be eliminated from the automotive exhaust [**11**].

In Diesel engines, the amount of oxygen present in the gas mixture is much lower ($\lambda < 1$). Using catalysts based on Pt, it is relatively easy to remove the unburned hydrocarbons and the carbon monoxide from the automotive exhaust with an oxidation catalyst. However, the reductive elimination of the nitrogen oxides is almost impossible with such a catalysts.

4.1. Selective Catalytic Reduction (SCR)

SCR catalysts are manufactured from various ceramic materials used as a carrier, such as titanium oxide, and the active catalytic components are usually oxides of base metals (such as vanadium and tungsten), zeolites, and various precious metals. An example of a selective catalytic reduction catalyst is $V_2O_5/TiO_2/WO_3$. That technology is known since the 70s and it is currently used in diesel trucks. The elimination of the nitrogen oxides from the diesel automotive exhaust under strong oxidizing conditions occurs due to the performance of a reducting agent (NH_3, H_2 or hydrocarbons) on the SCR catalyst surface [**12**] [**13**].

4.1.1. SCR-NH_3.

If no NO_2 is contained in the feed, the reduction of NO by NH_3 takes place according to equations (4.1) and (4.2). That is known as standard SCR.

$$6\,NO\;+\;4\,NH_3\;\leftrightarrow\;5\,N_2\;+\;6\,H_2O \tag{4.1}$$

$$4\,NO\;+\;4\,NH_3\;+\;O_2\;\leftrightarrow\;4\,N_2\;+\;6\,H_2O \tag{4.2}$$

By means of a diesel oxidation pre-catalyst (DOC), the previous oxidation of NO to NO_2 occurs. When NO and NO_2 are present in the exhaust in equimolar concentrations, reaction (4.3) take place (the so-called fast-SCR) that is faster than the standard SCR. When the NO_2/NO ratio is larger than 1, the reduction reaction occurs according to equation (4.3) and (4.5) which are demonstrated to be slower than the fast-SCR reaction [**136**] - [**138**]. The temperature at which the fast-SCR reaction takes place is lower than the temperature needed for the standard SCR but it has to be kept above 200°C since the fast SCR conversion drops with decreasing temperature under 200°C which is probably originated by the ammonium nitrate formation that leads to an inhibition of the rate-determining step for fast- SCR [**139**]. Furthermore, a kinetic inhibition of the NO oxidation on the Pt surface occurs at temperatures lower than 170°C [**16**].

$$NO\;+\;NO_2\;+\;2\,NH_3\;\leftrightarrow\;2\,N_2\;+\;3\,H_2O \tag{4.3}$$

$$2\,NO_2\;+\;2\,NH_3\;\leftrightarrow\;7\,N_2\;+\;12\,H_2O \tag{4.4}$$

$$6\,NO_2\;+\;8\,NH_3\;\leftrightarrow\;N_2\;+\;N_2O\;+\;3\,H_2O \tag{4.5}$$

For the application of that catalysts technology to vehicles, the NH_3 has to be stored inside of them. Due to the toxicity of NH_3 its storage inside of the vehicles is not feasible. Instead of that, the NH_3 can be generated in-situ using an aqueous urea solution commercially available as "AdBlue" [**14**]. That urea solution give rise to NH_3 according to the equation (4.6) [**15**].

$$(NH_2)_2CO\;+\;H_2O\;\rightarrow\;2\,NH_3\;+\;CO_2 \tag{4.6}$$

Another application problem of the NH_3-SCR technology in diesel vehicles is that the temperature needed for the regeneration of the particles filter is higher than 650°C and the thermal stability of V_2O_5 is not good enough since its melting point is relatively low (690°C). Hence, the continuous performance of that catalysts containing V_2O_5 has to be kept at a temperature lower than 550°C [**17**].

As seen previously, the SCR-NH_3 technology presents some problems since it requires a complex catalyst, a lot of space for the reagents storage and it is necessary to refill the urea container periodically. Besides that, the V_2O_5 is toxic and it presents a too low thermal stability. Hence, some research works aim to eliminate the V_2O_5 from the catalyst and replace it with iron or zeolites. All that problems make he SCR-NH_3 technology not suitable for applications in diesel vehicles.

4.1.2. SCR-H_2.

SCR-H_2 is an effective method for the decomposition of nitrogen oxides contained in the diesel exhaust at low temperatures. It is known [**18**] [**12**] that the nitrogen oxides can be decomposed on the Pt surface when they react with hydrogen in stoichiometric and not stoichiometric conditions. Therefore, it is possible to obtain good conversion rates even if the reaction takes place under high oxidant rich conditions. Shelef et al. [**19**] concluded that there is a definite selectivity of the catalytic reduction of NO molecules by H_2 with respect to the reduction of O_2 molecules by H_2 over Pt and Pd catalysts at temperatures lower than 200°C. However, the temperature interval in which good conversion rates can be achieved is not very large since a good activity is not observed at temperatures lower than 150°C. The reduction of the nitrogen oxides with H_2 can give rise to both N_2 (4.7) and N_2O with N_2O as the main product [**20**] - [**23**]. That makes that catalyst not suitable for the elimination of the nitrogen oxides contained in the diesel exhaust.

$$2\,NO\,+\,2\,H_2\,\rightarrow\,N_2\,+\,2\,H_2O \tag{4.7}$$

The reduction mechanism of NO_x with H_2 on a Pt/Al_2O_3 has been studied by Burch et al. [**24**] and according to that work, it is possible to conclude that the reduction of the surface of the catalyst by H_2 create a certain number of active centers which can participate in the dissociative adsorption of the NO molecules on the catalyst surface. The reaction product N_2 is formed as a consequence of the recombination of the nitrogen atoms originated during the dissociative adsorption of two NO molecules on the catalyst surface. The reaction product N_2O is produced by the reaction of a gas NO molecule with a nitrogen atom adsorbed on the catalyst surface. The oxygen produced during the dissociative reduction remains adsorbed on the catalyst surface and it will play a role on the re-oxidation of the catalyst.

In order to improve the activity of the SCR-H_2 catalysts, some studies have been done with the purpose of replacing the TiO with another binary oxides which can work as catalyst support [**25**] [**26**]. Other types of systems have been also studied [**27**] [**28**] but none of them presented a significant improvement on the activity and selectivity of the catalytic reaction of N_2 formation. It has been also proved that Pd, Rh, Ir and Ru are much less active than Pt on the SCR-H_2 reaction [**29**] [**30**] [**31**]. Frank et al. [**32**] studied the system $Pt-Mo-Co/\alpha-Al_2O_3$. They found a first significant improvement on the catalytic activity of the SCR-H_2 system as regards to the formation of N_2. Costa et al. [**33**] could achieve conversions between 80 and 90 % working with a $Pt/La_{0.7}Sr_{0.2}Ce_{0.1}FeO_3$ in the temperature range between 100 and 250°C.

For the application of the SCR-H_2 catalyst to diesel vehicles, it is necessary to store and refill the H_2 container inside them. Since the H_2 supply from high-pressure bottles can be problematic from the security point of view, an alternative H_2 supply method would be required. A possibility could be the in-situ H_2 generation by means of water hydrolysis or starting from methanol [**34**] [**35**] according to reaction (4.8).

$$CH_3OH \;\rightarrow\; CO \;+\; 2\,H_2 \tag{4.8}$$

But even that variant presents disadvantages. The energy consumption is high and the reagent containers need a lot of place. They also increase the vehicles weight. Another possibility would be the H_2 obtaining from the diesel fuel partial oxidation [**36**] [**37**] [**38**].

4.1.3. HC-SCR.

In the *HC-SCR* technology, the reduction reagents used to decompose the nitrogen oxides are hydrocarbons ("HC"). The reaction that takes place is shown in equation (4.9) where "CH_2" indicates an hydrocarbon fragment.

$$6\,NO \;+\; 2\,"CH_2" \;\rightarrow\; 3\,N_2 \;+\; 2\,CO_2 \;+\; 2\,H_2O \tag{4.9}$$

The utilized catalysts are based on Pt and Ir as well as on transition metals like Ag and Cu. Zeolites can also being used [**39**] [**40**]. The advantage that the *HC-SCR* presents with regard to the other *SCR* variants is that it is not necessary to refill the reducing reagent because it is generated in the vehicle. The generation of the hydrocarbons can take place through diesel fuel catalytic cracking with zeolite based catalysts [**41**]. The processing of the fuels is necessary since the short-chain hydrocarbons present a higher reactivity than the long-chain and ramified hydrocarbons [**40**]. Due to the great oxygen excess present in the diesel exhaust (3-21 vol %), the most hydrocarbons which are supposed to reduce the NO_x will be oxidize by the catalyst. Another problem presented by the noble metal-based catalysts is that part of the NO_x will be reduced in order to form N_2O as shown in equation (4.10)

$$6\,NO \;+\; "CH_2" \;\rightarrow\; 3\,N_2O \;+\; CO_2 \;+\; H_2O \tag{4.10}$$

So far, the catalysts with Ag show the best activity and selectivity but the SO_x originates its poisoning. Hence, the catalyst will be deactivated with the operating time.

4.2. NO_x-storage-reduction technology (NSR)

NSR was developed and first applied in vehicles by Toyota. A promising approach to NO_x removal under lean burning conditions (i.e. oxygen rich) is based on the NO_x storage-reduction (NSR) concept. NSR catalytic systems, also referred to lean NO_x traps ($LNTs$), are operated alternatively under lean and rich (i.e. oxygen poor) burning conditions: NO_x is stored on the catalyst under lean conditions and subsequently converted to nitrogen by unburned hydrocarbons under rich conditions. Typical NSR catalysts consist of a high-surface-area support (e.g., α - alumina), a NO_x-storage component (an alkaline or an alkaline earth metal oxide like BaO), and a noble metal (Pt), for both the oxidation of NO and hydrocarbons and the reduction of stored NO_x. The NO emitted is oxidized to NO_2 under lean burning conditions ($\lambda > 1$) by the excess oxygen present in the gas mixture on the noble metal (generally Pt) based catalyst. The NO_2 is then retained by the $Ba(OH)_2$ or $BaCO_3$ as nitrites and nitrates [**42**] [**43**]. That happens until the catalyst is almost saturated and then a catalyst regeneration phase follows which is achieved through the change from lean to rich burning conditions ($\lambda < 1$). That originates the desorption of NO_2 which will be then reduced by the excess of reduction reagents like H_2, CO and "HC" giving rise to N_2 and water. After that the system is returned to the lean burning conditions to start again the catalytic cycle. That kind of catalyst presents a deactivation problem due to the SO_2 present in the fuel. These catalysts are currently being used in automotive applications.

In the literature it is possible to find a large amount of works aimed to elucidate the performance mechanism of that type of catalysts. Fridell et al. [**44**] studied the system $Pt/BaO/Al_2O_3$ and proposed a four-step mechanism which is generally accepted: (i) NO to NO_2 oxidation on Pt, (ii) NO_2 storage on BaO, (iii) NO_x release, and (iv) NO_x reduction to N_2. Many works have been done in order to elucidate the NO_x storage mechanism [**44**]-[**56**] and the reduction mechanism of the trapped nitrogen oxides [**57**]-[**59**].

4.3. $DeNO_x$ Technology

The $deNO_x$ technology is aimed at eliminating the nitrogen oxides by converting them into N_2 and O_2. The NO_x dissociation is thermodynamically favorable at temperatures under 1000°C. Therefore, that reaction can be used in order to remove the nitrogen oxides which are contained in the diesel and Otto automotive exhaust. A clear advantage of that technology is that no reduction agent is necessary for the adequate performance of the catalyst.

The active materials used in the catalyst have been noble metals, zeolites and perovskites. Already in 1906, Karl Jellinek [**60**] studied the NO decomposition reaction on Pt giving rise to N_2 and O_2. He established the dependence of that reaction with the temperature concluding that it took place in the temperature range between 650 and 1750°C.

It is known [**61**]-[**63**] that the noble metals Rh, Pd and Pt present a considerable activity in the NO_x decomposition but when oxygen is also present in the gas mixture, the activity decreases and the NO_x decomposition is inhibited [**64**] [**65**]. The strength of the bound formed between the oxygen and the Pt gives rise to the fast deactivation of the Pt since just a small fraction of the active centers on the platinum surface remain free and available for the NO_x decomposition reaction to take place. The liberation of the adsorbed oxygen can be sped up by means of the use of promoters. The tested promoters which showed a better effect were the rare earth element oxides like Tb since these compounds have the capacity of capturing and storing oxygen. However the oxygen desorption occurs significantly only up to 593°C [**66**].

The zeolite-based system Cu-ZMS5 showed an improved NO_x decomposition activity when Ca or Mg co-cations were added [**68**]. The disadvantages of these catalyst are that they show a drastic deactivation when oxygen is contained in the gas mixture and apart from that, the zeolite structure do not present a thermal stability enough to be applied on the vehicle exhaust purification.

Unlike the zeolites $ZMS5$, the perovskites are thermal stable. The perovskite capacity of decomposing the nitrogen oxides is known since the middle of the 60 s [**69**] [**70**]. The development of that kind of catalysts in order to achieve better results in the decomposition of the nitrogen oxides have been intensified during the last 20 years. Teraoka et al. [**71**] developed a model for the NO_x decomposition using the perovskites $La_{0.8}Sr_{0.2}CoO_3$ and $La_{0.4}Sr_{0.6}Mn_{0.8}Ni_{0.2}O_3$ as catalyst. That model is not based on detailed mechanistic experiments but on global kinetic data. According to Teraoka et al. two oxygen vacancies participate in the adsorption of two NO molecules. As a consequence of the adsorption, both NO molecules dissociates and the two nitrogen atoms will combine giving rise to a nitrogen molecule. Whereas the nitrogen molecule rapidly abandon the catalyst surface, the oxygen atoms do not since its desorption occurs very slowly. Hence, an equilibrium between the adsorbed and gas oxygen take place originating a decrease of the catalyst activity. Teraoka et al. found a decrease of about 50 % on the catalytic activity when the oxygen concentration was increased from a 0 vol% to a 5.5 vol%. The influence of another gases which are present in the automotive exhaust were not taken in consideration on this work. Kirchnerova et al. [**72**] demonstrated that the NO_x decomposition activity presented by some perovskites like $La_{0.8}Sr_{0.13}Mn_{0.2}Ni_{0.8}O_{3-\delta}$ clearly decreases when both CO_2 and H_2O are present in the gas mixture. Yokoi and Uchida [**73**] investigated the relationship between NO decomposition activity on lanthanum transition metal oxide ($LaMO_3$) catalysts (where M can be Cr, Mn, Fe, Co and Ni) and their oxygen desorption properties and they found that the catalyitc activity decreases as follows: $LaNiO_3 > LaCoO_3 > LaFeO_3 > LaMnO_3 > LaCrO_3$. These results correlate with the oxygen desorption temperature since the best catalyst is the one which presents a lower temperature for the oxygen desorption. Molecular orbital calculations support these results and indicate that the bond between the oxygen and the active centers of the most active catalyst is the bond that easiest breaks up. When oxygen and NO co-exist in the gas mixture, an equilibrium between the adsorbed and gas oxygen occurs which leads to a decrease of the catalytic activity. Voorhoeve et al. reported a total deactivation of the NO_x decomposition reaction when oxygen was also present [**61**].

In order to solve the problem derived from the strong adsorption of the oxygen molecules on the catalyst surface, a new concept was developed which consist of the use of an electro-chemical cells. That system can eliminate the adsorbed oxygen from the catalyst surface by pumping it out of it. Hence, the continuous regeneration of the catalyst may occur. Huggins et al. [**74**] were the first to demonstrate that it was possible to obtain an effective NO decomposition using a $Pt/YSZ/Pt$ and $Au/YSZ/Au$ electrochemical cell when no oxygen was present in the gas mixture. They found a tremendous enhancement of the rate of NO decomposition in the case of either porous platinum or gold compared with the one obtained with no porous electrodes. The catalytic enhancement for zirconia covered with a nonporous layer of platinum is that typical for pure platinum in a non-electrolytic system. Those results support the hypothesis that the catalytic reactions do not take place on the Pt or Au surface but on the YSZ/Pt border and that the F-centers, created by the voltage applied to the cell, are responsible for the catalytic activity. T. Hibino et al. [**75**] worked with the system $Pt/YSZ/Pt$ and concluded that when oxygen is present in the gas mixture, a very high current is necessary to get an appreciable NO_x conversion and that the oxygen molecules adsorb preferably than the NO or NO_2 molecules.

To solve the problem of effective NO decomposition in the presence of excess oxygen, a functional multilayer electrode concept was developed. in which the noble metal layer is covered by a catalyst layer. As catalyst, mixed ionic-electronic conductors (MIECs) which have both ionic and electronic species as charge carriers will be used. Perovskite-based oxides $LnMO_3$ ($Ln = La$, Sr, Y and $M = Co$, Mn, Cr) have been studied for their use in zirconia-based SOFC due to their high electronic and significant oxygen ion conductivity [**77**]-[**81**]. Examples of another class of mixed conductors, fabricated by mixing two different phases of materials, can be also found in the literature. As examples we can mention LiI/Al_2O3 [**82**], NiO/NiS, NiO/Ni and NiO/Pd [**83**] [**84**], ZrO_2/In_2O_3 [**85**] and CeO_2/NiO [**86**].

Another $MIEC$ material is YSZ/NiO. Min Park and Gyeong Man Choi [**87**] studied the electrical properties of a YSZ/NiO mixed ionic-electronic conductors in the temperature range between 400 and 1000°C and a complete concentration range of the YSZ/NiO material. Bredikhin et al studied the NO_x decomposition activity of the $Pt/YSZ/Pt/YSZ - NiO$ cell and they observed that the covering of the Pt layer with a YSZ/NiO MIEC gave rise to the improvement of the nitrogen oxide decomposition results in oxygen excess [**88**] [**89**]. They studied also the correlation between the NO conversion rate and the micro-structure of the working electrode. Before these works, Xueping Xu and D. Wayne Goodman [**90**] studied the influence of the size of the Pd particles in the catalytic activity in the nitrogen oxide decomposition and they observed that no N_2O was produced but just N_2 and O_2 when the Pd particle size was small (< 50 $\AA$), but it was detected when the particle size was larger. In addition, more extensively NO decomposition was observed on the smaller Pd particles.

S. Bredikhin et al. studied the correlation between the micro-structure of the working electrode and the NO conversion rate [**91**]. They found that the micro-structure of the working electrode changed after cell operation. They also assert that an increase of the YSZ particles and a decrease of the NiO particles occur and the challenges of the working electrode micro-structure take place on the boundaries between two YSZ particles. They observed also that the catalytic activity of the electrochemical cell improved as the micro-structure of the working electrode changed. They also reported [**76**] that the increase of the sintering temperature leads to a decrease of the size of the pores and as a result, an improvement of the cell performance since a lower current value was then required for the NO decomposition.

Challenges of the micro-structure were also observed in another work (fig. 4.1) [**92**] but the growth of new NiO particles are in that case observed in the boundaries between a NiO and a YSZ particle and not between two YSZ particles. A growth of the new NiO particles on the boundaries between two NiO particles has been also reported [**93**].

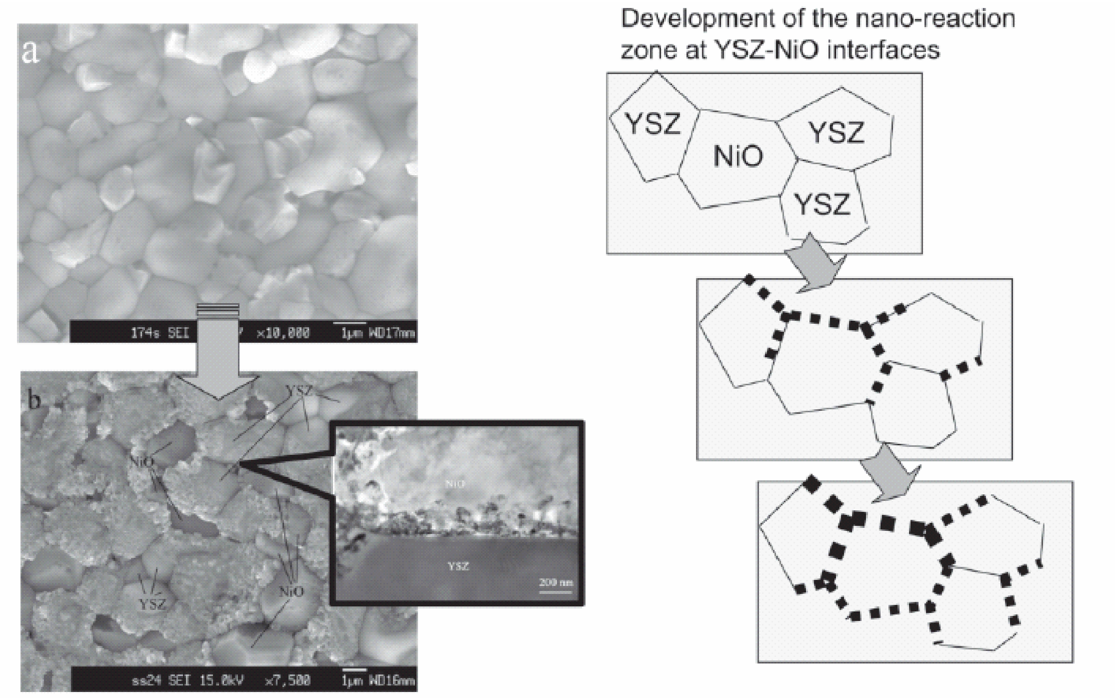

Fig. 3. Microstructure of the electro-catalytic electrode observed by SEM and TEM. The sample was electrochemically treated to develop the nano-structure.

FIGURE 4.1. Challenges in the micro-structure of the working electrode after cell operation

The mechanism of the decomposition of nitrogen oxide on the YSZ/NiO catalyst was also studied [**92**] [**93**] . These works assert that the NO molecules are first chemisorbed on Ni. Then two molecules of $Ni - NO$ recombine to form N_2 and NiO. The active centers of the catalyst are then regenerated as a voltage is applied between the electrodes and the oxygen adsorbed on Ni is pumped out from the cathode to the anode near region where an oxidation reaction is produced and O_2 molecules are formed. In the present work, the decomposition reactions of NO_x on Ni based catalysts on an electrochemical system (section 8.6) and the regeneration of its active centers was also studied (section 8.2)

CHAPTER 5

Experimental methods

5.1. Chemiluminiscence

Chemiluminiscence is the emission of light with limited emission of heat as a result of a chemical reaction. That method is generally highly sensitive because low light levels are readily monitored in the absence of noise. It is considered one of the most widely used technique for the measurement of nitrogen oxides. It is capable to proportionate a linear relationship between signal and concentration over the range of measurement between 1 ppb and 10000 ppm and it makes possible to obtain a continuous signal for NO, NO_2 and NO_x.

Both ozone and the gas sample are conduced continuously into the analyzer of the instrument where NO and ozone reacts giving rise to the reactions (5.1) and (5.2).

$$NO + O_3 \rightarrow NO_2^* + O_2 \tag{5.1}$$

$$NO + O_3 \rightarrow NO_2 + O_2 \tag{5.2}$$

20% of all the reactions between nitrogen monoxide and ozone produce nitrogen dioxide in an excited state (NO_2^*) which can suffer a deactivation to return to the ground state in two ways: through emission of electromagnetic radiation (5.3) or by means of collision with a gas molecule M (5.4). The deactivation of the NO_2^* molecules due to collisions is the most frequent way, for which they return to the ground state.

$$NO_2^* \rightarrow NO_2 + h\nu \tag{5.3}$$

$$NO_2^* + M \rightarrow NO_2 + M \quad \text{Main reaction} \tag{5.4}$$

The emitted radiation is photo-electrical detected. If an adequate excess of ozone is available, the above mentioned photo-electrical signal is proportional to the concentration of the NO to be analyzed.

Since the deactivation of NO_2* molecules occur mainly through collision with another gas molecules, it is necessary to work in high vacuum to minimize the loss of electromagnetic radiation due to the reaction (5.4). Working in high vacuum reduces the probability of a deactivation through collision with another gas molecule.

In order to determine the concentration of NO_2 in the gas sample, we have to convert it first to NO before it arrives to the measurement vessel, where the reaction with ozone will take place. The gas sample is conduced into a converter which works at 415°C and which contains a reduction material (carbon). The NO_2 is reduced by the carbon (5.5) in order to form NO which then can be detected.

$$NO_2 + C \rightarrow NO + CO \tag{5.5}$$

Normally both NO and NO_2 are present in the gas sample. The use of a converter allows us to measure the NO together with NO_2 ($NO_x = NO + NO_2$). The simultaneous measurement of both NO and NO_2 is possible by using the principle of two chamber which is described in fig. 5.1.

The gas sample is separated in two equal flows which are conducted by two different capillaries (canal 1 and canal 2) through the instrument. One of the capillaries (the canal 2 in fig. 5.1) conduces the gas sample first into the converter and finally into the analyzer. Hence, a signal corresponding to NO_x can be achieved. The other capillary (canal 1 in fig. 5.1), conduces the gas sample directly into the analyzer giving rise to the NO concentration signal. The NO_2 concentration can be calculated as the difference between the NO_x and NO signal.

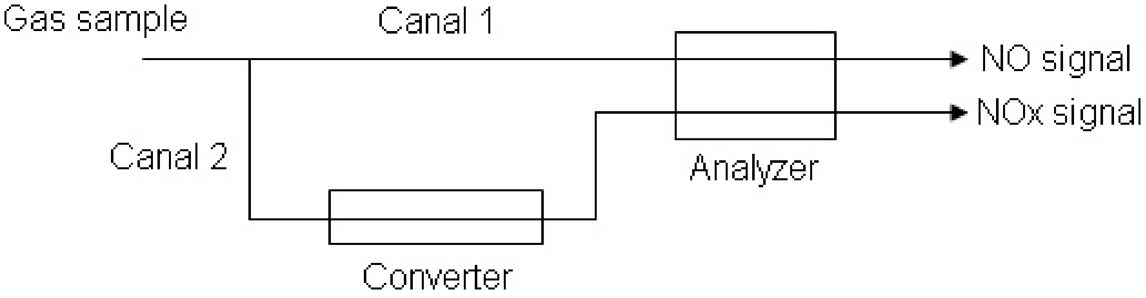

FIGURE 5.1. The principle of two chamber

The instrument used in this work was a CLD 700 El ht provided by ECO PHYSICS (München). The concentration range was 1-1000 ppm.

5.2. Electron microscopy

The electron microscope combines the possibility of obtaining high resolution images with the possibility of chemical analyzing of small sample areas. The electron microscope resolving power is determined by the wavelength of the particles which are used to irradiate the specimen which has to be analyzed. The resolving power can be increased by decreasing the wavelength of the utilized radiation. The wavelength of an electron beam is much shorter than the one of visible and even UV light. The advantages of using an electron beam instead of another short wavelength particles is that electrons can be easily accelerated by applying a voltage and since they are charged particles, its trajectory can be easily modified by electric and magnetic fields.

The electron microscope works with electron beams which travel with a determined trajectory from its source to the sample. Therefore, the electron microscope always works under high vacuum conditions in order to avoid that another atoms or molecules different from the sample alter the course of the electrons path. The work pressures are in the range between 10^{-7} and 10^{-10} bar.

An electron cannon generate the electron beam which is then accelerated by a voltage and focused by magnetic lenses. The electron beam reaches the sample and the signal obtained is amplified by a group of magnetic lenses which create an image on a screen which is sensitive to the impact of electrons. Then, that image is transmitted to a computer screen. The interaction between the sample and the electrons beam originate the emission of secondary radiations. The type of information achieved about the samples depends on the secondary radiations which are detected.

5.2.1. Scanning electron microscope (SEM).

Energies in the range between some hundred eV and some tens keV are utilized for the acceleration of a thin electron beam which come into contact with a thick electron-opaque sample. That electron beam is focused on the sample surface and it scans the sample in a raster scan pattern.

From all forms of radiation resulting from the interaction between the electron beam and the sample, the two of them which are really important in the scanning electron microscope are the secondary electrons and the back-scattered electrons. When the electrons beam interacts with the sample, the atoms which are located close to its surface emit electrons which are denominated as secondary electrons. They are responsible of the obtaining of a three-dimensional image of the sample. The back-scattered electrons are however electrons which come from the incident electron beam. They are electrons which have been reflected by the sample and they can reveal differences in the chemical sample composition since the heaviest atoms produce a higher number of electrons and therefore more intense signals. The intensity of both secondary and back-scattered electrons signals depends on the angle between the incident electron beam and the sample surface, that is, it depends on the sample topography. The x-ray radiation spectrum emitted by the atoms can also be used in order to obtain quantitative and qualitative information about the chemical composition of a small portion of the sample making use of the analytical technique known as energy-dispersive X-ray spectroscopy (EDS or EDX). When the electron beam removes a sample inner shell electron, another electron, which has a higher energy than the one released, can fill the shell giving rise to the emission of x-ray. The wavelengths of this emitted x-ray are characteristic of the elements present in the sample and the radiation intensities at each wavelength are proportional to the different element concentrations.

5.3. X-ray diffraction

The x-rays are electromagnetic radiations which have wavelengths in the Ångstrøm range, are sufficiently energetic to penetrate solids and are well suited to probe their internal structure. The x-rays are situated in the electromagnetic spectrum between the ultraviolet radiation and the gamma rays and this radiation is produced when high energy charged particles (for example electrons) are accelerated in a 3000 V field and then, they collide with matter.

The principle in which that method for the determination of crystal structures is based, lays in the fact that diffraction occurs when a wave encounters a series of regularly spaced obstacles which both are capable of scattering the radiation wave and have spacing that are comparable in magnitude to the radiation wavelength. Furthermore, diffraction is a consequence of specific phase relationships established between two or more waves that have been scattered by the obstacles.

When the scattered waves are out of phase, their amplitudes destructively interfere. When the scattered waves are in phase, their amplitudes reinforce one another and that is a manifestation of diffraction. In that case (constructive interference), the Bragg law is valid.

$$\lambda = 2\, d_{hkl} \sin\Theta \tag{5.6}$$

where:

λ is the wavelength of the X-rays

d_{hkl} is the distance between two lattice planes

Θ is the angle between the incoming X-rays and the normal to the reflecting lattice plane.

The XRD spectrum is characteristic of a crystal type in particular and that makes possible the characterization of crystalline compounds through x-ray diffraction.

The analysis were performed with a diffractometer 501 provided by Siemens (Karlsruhe). The X-radiation source was the $Cu-Ka_{1/2}$ radiation with a wavelength of 1.5405 Å. The measurement time per increment was 4 s, the 2Θ angle increments were 0,02° and the rotation frequency was 2 Hz.

5.4. Molecular mass spectrometry

In the mass spectrometry technique, ionized gas molecules of a sample will be separated in a separation field according to their masses and finally the ions will be detected. There are several methods to ionize the sample molecules. Historically, ions for mass analysis were produced by electron impact. In order to do so, electrons are emitted from a heated tungsten or rhenium filament and accelerated by applying approximately 70 V between the filament and the anode. Those electrons collide with the gas molecules of the sample giving rise to its ionization. In chemical ionization, gaseous molecules of the sample are ionized by collision with ions produced by electron bombardment of an excess of a reagent gas. The chemical ionization provides less energy to the sample molecules than the electron impact. As a consequence of that, the molecules will be ionized but they will remain almost completely not fragmented. More details referred to the chemical ionization are given in appendix 10.1. The separation of the ionized molecules according to their relation mass/charge occurs through a quadrupole mass analyze which separation principle is based in the different performance of the charged molecules in an electrical field. A secondary electron multiplier will be used as detector.

For the experiments contained in that work, a mass-spectrometer with chemical ionization airsense 500 provided by v & f (Absam, Austria) was utilized.

5.5. Nitrogen-physisorption

According to Brunauer, Emmett and Teller (BET), the specific surface area of a porous solid material (S_{BET}) can be measured making use of the nitrogen-physisorption isotherm (DIN 66131) [**123**]. The BET-equation 5.7 can be utilized to calculate the specific amount of nitrogen which is needed in order to form a mono-molecular layer (n_m).

$$\frac{p/p_0}{n_{ads}(1-p/p_0)} = \frac{1}{n_m\,C} + \frac{C-1}{n_m\,C}\,(p/p_0) \tag{5.7}$$

Where

p is the equilibrium pressure of adsorbates at the temperature of adsorption in bar

p_0 is the saturation pressure of adsorbates at the temperature of adsorption in bar.

n_{ads} is the adsorbed gas quantity in mol/g.

C is the BET constant.

n_m is the mono-layer adsorbed gas quantity in mol/g.

Then the S_{BET} can be calculated according to equation (5.8)

$$S_{BET} = n_m \, S \, N_L \tag{5.8}$$

Where

S is the space required by an adsorbate in m^2

N_L is the Avogadro constant.

The samples were first pretreated for 30 min at 300°C. The nitrogen-physisorption experiments were then performed at the N_2 boiling temperature (-196°C) making use of a Sorptomatic 1990 instrument provided by Porotec (Hofheim). The experimental error of the specific surface area determination was induced by the experimental error obtained as a consequence of weighing the sample. That error has a maximal value of 0.3 % which is so small that it can be disregarded.

5.6. Temperature programmed desorption

The temperature programmed desorption (TPD) can be used in order to determine the different adsorption sites of a solid material or the amount of gas species which are adsorbed on a solid material like catalysts under determined experimental conditions.

To prepare the sample for the TPD experiment, the species which could be adsorbed on the catalyst surface must be first eliminated. In order to do so, 1 g catalyst was heated at 450°C for 15 min in N_2 and then it was cooled down, also in N_2, to the temperature at which the saturation treatment would take place.

For the study of the NO_x and O_2 catalyst adsorption capacity, a gas mixture containing NO_x and O_2 respectively in N_2 was passed through the catalyst powder until the out-coming NO_x or O_2 concentration presented the same value than the incoming NO_x or O_2 concentration. Then, the catalyst was purged with a N_2 flow until no NO_x or O_2 was detected. The performance of the TPD experimental method occurs with a heating rate of 10 °C/min in a N_2 flow. The NO_x and O_2 gas detection was continuously performed during the TPD making use of the appropriate detection methods for each gas. The integration of the TPD signals as explained in appendix 10.5 can proportionate the information related to the amount of adsorbed species on the catalyst surface.

For the quantitative determination of the adsorbed species, experimental errors can interfere since it is possible that not all the adsorbed species are removed during the TPD.

5.7. Diffuse reflectance infrared Fourier transform spectroscopy ($DRIFT$)

The Fourier transform infrared spectroscopy ($FTIR$) measurement principle is based on the molecule capacity of absorbing electromagnetic radiation in the infrared range. The molecule vibrations and rotations are excited due to the radiation absorption and it can provide information about the molecule structure. By the diffuse Reflectance Infrared Fourier Transform Spectroscopy ($DRIFT$), the radiation which is reflected by a solid material surface is collected by mirrors and then it is conducted to the detector. Thereby, the identification of the different adsorbed species on the solid material surface can be possible.

Within the scope of the present study, a heatable sample carrier which is located inside a gas-tight sample chamber was utilized. Thus, the experiments can be performed under controlled temperature and atmosphere.

For the experiments accomplishment, a P/N 19930 sample chamber with a zinc selenide window (Fa. Specac/London, UK) was employed. The spectrometer used to run the spectra was a Nicolet 5700 (provided by Thermo Electron Corporation/Waltham) which possesses a MCT detector.

$$F(R) = \frac{(1-R)^2}{2\,R} = \frac{k}{s} \tag{5.9}$$

The basis of the diffuse reflectance theory used to quantify the concentration of a solid solute in a non-absorbing matrix was developed by Kubelka and Munk. The Kubelka-Munk formula (equation 5.9) relates the absolute reflectance R of the scattered radiation (R is defined as the intensity scattered divided by that of the incident radiation) to the sample absorption and scattering coefficients k and s, respectively [**140**] [**141**]. That formula is used to describe the adsorption and transmission spectra which have been obtained in the $DRIFT$ experiments.

CHAPTER 6

Assembly of the experimental equipment

6.1. Equipment assembly for the electro-catalytic experiments

In fig. 6.1, a schema of the equipment used for the electro-catalytic experiments is illustrated.

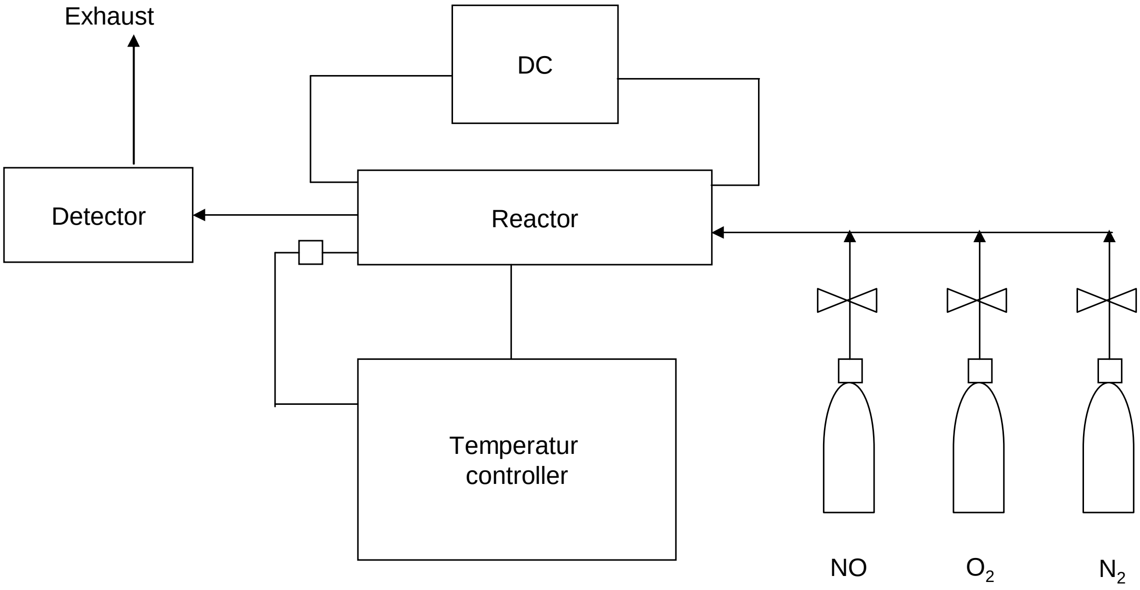

Figure 6.1. Equipment used for the electro-catalytic experiments

The thermocouple placed in the reactor and the heating tape used to heat it are connected to a temperature controller device (Eurotherm) which can be programmed in order to control the heating rate and the temperature. The N_2, O_2 and NO flows are determined by mass flow controllers (MKS Instruments, München). The gases are conducted through tubes from the mass flow controllers to the reactor and from there to the detector. The gas conduction tubes are fixed to the reactor entry and exit through leak-proof tube fittings. The electric cable connected to the reactor cathode and the cable connected to the reactor anode are respectively connected to the positive and negative pole of a DC device (Voltcraft).

For the electro-catalytic experiments, two different reactors will be used in the present work.

6.1.1. Tubular reactor.

The reactor is illustrated in fig. 6.2.

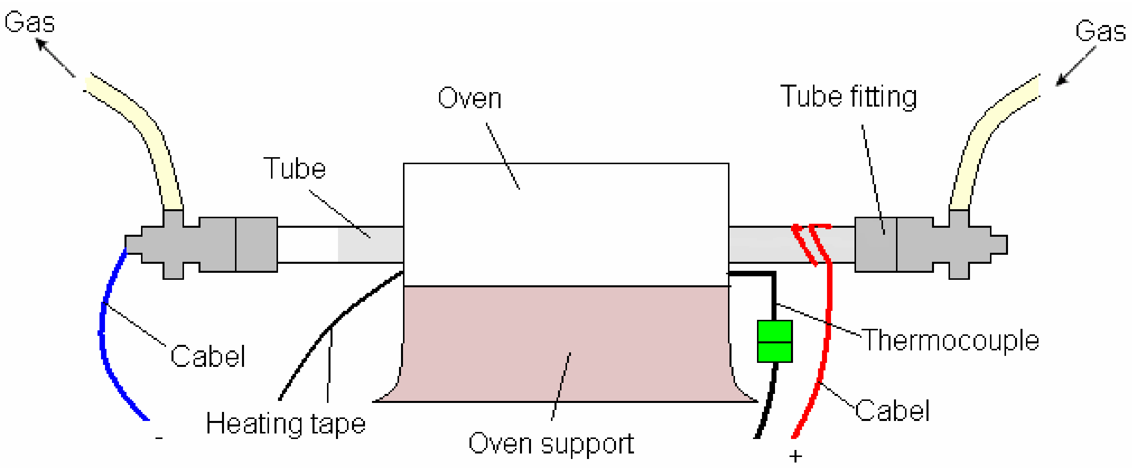

FIGURE 6.2. Tubular reactor

In the present work, different tubular electro-catalytic systems were used. Its preparation is described as follows.

6.1.1.1. *Pt/YSZ/Pt, Pt/YSZ/Pt/YSZ-NiO and Pt/YSZ/Pt/YSZ-perovskite systems.*

A yttria-stabilized zirconia (YSZ composed of 8.5 wt% Y_2O_3 and ZrO_2) tube manufactured by Degussa (length; 20 cm, thickness; 0.3 cm and internal diameter; 0.7 cm) was used. The YSZ tube was first cleaned for 30min in acetone and then, its internal and external side was covered by a Pt layer. In order to do so, a small paint brush and a Pt paste (ESL, Typ 5542, fritless. 73 wt% Pt powder, 20 wt% ethylcelulose and 17 wt% terpineol), which contains suspended crystalline platinum particles in an organic matrix, were used. The platinum coating should be as homogeneous and thin as possible in order to get a good conductivity and to minimize the cell resistance caused by the diffusion process of the ionic species through it. The first 5 cm of one of the external sides of the tube and the first 5 cm of the internal opposite side of the tube were left free from Pt in order to avoid a direct electric contact between the external and internal tube sides (the cathode and anode) since it would originate a short-circuit in the electrocatalytic cell. To fix the Pt layer to the YSZ tube, the calcination program illustrated in table 6.1 was utilized [**103**].

Starting temperature [°*C*]	*End temperature* [°*C*]	*Rate* [°*C*/*min*]	*Time* [*min*]
25	130	5	360
130	390	5	120
390	1060	5	20

TABLE 6.1. Temperature program used for the calcination of the Pt paste

After calcination, the volatile components of the Pt paste have been eliminated and its organic matrix has been burnt which leads to the formation of a porous Pt layer which remains adequately fixed to the YSZ surface. Then, the conductivity of the platinum coat is checked for which purpose, the electric resistance between the two extremes of the internal and external Pt layer are measured. If the resistance is much higher than 10 $m\Omega$, the conductivity would not be considered to be high enough for the electro-catalytic experiments. The reason for the poor electrical conductivity could be an inhomogeneous platinum layer. If the resistance is less than to 10 $m\Omega$, the catalyst can be deposited on the cathode.

For the preparation of the $Pt/YSZ/Pt/YSZ - catalyst$ (where the catalyst is NiO or perovskites) a $YSZ - catalyst$ paste was first prepared. In order to do so, 40 wt% of NiO (99.8 wt% purity, 10-20 nm particlesize, ChemPur Feinchemikalien und Forschungsbedarf GmbH, Karlsruhe) or perovskite powder and 60 wt% of a YSZ paste (20 wt% solid matter, 80wt % terpineol, Robert Bosch GmbH, Stuttgart) were mixed during 15 min with a mortar.

Then, the $YSZ - catalyst$ (where the catalyst can be NiO or a perovskite) paste was distributed homogeneously with a small paintbrush in the internal side of the YSZ tube. The first 5 cm of the internal side of the tube which are already covered with a Pt layer were left free from the paste in order to make there the electric contact with the cable which was connected to the DC device. Finally, the so prepared tube was placed in an oven. The temperature program used for the calcination of the tube is shown in table 7.1

6.1.1.2. $Pt/YSZ/Pt - NiO$ *system.*

A yttria-stabilized zirconia (YSZ composed of 8.5 wt% Y_2O_3 and ZrO_2) tube manufactured by Degussa (length; 20 cm, thickness; 0.3 cm and internal diameter; 0.7 cm) was used. The YSZ tube was first cleaned for 30 min in acetone and then, its external side was covered by a Pt layer. In order to do so, a small paint brush and a Pt paste (ESL, Typ 5542, fritless. 73 wt% Pt powder, 20 wt% ethylcellulose and 17 wt% terpineol), which contains suspended crystalline platinum particles in an organic matrix, were used. The internal side of the YSZ tube was covered with a paste composed of a mixture consisting of a platin paste and the NiO nanopowder. In order to decrease the viscosity of the $Pt-NiO$ paste, terpineol was added to the mixture. Both the platin and $Pt-NiO$ coat should be as homogeneous and thin as possible in order to get a good conductivity and to minimize the cell resistance caused by the diffusion process of the ionic species through the Pt or $Pt-NiO$ layer. The first 5 cm of one of the external sides of the tube and the first 5 cm of the internal opposite side of the tube were left free from Pt in order to avoid a direct electric contact between the external and internal tube side since it would originate a short-circuit in the electrocatalytic cell. To fix the Pt and $Pt-NiO$ layer to the YSZ tube, a calcination program [**103**] was utilized (table 6.1).

6.1.1.3. *$Pt/YSZ/Pt/YSZ/NiO$ system.*

A yttria-stabilized zirconia (YSZ composed of 8.5 wt% Y_2O_3 and ZrO_2) tube manufactured by Degussa (length; 20 cm, thickness; 0.3 cm and internal diameter; 0.7 cm) was used. The YSZ tube was first cleaned for 30 min in acetone and then, its internal and external side was covered by a Pt layer. In order to do so, a small paint brush and a Pt paste (ESL, Typ 5542, fritless. 73 wt% Pt powder, 20 wt% ethylcelulose and 17 wt% terpineol), which contains suspended crystalline platin particles in an organic matrix, were used. The platinum coat should be as homogeneous and thin as possible in order to get a good conductivity and to minimize the cell resistance derived from the diffusion process of the ionic species through it. The first 5 cm of one of the external sides of the tube and the first 5 cm of the internal opposite side of the tube were left free from Pt in order to avoid a direct electric contact between the external and internal tube side since it would originate a short-circuit in the electrocatalytic cell. To fix the Pt layer to the YSZ tube, a calcination program [**103**] was performed (table 6.1).

Then, the YSZ paste was applied homogeneously with a small paintbrush in the internal side of the $Pt/YSZ/Pt$ tube. The first 5cm of the internal side of the tube which are already covered with a Pt layer were left free from the paste in order to make there the electric contact with the cable which was connected to the DC device. Finally, the so prepared tube was placed in an oven. The temperature program used for the calcination of the tube is shown in table 7.1

The NiO catalyst was now placed in the internal side of the tube through a post-impregnation. For that purpose, a water 1 M $Ni(NO_3)_2$ solution was first prepared. The side of the tube that has the first internal 5 cm free from platinum was closed with adhesive tape. The tube was placed in a vertical position and the 1 M $Ni(NO_3)_2$ solution was introduced in the tube with a small pipette taking care that the internal first 5 cm, which are already covered by the platinum layer, do not come in contact with the $Ni(NO_3)_2$ solution. After 30 min, the tube was placed in a glass and keeping the vertical position, the adhesive tape was removed but taking care that the solution evacuation occurs very slow. Then, the tube was dried at 130°C for 15 min and finally it was calcinated at 600°C for 1 h.

6.1.2. Planar substrate reactor.

In order to improve the reproducibility of the preparation procedure and to test the electrochemically enhanced NO decomposition with a more practical reactor configuration a planar substrate was developed. The resulting reactor section involving a substrate surface area of about 22 cm^2 is depicted in fig. 6.3; this substrate provides a ten times lower surface area than the tubular one. The thickness of the catalytic layer was established to be in the range of 5 to 25 μm.

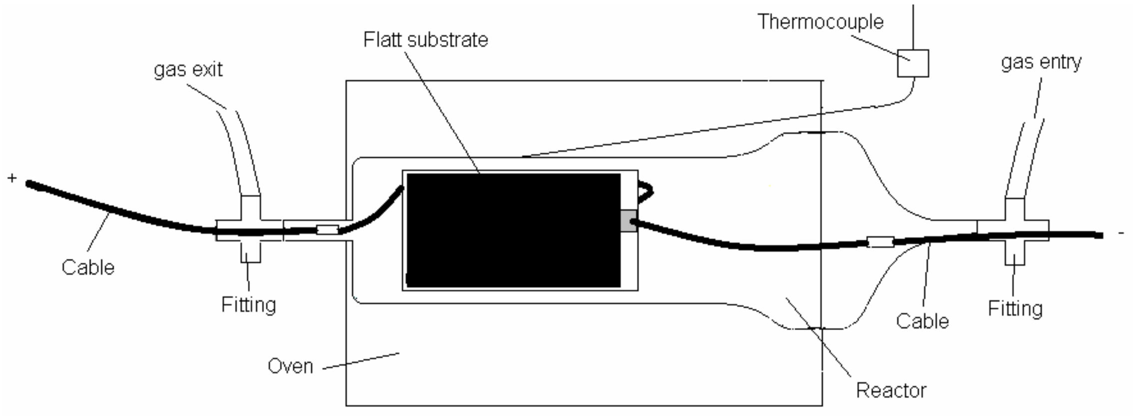

FIGURE 6.3. Planar substrate reactor

For the preparation of the planar substrate reactor, planar YSZ substrates covered in both sides by a porous Pt layer which were connected in both sides to two silver cables were provided by Robert Bosch GmbH (Stuttgart).

One side of the planar substrate was covered by the YSZ/NiO paste and then calcinated as described in section 6.1.1.1. The reactor is a quartz oval tube which has a close and an open side. The open side can be closed with a quartz fitting after the planar substrate has be placed inside. The planar substrate was placed in the reactor as described in fig. 6.4 and then the silver cable connected to the side of the planar $Pt/YSZ/Pt/NiO-YSZ$ substrate which contains the catalyst layer was connected to the negative pole of a DC device and the other silver cable was connected to the positive pole. Tube fittings were used in order to fix the gas conducting tubes to the reactor.

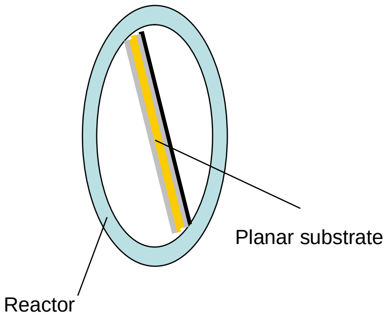

FIGURE 6.4. Placement of the planar substrate inside of the reactor

6.2. Equipment assembly for the powder experiments

The reactor illustrated in fig. 6.5 was used for the non-electro-catalytic experiments.

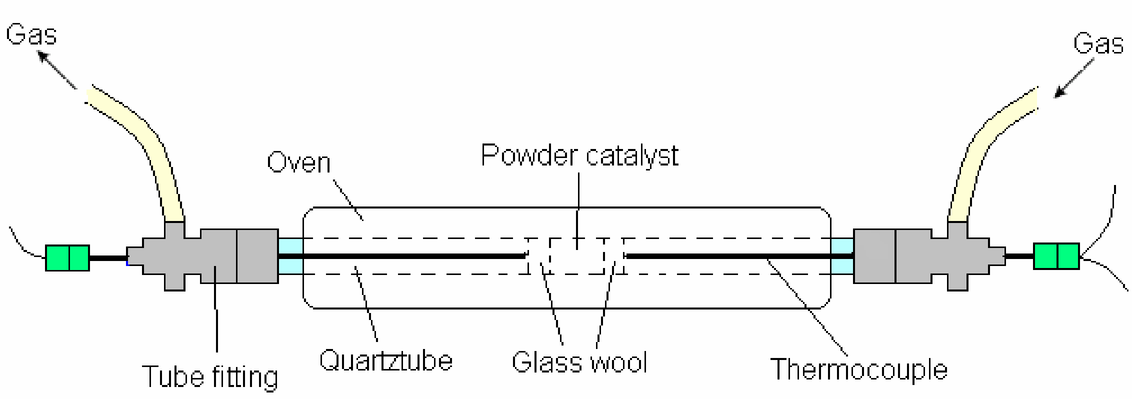

FIGURE 6.5. Non electro-catalytic experiments reactor

1 g of the NiO/YSZ powder catalyst (synthesized as section 7.1 indicates) was pressed and granulated in order to obtain particle sizes between 125 and 250 μm. The catalyst was placed in the middle of the quartz reactor (length; 110 cm, thickness; 1 mm and internal diameter; 1 cm). A piece of glass wool was placed before and after the catalyst in order to fix its position in the reactor. The quartz tube was placed inside of a ZrO_2 tube (length; 80 cm, thickness; 4 mm and external diameter; 3.5 cm). A heating tape was coiled to the ZrO_2 tube and it was connected to a temperature controller device. Two thermocouples were placed next to the glass wool (one at each sides of the catalyst). One of the thermocouple is connected to the temperature controller device and the other is connected to a temperature indicator. During the experiments, the temperature differences showed by both the

temperature indicator and the temperature controller device should be smaller than 10°C in order to obtain a good reproducibility in the experimental results. Two tube fittings were used to connect the gas conducting tubes to the reactor entry and exit. Two different gas conducting tubes were used in order to change from the reductive gas mixture (H_2/N_2) to the oxidizing gas mixture ($NO/O_2/N_2$). The gas flows were controlled through mass flow controllers. The gas conducting tube which came out of the reactor was connected to the detector. The equipment assembly is illustrated in fig. 6.6.

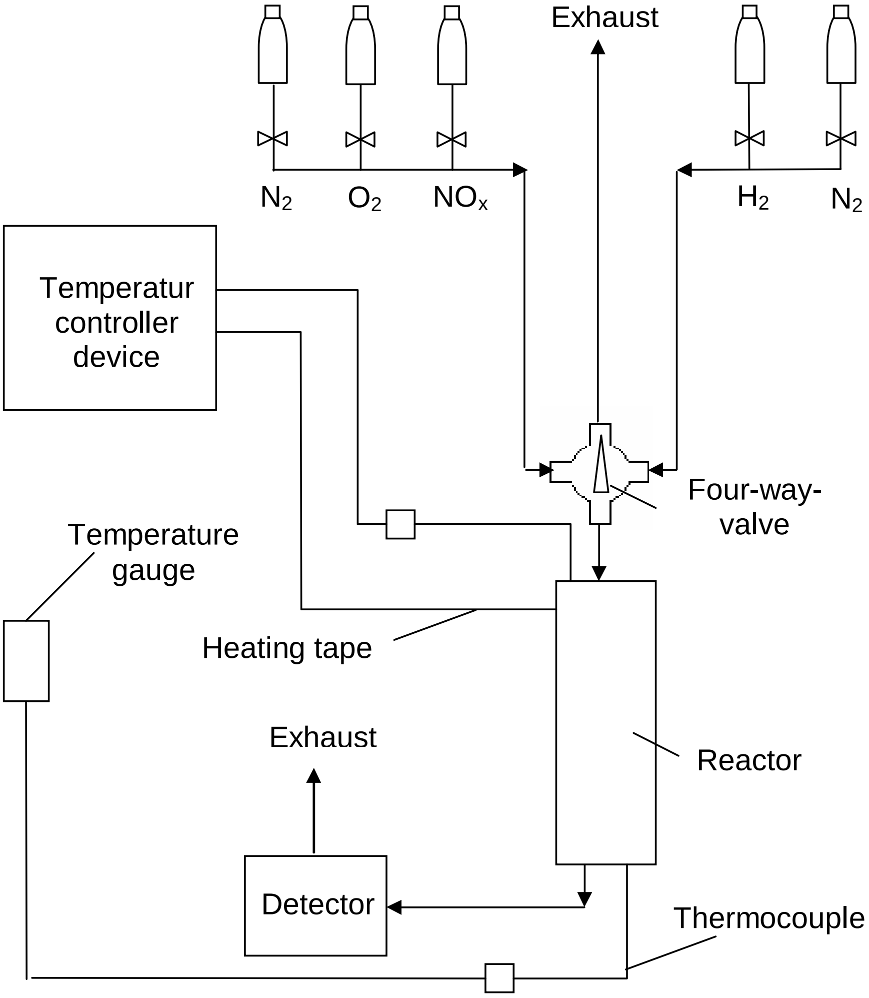

FIGURE 6.6. Equipment assembly used in the non electro-catalytic experiments

CHAPTER 7

Experimental results

7.1. Synthesis of the powder catalysts

7.1.1. Synthesis of the NiO/YSZ powder catalyst.

A paste composed of 40 wt% of NiO nanopowder (99.8 wt% purity, 10-20 nm particle size, ChemPur Feinchemikalien und Forschungsbedarf GmbH, Karlsruhe) and 60 wt% of a YSZ paste (20 wt% solid matter, 80wt % terpineol, Robert Bosch GmbH, Stuttgart) was prepared. The paste was mixed during 15 min with a mortar. Then, it was put inside of a porcelain container and it was calcinated according to the temperature program shown in table 7.1. After calcination, a dark blue almost black solid was obtained.

Starting temperature [°C]	End temperature [°C]	Rate [°C/h]	Time [h]
25	60	100	1
60	80	100	1
80	100	100	0
100	130	30	0
130	180	10	0
180	600	30	0

TABLE 7.1. NiO/YSZ calcination temperature program

7.1.2. Synthesis of the perovskites and spinel powder catalyst.

The Polyvinyl alcohol method (PVA-method) was chosen to prepare the perovskite catalysts. A modification [**101**] of the method described by Saha and Pramanik [**102**] was used. Granulated PVA (Polyvinyl alcohol, $M = 145000\ g/mol$, Merck) was solved in distilled water in a 1:10 ratio. In order to accelerate the solution process, the mixture was heated at 80-90°C and it was continuously stirred up with a magnetic stirrer until a clear transparent gel was formed.

The nitrates of the metals contained in the perovskite or spinel structure were solved separately in the smallest possible amount of water and finally they were added to the stirring PVA solution. The PVA monomer to metal-ion ratio was 2.5:1.

The solution was then evaporated at 100°C under continuous stirring. When the bigger part of the water was eliminated, the solution became very viscous. At that point, the temperature was slowly increased until a solid was obtained. In order to prevent the solid to spatter out of the container during the synthesis, a powder sieve was placed above it. When the solid was obtained, a mortar was used to reduce its grain size and it was then calcinated at 650°C for six hours. The heating rate was 5 °C/min.

7.2. Characterization of the powder catalysts

The characterization of the NiO/YSZ, perovskite and spinel powder catalyst was done through XRD, BET and SEM

7.2.1. Characterization through XRD.

In order to check the correct preparation of the catalyst and to identify its crystalline phases, a sample of each powder catalyst was taken to obtain a XRD spectrum.

7.2.1.1. NiO/YSZ.

The peaks identification were done by comparing the experimental data with the "Powder Diffraction Files" pattern. In order to do so, the Bragg law was first used to convert the 2Θ data in d_{hkl}. A λ value of 1.5406 $\mathring{A}$ was utilized. The NiO/YSZ XRD spectrum is shown in fig. 7.1.

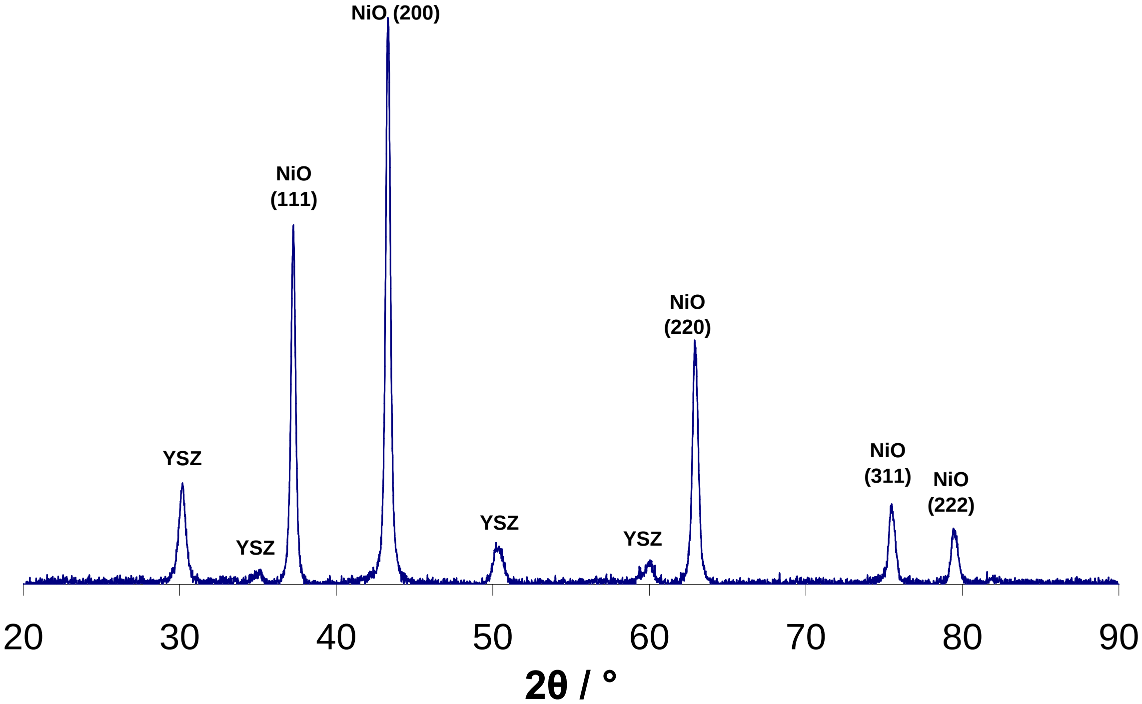

FIGURE 7.1. XRD spectrum of the NiO/YSZ powder catalyst

The peaks at 37.28, 43.26, 62.96, 75.56 and 79.64° correspond to the plane (111), (200), (220), (311) and (222) of the cubic NiO [**124**]. The presence of the hexagonal NiO phase can be dismissed since then, a splitting of the signals which appear at 62.94 and 79.46° should be observed [**125**].

The absence of a signal at 28.2° can indicate that the monoclinic ZrO_2 phase is not present since it is the most intense signal which should be expected [**126**]. If the hexagonal phase of the ZrO_2 is present, a signal at 27° should be observed [**127**]. Hence, it can be concluded that there is no hexagonal YSZ in the catalyst. Due to the similarity between the signals expected for the tetragonal and cubic ZrO_2 phases, and also due to the small signals corresponding to YSZ, the absence or presence of the cubic or the tetragonal phases can not be asserted. The reason for the obtaining of such small XRD signals is that in the NiO/YSZ powder, a much higher amount of NiO is present. To obtain better XRD signals, YSZ pure powder was prepared making use of the same calcination program utilized for the NiO/YSZ preparation and an XRD spectrum was then obtained. The experimental results are shown in fig. 7.2. The Miller indices in red correspond to the different planes of the cubic ZrO_2 phase and the black ones correspond to the tetragonal ZrO_2 phase.

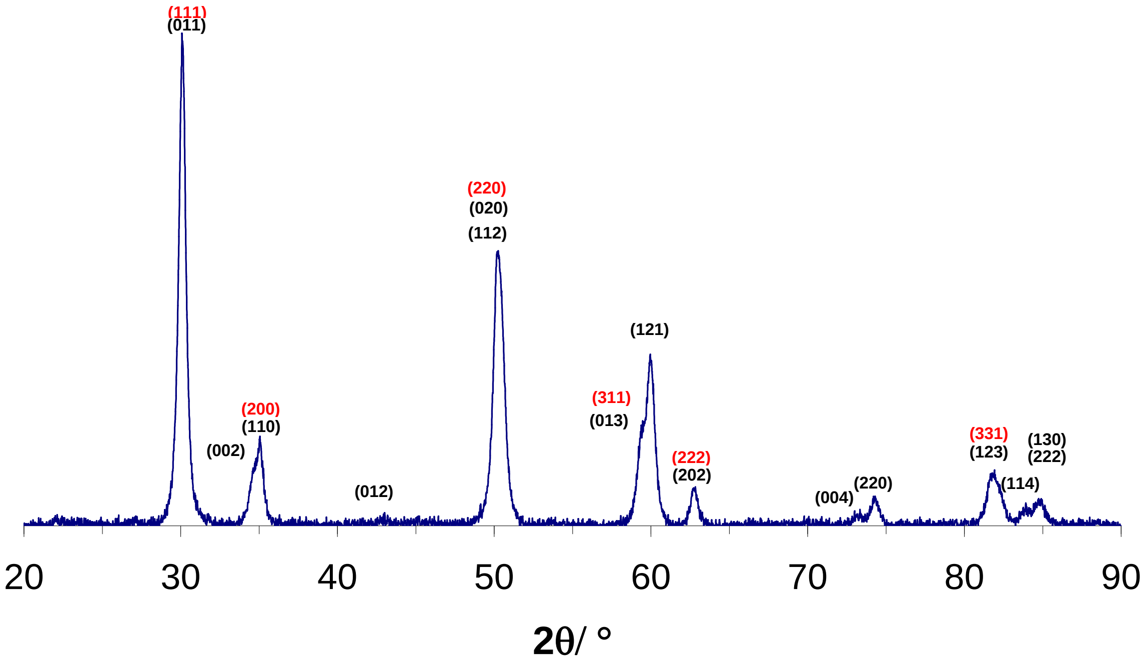

FIGURE 7.2. XRD spectrum of the YSZ pure powder

The presence of the signals at 73.52, 74.46 and 84.14° can just correspond to the (004), (200) and (123) planes of the tetragonal ZrO_2 phase [**128**]. The band at 85.14° is also characteristic of the tetragonal phase and can correspond to the overlapping of the peaks expected from the (130) and (222) planes. It is possible then to conclude that the tetragonal ZrO_2 phase is present. The characteristic peaks expected if the cubic phase is also present, overlap with the peaks expected from the tetragonal phase [**129**]. As a consequence, it is not possible to conclude if the cubic NiO phase is present or not.

7.2.1.2. $LaNiO_3$.

A sample of the $LaNiO_3$ powder was taken to run a XRD experiment. The results are shown in fig. 7.3. The signals obtained correspond to the hexagonal phase of the $LaNiO_3$ [**130**].

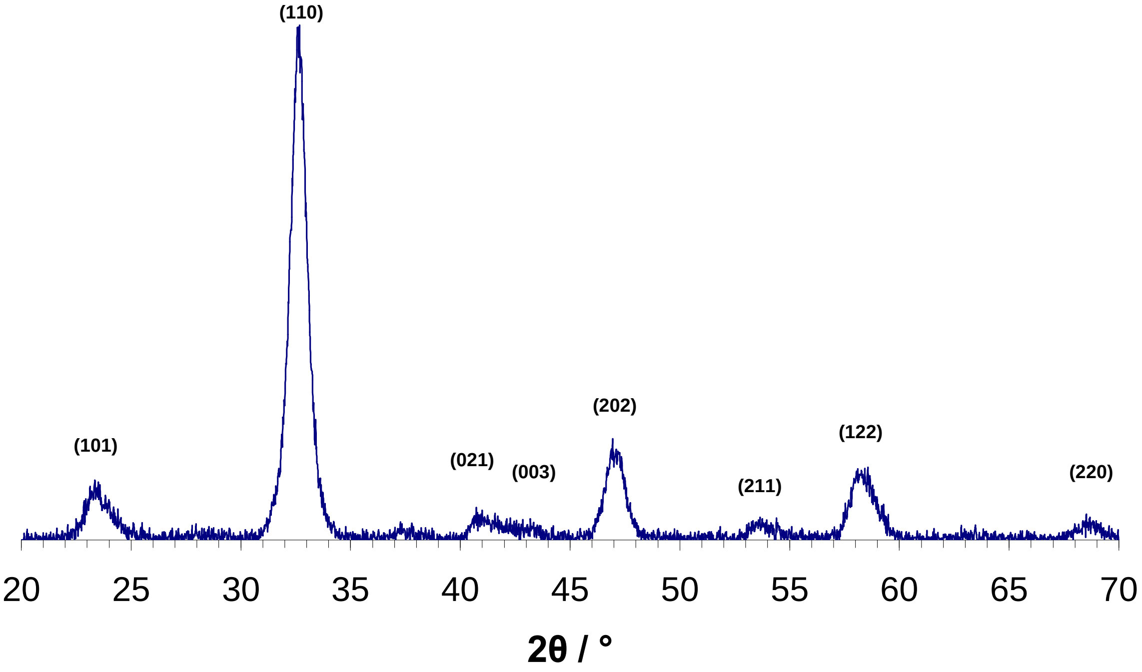

FIGURE 7.3. XRD spectrum of the $LaNiO_3$ powder catalyst

7.2.1.3. La_2NiO_4.

A sample of the La_2NiO_4 powder was taken to run a XRD experiment. The results are shown in fig. 7.4.

In the XRD spectrum, the characteristic peaks of the La_2NiO_4 spinel were obtained [**131**]. However, some peaks which do not correspond to the La_2NiO_4 have to be assigned. The signal obtained at 28.26° could correspond to the La_2O_3 [**132**] and the signals at 52.34 and 26.24° could result from the presence of Ni_2O_3 [**133**]. The signal at 39.72° could be assigned to both La_2O_3 and Ni_2O_3. The signal which appears at 29.4° could be originated by the presence of Ni [**134**].

7.2.2. Characterization through *BET*.

The measurement of the specific surface area of the catalysts was also performed through nitrogen-physisorption experiments. The results are shown in appendix.

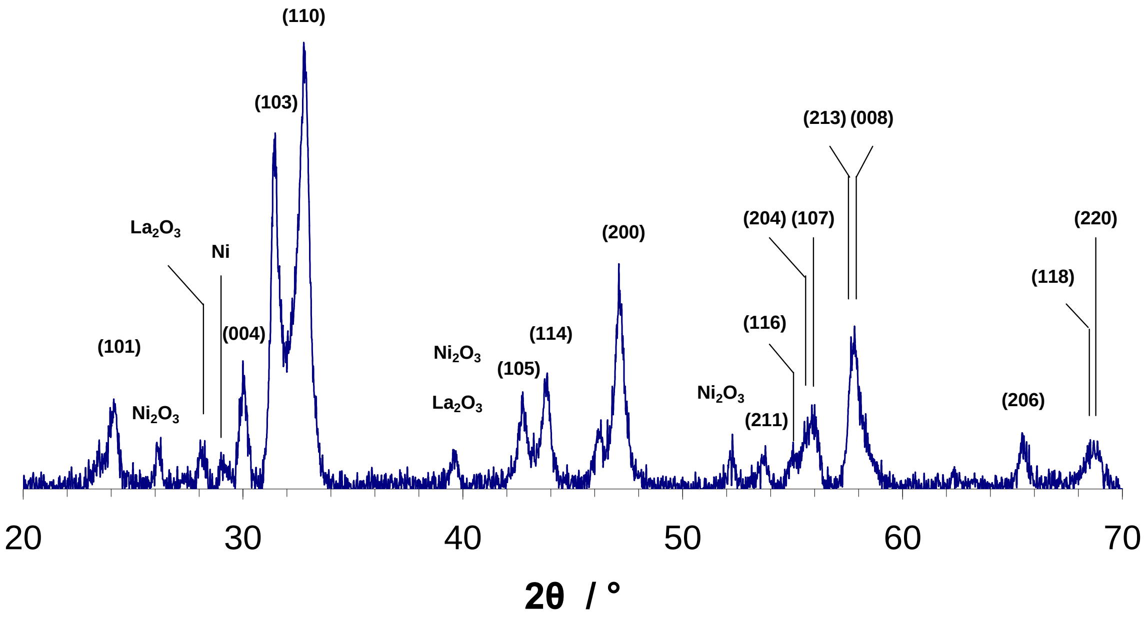

Figure 7.4. XRD spectrum of the La_2NiO_4 powder catalyst

Table 7.2 summarizes the specific surface area ($a_{s,BET}$) and total pore volume values obtained for each catalyst powder. The higher specific surface area and total pore volume was obtained for the NiO/YSZ catalyst and the smaller values were achieved for the La_2NiO_4 spinel.

	$a_{s,BET}[m^2g^{-1}]$	Total pore volume . $10^{-2}[cm^3g^{-1}]$
NiO/YSZ	18.578	23.62
$LaNiO_3$	16.240	13.47
La_2NiO_4	12.174	6.145

Table 7.2. Results obtained from the BET experiments

7.2.3. Characterization through SEM.

The morphology of the catalyst was studied through SEM/EDS (fig. 7.5 and fig. 7.6) and mapping (fig. 7.7)

As we can see in fig. 7.5, the NiO/YSZ powder catalyst is composed of particles whose size ranges between 2 and 10 μm. A dark and a brighter zone can be distinguished in the SEM picture. An EDS experiment was done in the dark zone and another one was done in the brighter zone. As we can see in the EDS spectra, the brighter zone contains a bigger amount of Zr and Y than the dark zone.

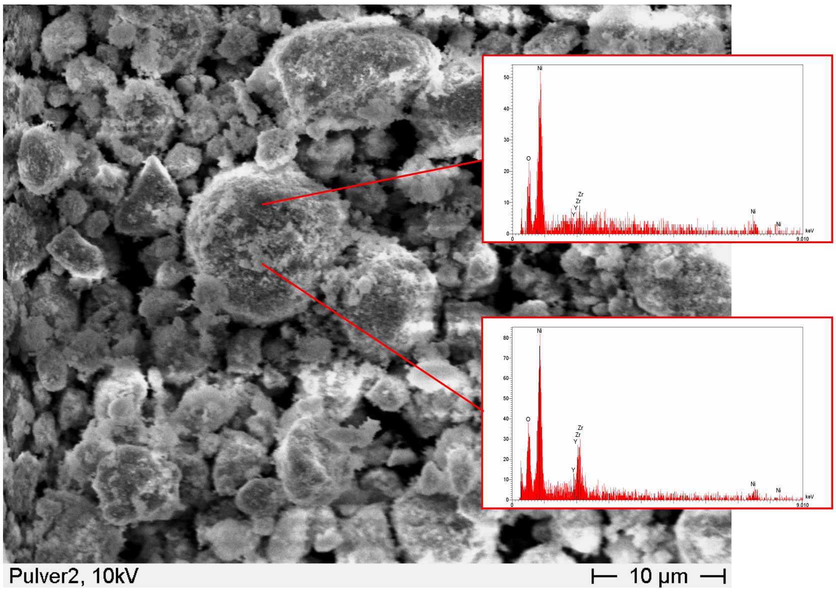

FIGURE 7.5. SEM/EDS of the NiO/YSZ powder catalyst

Another EDS experiment performed in order to determinate the elemental composition of the $NiOYSZ$ powder catalyst which is 19.61 wt% O, 67.24 wt% Ni, 2.32 wt% Y and 10.84 wt% Zr is depicted in fig. 7.6

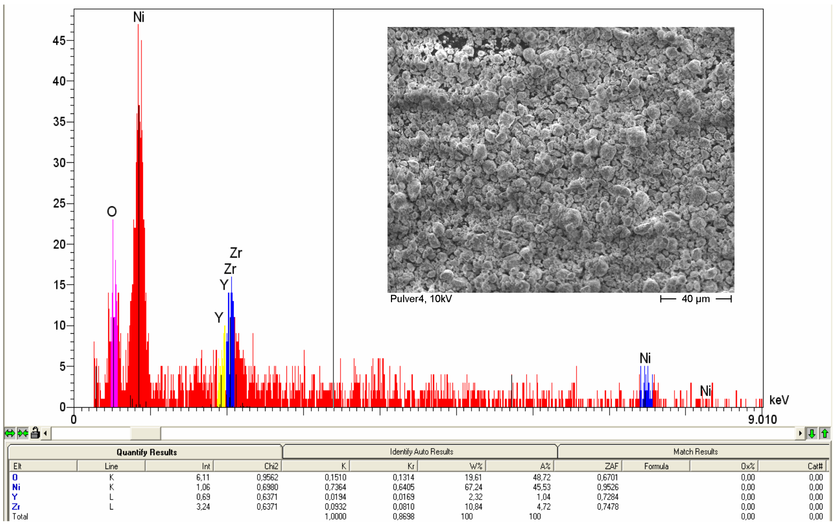

Elt	Line	Int	Chi2	K	Kr	W%	A%	ZAF	Formula	Ox%	Cat#
O	K	6,11	0,9562	0,1510	0,1314	19,61	48,72	0,6701		0,00	0,00
Ni	K	1,06	0,6980	0,7364	0,6405	67,24	45,53	0,9526		0,00	0,00
Y	L	0,69	0,6371	0,0194	0,0169	2,32	1,04	0,7284		0,00	0,00
Zr	L	3,24	0,6371	0,0932	0,0810	10,84	4,72	0,7478		0,00	0,00
Total				1,0000	0,8698	100	100			0,00	0,00

FIGURE 7.6. SEM/EDS obtained with a NiO/YSZ powder sample in order to determinate the catalyst composition

It is also interesting to know if the elements which compose the catalyst are homogeneously distributed for which purpose, a mapping of a probe sample was done. As we can observe in fig. 7.7, O, Ni and Zr are homogeneously distributed in the catalyst sample.

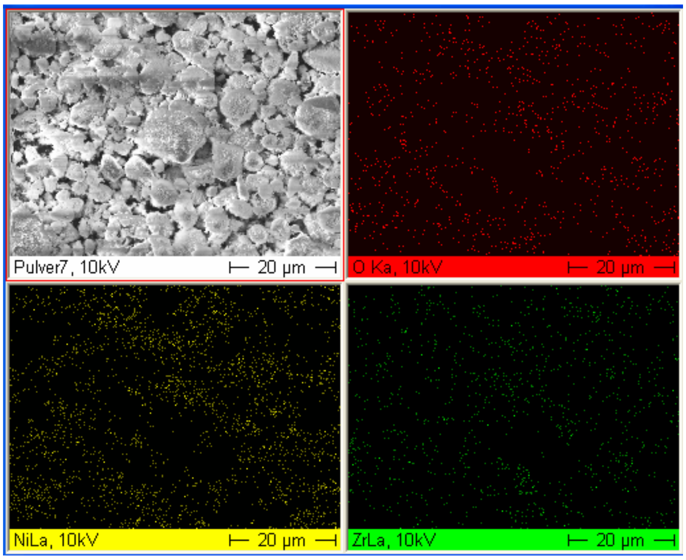

FIGURE 7.7. Mapping of the NiO/YSZ powder catalyst

7.3. Characterization of different system surfaces through SEM

A flat YSZ sample was used in order to study the structure of the surface of different systems.

7.3.1. YSZ/Pt. The YSZ sample was covered with a Pt paste layer and was finally calcinated for 20 min at 1060°C. The results of the SEM studies are shown in fig. 7.8. It can be observed that not all the surface of the YSZ sample is covered by Pt but the most of the Pt agglomerates are connected.

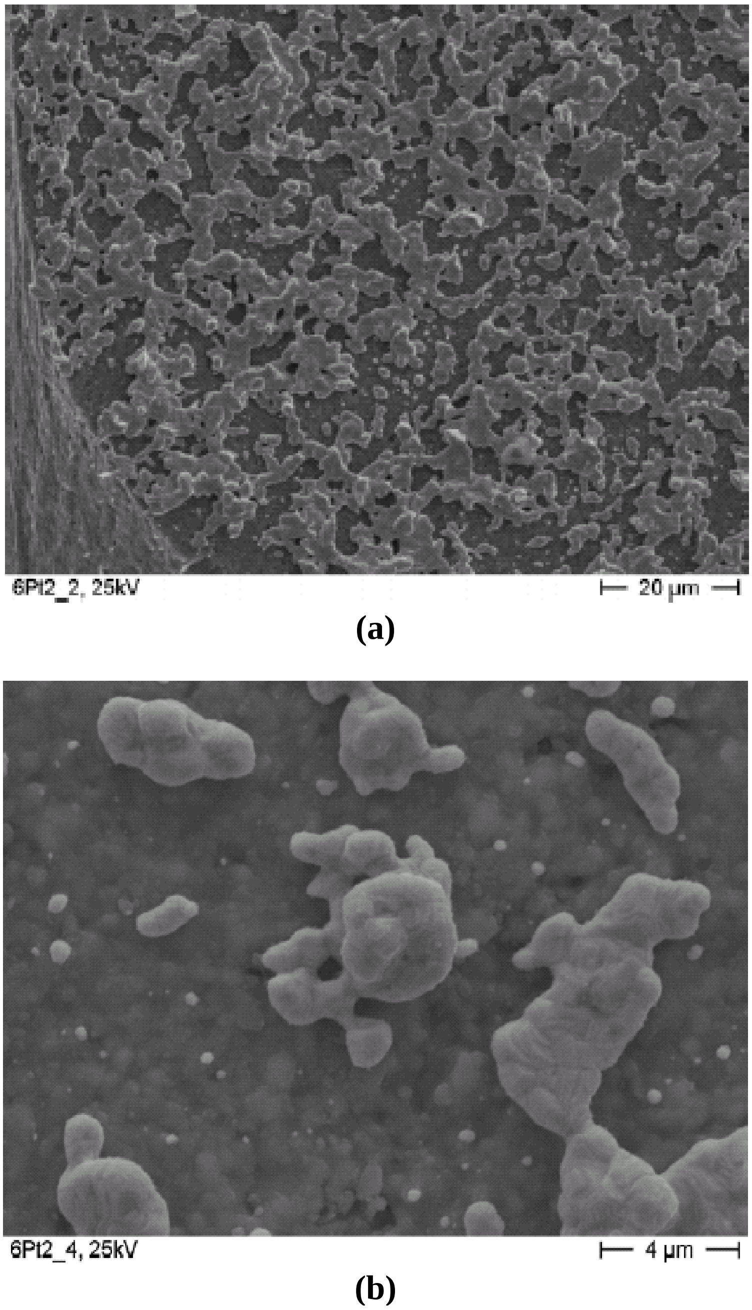

FIGURE 7.8. SEM study of the Pt surface

7.3.2. YSZ/Pt/YSZ. The YSZ sample was covered with a Pt paste layer and was calcinated for 20 min at 1060°C. Then, the Pt layer was covered with a YSZ layer and the system was finally calcinated for at 600°C. The results of the SEM studies are shown in fig. 7.9. The YSZ layer covers completely the Pt layer. Pores of approximately 4 μm are observed.

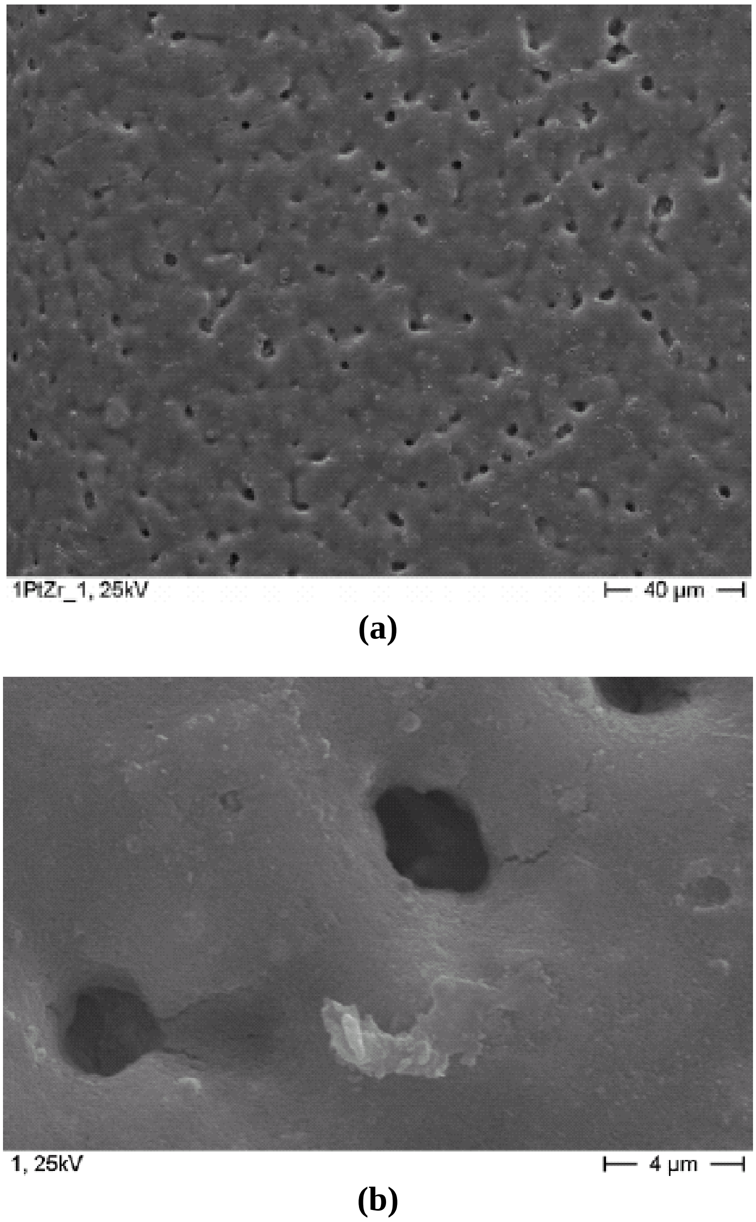

FIGURE 7.9. SEM study of the YSZ surface

7.3.3. YSZ/Pt-NiO. The YSZ sample was covered with a Pt-NiO paste layer and was calcinated for 20 min at 1060°C. The results of the SEM studies are shown in fig. 7.10. The agglomerates observed are bigger than the ones observed in the system YSZ/Pt (7.8).

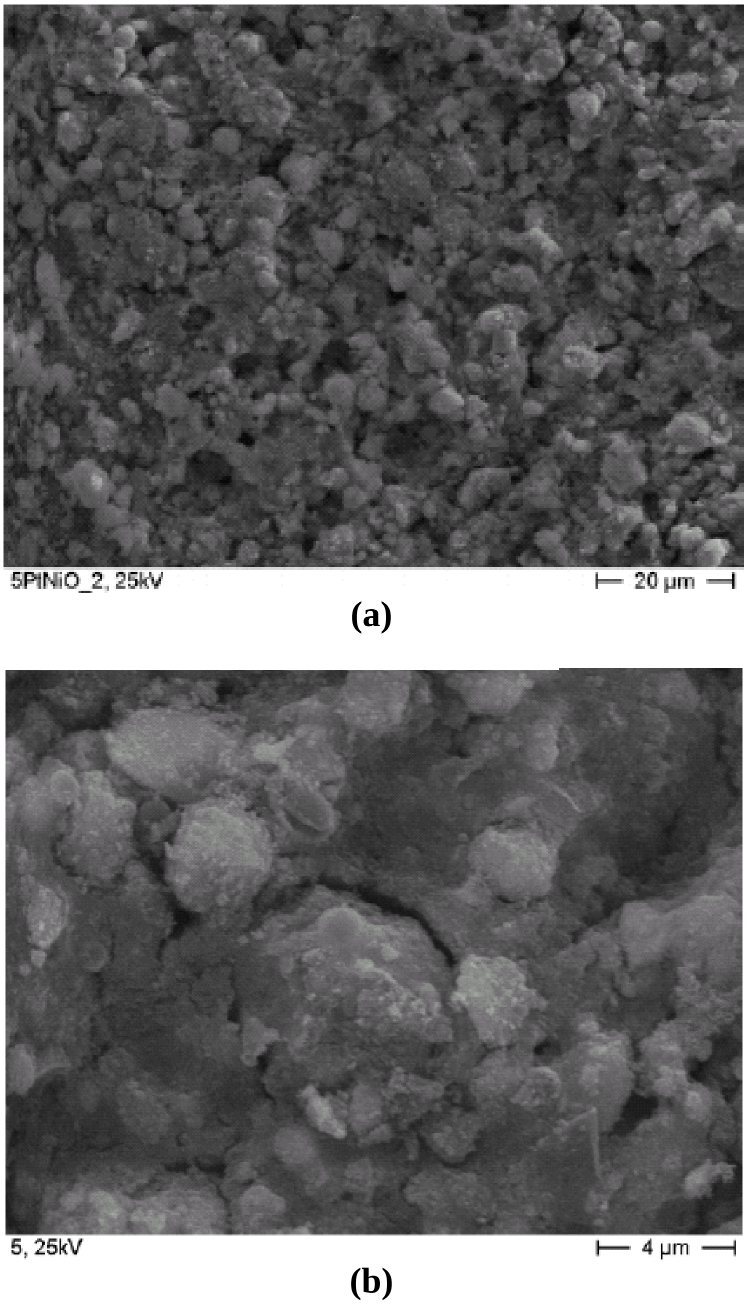

FIGURE 7.10. SEM study of the $Pt - NiO$ surface

7.3.4. YSZ/Pt/YSZ-NiO. The YSZ sample was covered with a Pt paste layer and was calcinated for 20 min at 1060°C. Then, the Pt layer was covered with a layer of a YSZ-NiO paste and the system was finally calcinated at 600°C. The results of the SEM studies are shown in fig. 7.11. The agglomerates observed are bigger than the ones observed in the system YSZ/Pt (7.8).

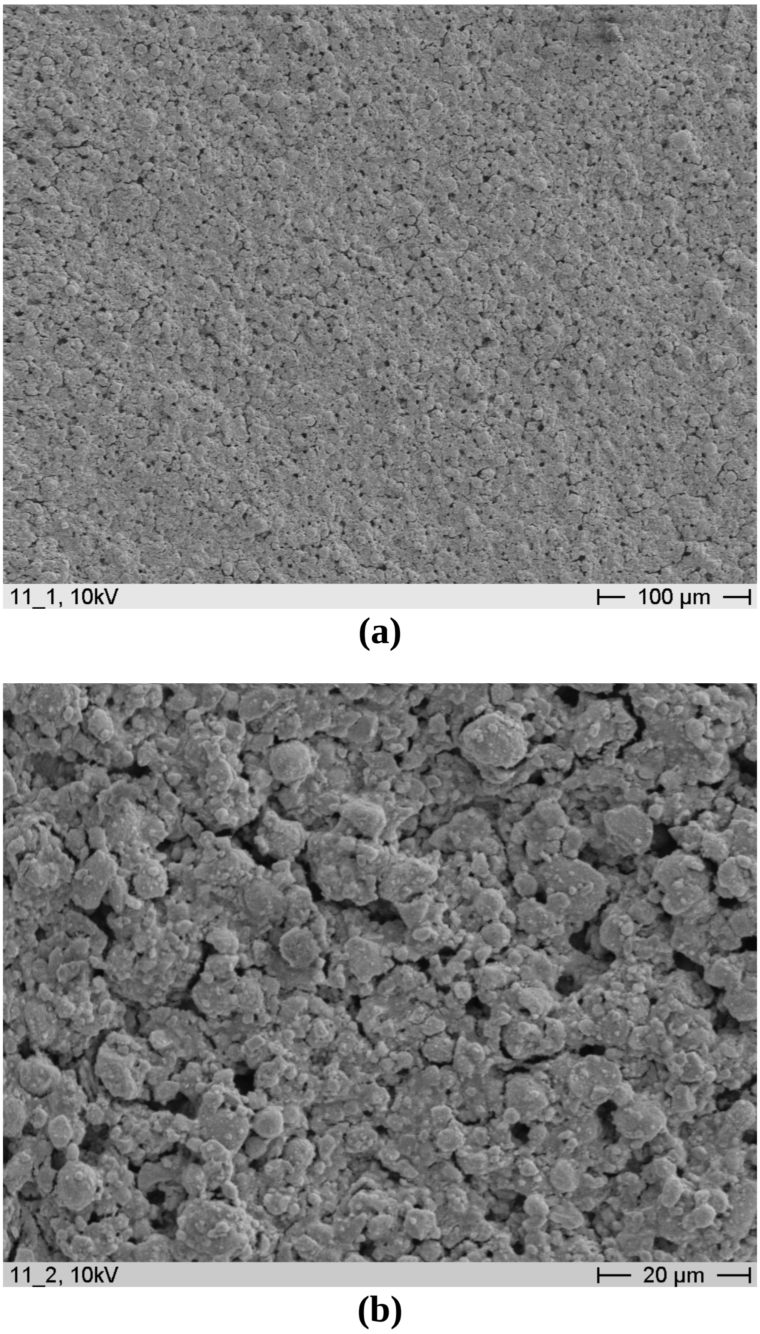

FIGURE 7.11. SEM study of the $YSZ - NiO$ surface

7.3.5. $YSZ/YSZ - La_2NiO_4$**.** The YSZ sample was covered with a Pt paste layer and was calcinated for 20 min at 1060°C. Then, the Pt layer was covered with a layer of a $YSZ - La_2NiO_4$ paste and the system was finally calcinated for at 600°C. The results of the SEM studies are shown in fig. 7.12

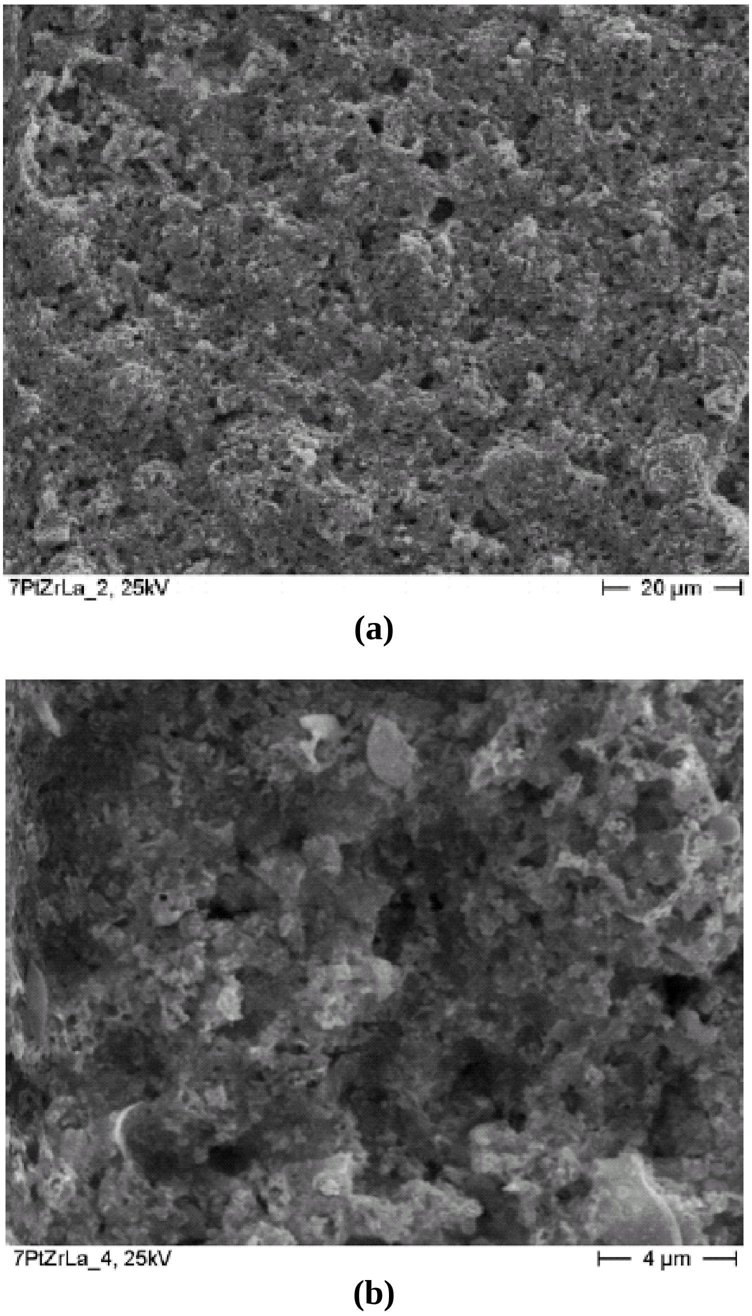

(a)

(b)

FIGURE 7.12. SEM study of the $YSZ - La_2NiO_4$ surface

7.3.6. YSZ/Pt/YSZ/NiO. The YSZ sample was covered with a Pt paste layer and was calcinated for 20 min at 1060°C. Then, the Pt layer was impregnated with a water $Ni(NO_3)_2$ solution 1 M and the system was dried for 15min at 130°C and finally calcinated at 600°C. The results of the SEM studies are shown in fig. 7.13.

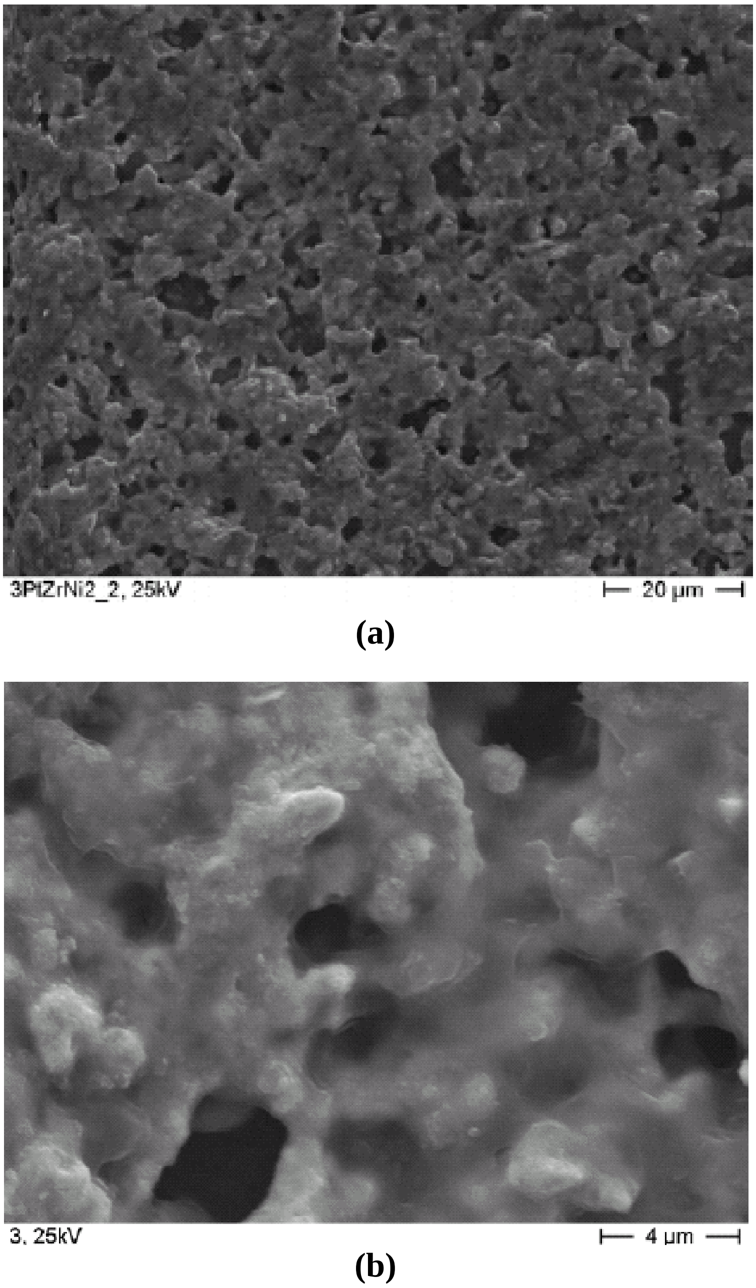

FIGURE 7.13. SEM study of the NiO surface deposited with a post-impregnation

7.4. Characterization of green NiO

The NiO/YSZ catalyst changes its color from almost black to pale green with the catalyst operating time. In order to characterize the green NiO, a sample was taken for the XRD experiments. The results shown in fig. 7.14 compares the XRD spectrum obtained with the black and green NiO.

The peaks of both XRD spectra appear at the same 2 Θ values. The spectrum of the green NiO shows peaks which are longer and more narrow than the ones observed in the black NiO spectrum. That is originated by an increase of the NiO crystallinity due to the increase of the calcination temperature.

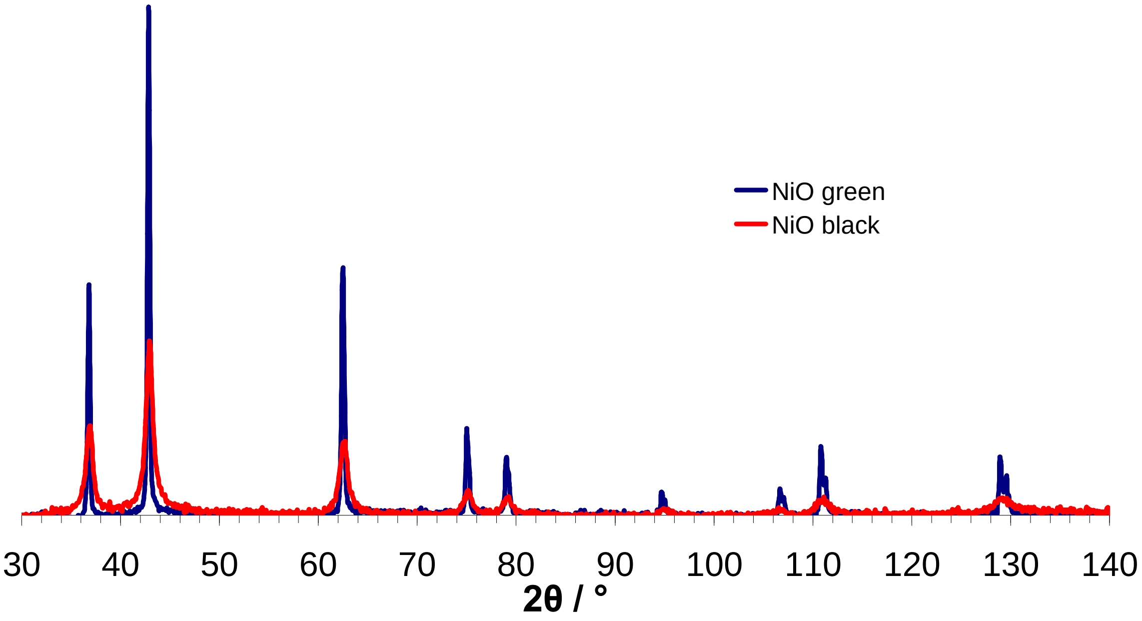

FIGURE 7.14. XRD experiments of the black and green NiO nano-powder

7.5. NOx-decomposition experiments

The NO decomposition reaction that occurs on the YSZ/NiO catalyst in order to build N_2 and O_2 is shown in equation (7.1)

$$NO \rightarrow \frac{1}{2}\,N_2 + \frac{1}{2}\,O_2 \tag{7.1}$$

Apart from equation (7.1), another two reactions involving NO can occur giving rise to the formation of N_2O and NO_2.

$$NO \rightarrow \frac{1}{2}\,N_2O + \frac{1}{4}\,O_2 \tag{7.2}$$

$$2\,NO + O_2 \rightarrow 2\,NO_2 \tag{7.3}$$

7.5.1. Activity and selectivity of the NO_x decomposition reaction.

The NO_x decomposition activity of some catalytic systems were studied. In order to compare the different experimental results obtained with different catalyst and catalytic systems, the NO_x conversion rate and the selectivity was calculated. The NO_x conversion rate ($X(NO_x)$) is used to estimate the amount of nitrogen oxide which is removed from the mixture gas and it is calculated as indicated in equation (7.4).

$$X(NO_x)\,\% = \frac{C(NO_x)}{C_0(NO_x)}\,100 \tag{7.4}$$

where:

$X(NO_x)\,\%$ is the NO_x conversion rate in percentage terms.

$C_0(NO_x)$ is the initial NO_x fraction in parts per million (ppm).

$C(NO_x)$ is the measured NO_x fraction in parts per million after catalyst performance.

As indicated at the beginning of that chapter, N_2 and N_2O can be formed as a consequence of the catalytic reduction of the nitrogen oxides on the NiO/YSZ catalyst. The selectivity in the formation of N_2 ($S(N_2)$) and the selectivity in the formation of N_2O ($S(N_2O)$) can be calculated according to equations (7.5) and (7.6).

$$S(N_2)\,\% = \frac{C(N_2)}{C(N_2) + C(N_2O)}\,100 \tag{7.5}$$

$$S(N_2O)\,\% \;=\; \frac{C(N_2O)}{C(N_2)\;+\;C(N_2O)}\,100 \tag{7.6}$$

where:

$S(N_2)\,\%$ is the selectivity of the catalyst in the formation of N_2 starting from NO_x in percentage terms.

$S(N_2O)\,\%$ is the selectivity of the catalyst in the formation of N_2O starting from NO_x in percentage terms.

$C(N_2)$ is the N_2 fraction in parts per million produced as a consequence of the NO_x reduction reaction.

$C(N_2O)$ is the N_2O fraction in parts per million produced as a consequence of the NO_x reduction reaction.

There is an excess of oxygen in the diesel exhaust. In the electro-catalytic reduction of the nitrogen oxides, O_2 can also decompose on the YSZ/NiO catalyst giving rise to an unwanted reaction which originates a higher current as the one expected when just the nitrogen oxides are decomposed on the cathode. The selectivity of the catalyst in the decomposition of NO in oxygen excess $S(NO)$ can be calculated according to equation (7.7)

$$S(NO)\,\% \;=\; \frac{I(NO)}{I}\,100 \tag{7.7}$$

where:

$S(NO)\,\%$ is the selectivity in the NO reduction in a cell in presence of excess O_2 in percentage terms.

$I(NO)$ is the current obtained when all the NO dosed is reduced on the cathode.

I is the total current obtained in the electrochemical reduction.

The $I(NO)$ value can be calculated as indicated in appendix 10.4

7.5.2. NO_x electro-catalytic decomposition with a tubular reactor.

The reactor was first heated at 450°C for 15 min in order to eliminate the nitrogen containing compounds that could be adsorbed on the catalyst surface. Then, it was heated at 600°C and the NO decomposition experiments were performed on different electro-catalytic systems. The experiments were done using a 500 ml/min flow of a gas mixture composed of 1000 ppm NO and 1 % O_2 in N_2 balance. Some catalytic systems were studied. The objective of that experiments was to measure the amount of NO which could be decomposed at different values of voltage and current with the different catalytic systems. The results are shown in fig. 7.15.

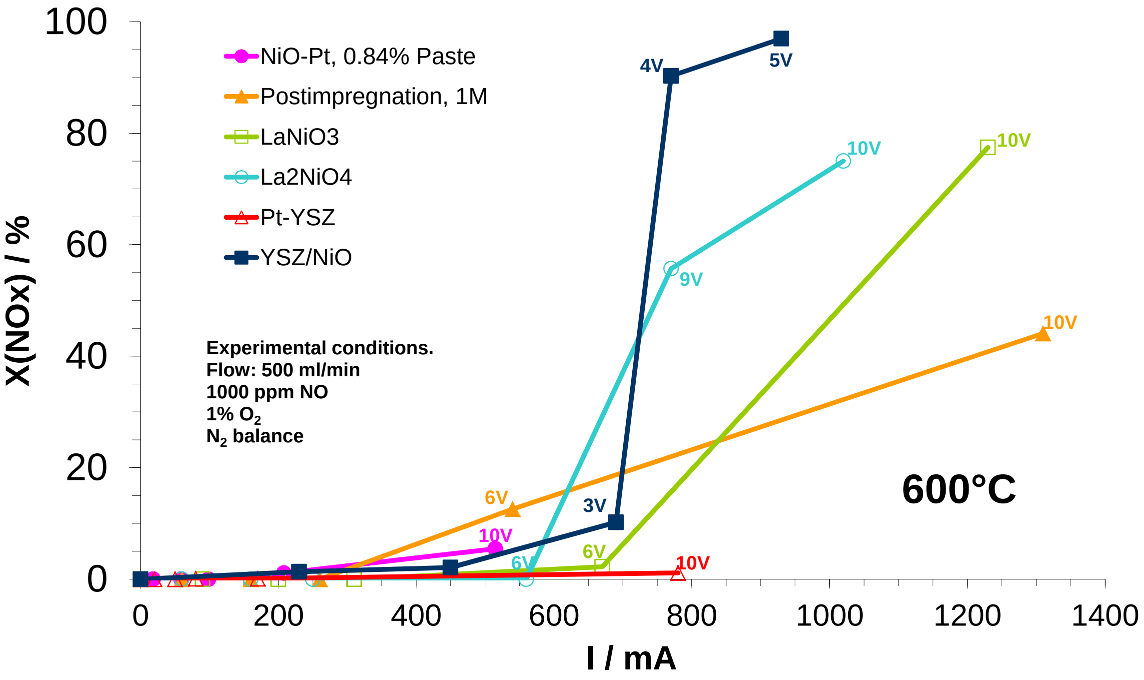

FIGURE 7.15. NOx decomposition activity presented by different electro-catalytic systems at 600°C

The system $Pt/YSZ/Pt/YSZ$ presents no catalytic activity for voltages between 0 and 10 V. The system $Pt/YSZ/Pt/YSZ/NiO$ obtained with a post-impregnation, achieved the highest conversion which was 42 % at 10 V and a current of 1300 mA is reached. The system $Pt/YSZ/Pt/YSZ - LaNiO_3$ presents a maximum conversion of about 78 % at 10 V and a current of 1200 mA. The system $Pt/YSZ/Pt/YSZ - La_2NiO_4$ achieve a 76 % conversion at 10 V with a 1000 mA current. The best system is $Pt/YSZ/Pt/YSZ - NiO$ which presents a conversion of 96 % at 5 V and with a 950 mA current.

The system which gave the best results ($Pt/YSZ/Pt/YSZ - NiO$) was chosen to make more experiments in order to understand the NO_X decomposition reaction.

The reactor was first heated at 450°C for 15min in order to eliminate the nitrogen containing compounds that could be adsorbed on the catalyst surface. Then, it was heated at 500°C and the NO decomposition experiments were performed on the $Pt/YSZ/Pt/YSZ - NiO$ system. The first, experiment was done using a 500 ml/min flow of a gas mixture composed of 1000 ppm NO and 1 % O_2 in N_2 balance. In order to study the performance of the catalytic system when NO_2 was dosed instead of NO, a second experiment at 500°C was done. In that second experiment, 500 ml/min flow of a gas mixture composed of 1000 ppm NO_2 and 1 % O_2 in N_2 balance was used. The experimental conditions of the third and fourth experiments were the same as the experimental conditions of the first experiment. The results are shown in fig. 7.16.

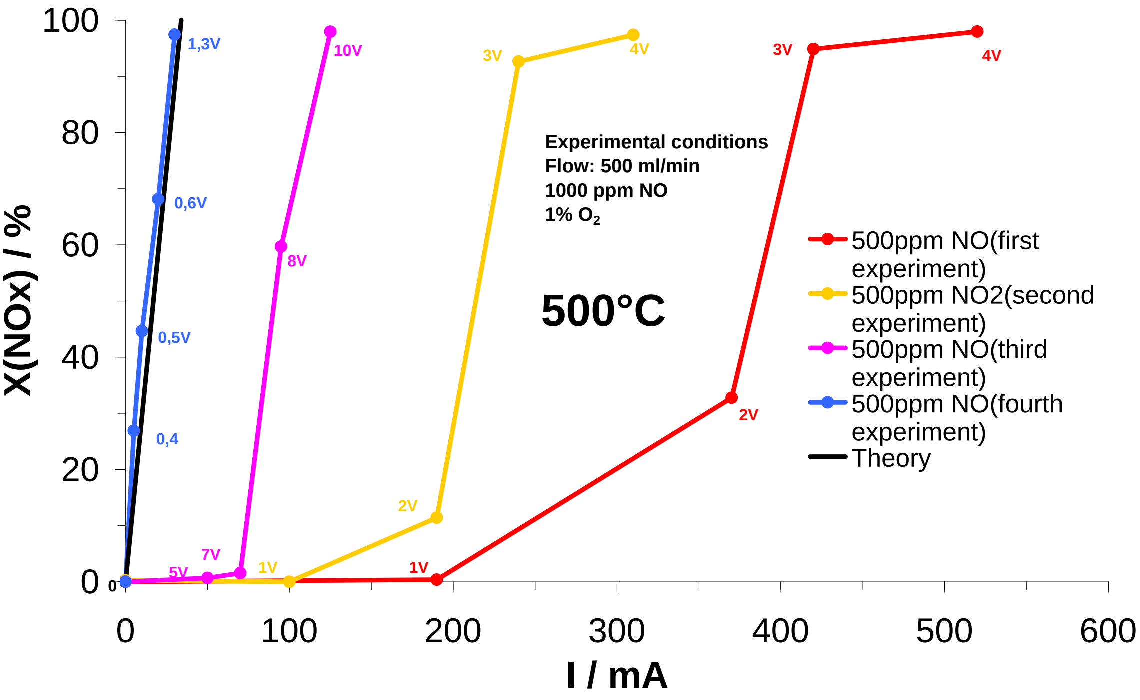

FIGURE 7.16. NOx decomposition activity of the NiO/YSZ catalyst at 500°C

An improvement of the catalytic performance of the $Pt/YSZ/Pt/YSZ-NiO$ system with the cell operating time was observed as shown in fig. 7.16. Finally, a 100 % conversion and selectivity was obtained. The theory-line in black correspond to the case in which just NO and no O_2 is decomposed at the cathode.

The system was then studied at different temperatures. The experimental conditions were 500 ml/min flow of a gas mixture composed of 1000 ppm NO and 1 % O_2 in N_2 balance. The results are shown in fig. 7.17. Between 500 and 300 °C 100 % of activity and selectivity are obtained but the conversion drops to 60 % at 250°C and the selectivity is no longer 100 %.

A comparison of the experimental results obtained when NO or NO_2 was dosed are illustrated in fig. 7.18. When NO was dosed, 100 % conversion rate and selectivity were achieved for all values of voltage. When NO_2 was dosed, the conversion rate and the selectivity increases from 0 % to 100 % as the voltage increases. The current obtained when NO_2 was dosed and 100 % conversion and selectivity was achieved is twice higher as the one achieved when NO was dosed.

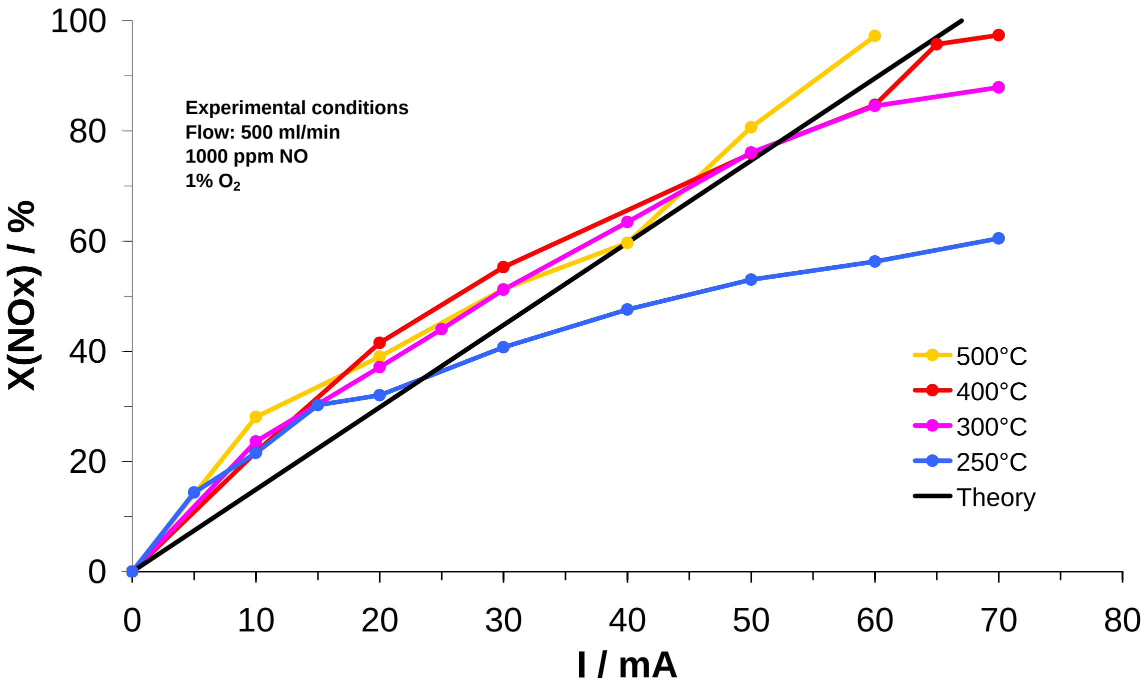

Figure 7.17. NOx decomposition activity of the NiO/YSZ catalyst at 500, 400, 300 and 250°C

The influence of the oxygen concentration in the conversion rate and the selectivity of the catalytic system was also studied. The reactor was heated at 450°C for 15 min and then at 500°C. The experimental conditions were 500 ml/min flow of a gas mixture composed of 1000 ppm NO and 2 % O_2 in N_2 balance. Then another two experiments with the same experimental conditions were done. Finally, experiments at 300, 400 and 600°C with 2 % O_2 were also performed.

The first experiment with 2 % O_2 shows that the selectivity decreases when the oxygen concentration is increased. An improvement of the electrocatalytic system with the operating time at 500°C is observed until finally 100 % selectivity is achieved. The subsequent experiment at 300, 400 and 600°C show 100 % selectivity. The results are illustrated in fig. 7.19.

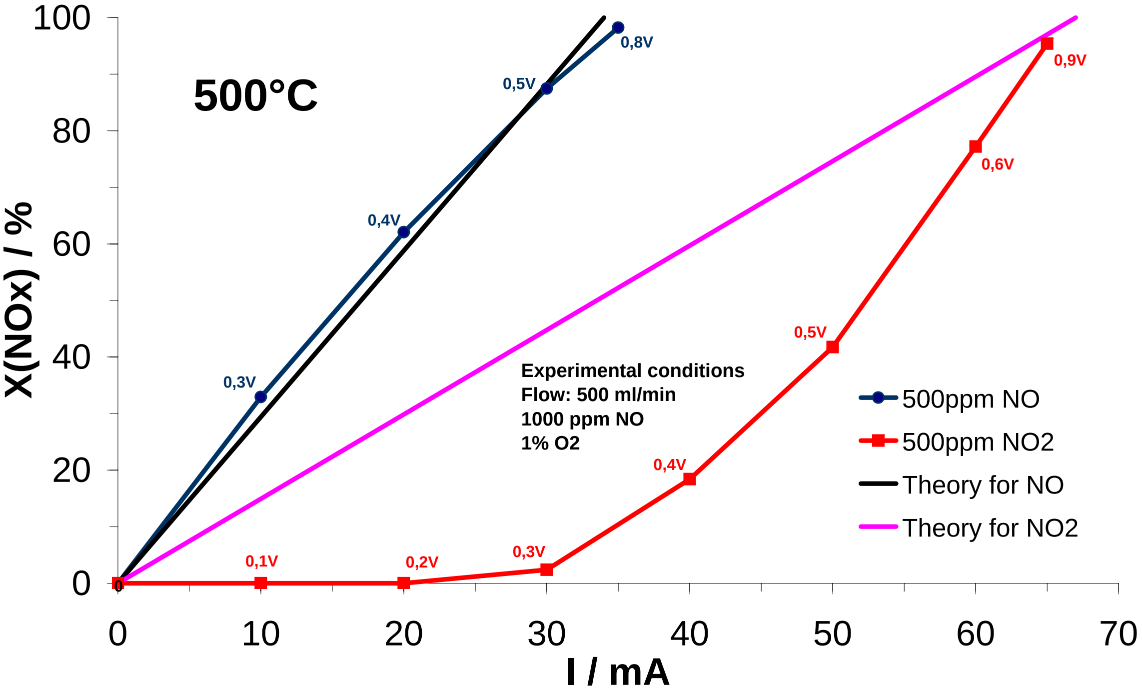

FIGURE 7.18. NOx decomposition activity of the NiO/YSZ catalyst when whether NO or NO_2 was dosed

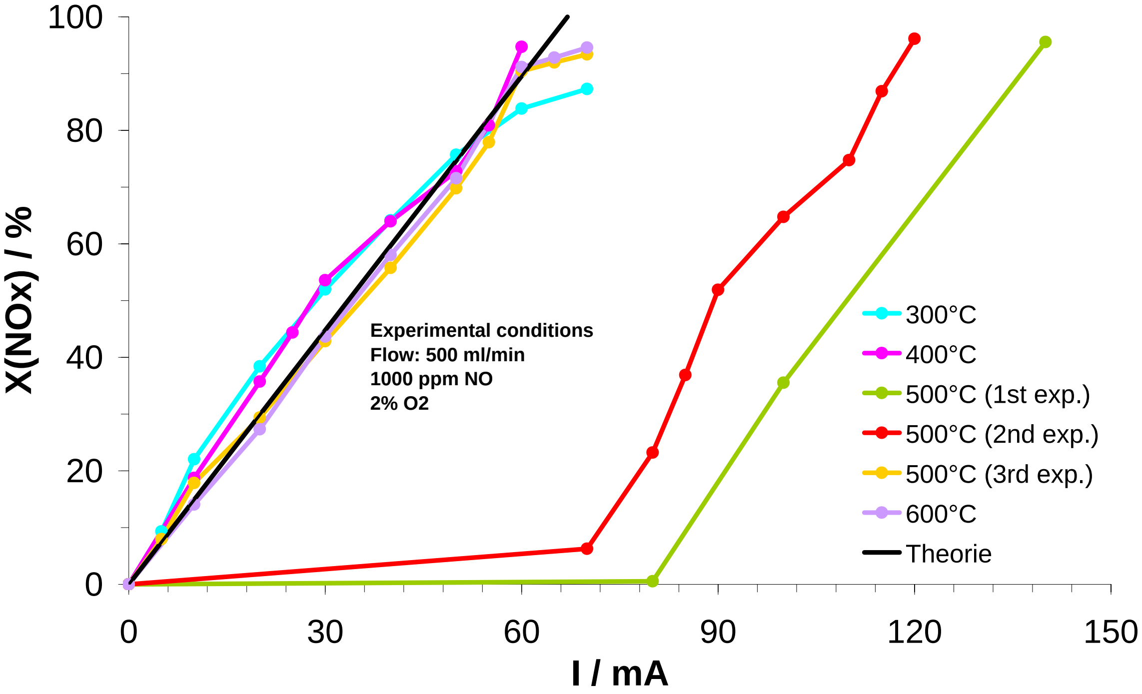

FIGURE 7.19. NOx decomposition activity of the NiO/YSZ catalyst when 2 % O_2 was present in the gas mixture

7.5.3. NO_x electro-catalytic decomposition with a planar substrate reactor.

In order to make the preparation of the catalyst more reproducible and the morphological studies easier, the tubular reactor was substituted for a flat substrate which has a surface of 21.87 cm^2. First two of the flat substrates were studied separately and then, both flat substrates were used in a "sandwich" conformation.

The experiments were done using a 500 ml/min flow of a gas mixture composed of 1000 ppm NO and 1 % O_2 in N_2 balance. The results are shown in fig. 7.20.

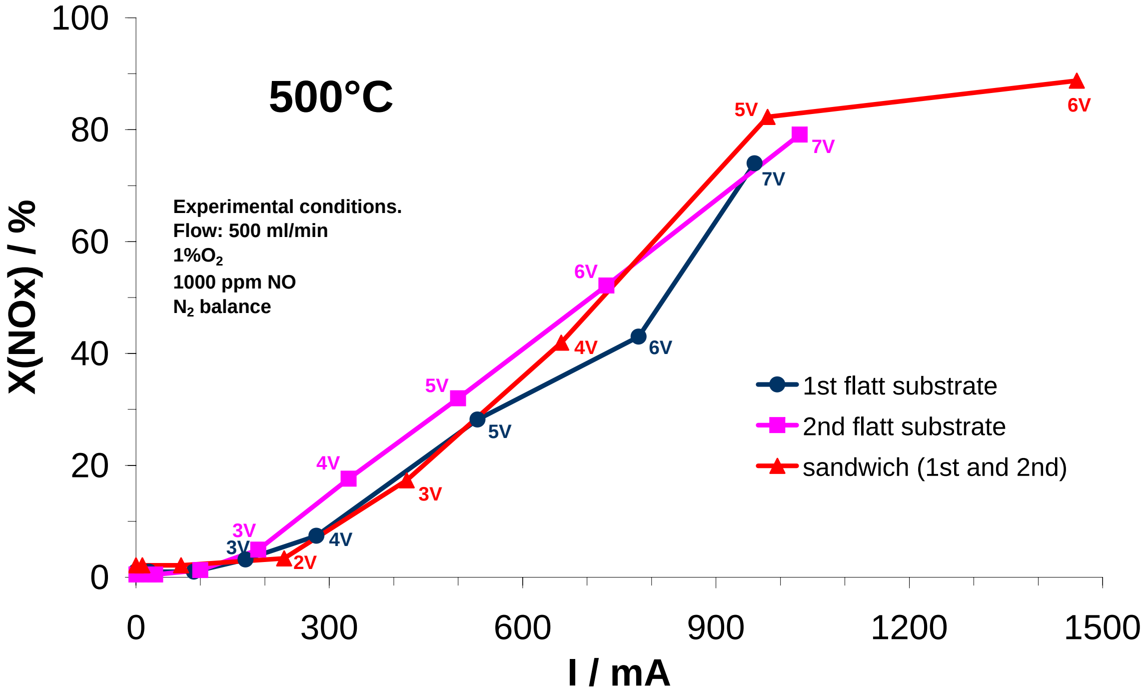

FIGURE 7.20. NOx decomposition activity of the NiO/YSZ catalyst on a planar substrate

The experiments done with the two planar substrates separately achieved the same conversion rates and selectivity values. When both planar substrates were used at the same time in a "sandwich" conformation, the voltage value needed in order to obtain the same conversion rate was lower for the "sandwich" conformation as fig. 7.20 shows.

Then, the oxygen influence on the NO_x catalytic activity was studied for which purpose, an experiment with 500 ml/min gas mixture composed of 1000 ppm NO and 5 % O_2 and another with 500 ml/min gas mixture composed of 1000 ppm NO and 10 % O_2 were done. The results were compared as shown in fig. 7.21. It is possible to observ that an increase of the oxygen concentration in the gas mixture leads to both a decrease in the NO_x catalytic activity and the NO_x conversion rate.

7.5.4. NO_x decomposition experiments on the NiO/YSZ powder catalyst as synthesized.

For all NO-decomposition experiments, 1 g of the NiO/YSZ powder catalyst pressed and granulated to obtain size particles between 125 and 250 μm was used.

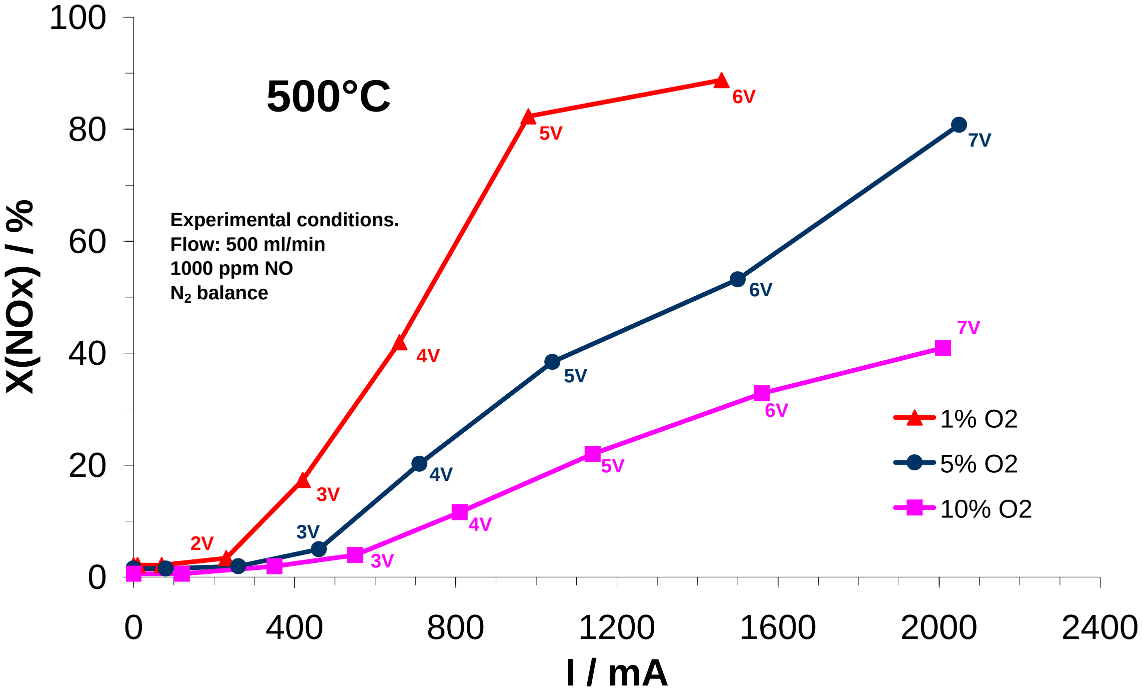

Figure 7.21. NOx decomposition activity of the NiO/YSZ catalyst when 1, 5 and 10 % O_2 wa present in the gas mixture

The catalyst was first heated at 450°C for 15min in order to eliminate the nitrogen-containing species which could be adsorbed on its surface. Finally, the temperature of the catalyst sample was driven to the temperature at which the NO decomposition was going to be studied (550, 450, 350, 250 and 150°C). The experimental conditions were 1 l/min N_2 and 1000 ppm NO. The NO_x conversion (U(NO_x)) was then calculated as indicated in 7.4. The results are shown in fig. 7.22

The NO_x conversion decreases very fast at all temperatures studied. Hence, the NO_x decomposition activity achieved in the temperature range between 150 and 550°C was very low. However, it is possible to observe an increase in the catalytic activity with increasing temperature.

7.5.5. NO-decomposition activity of the YSZ/NiO catalyst after previous reduction.

At 450°C no nitrogen-containing species are present on the catalyst surface but the oxygen originated as a result of the decomposition of the nitrogen oxide can strongly adsorb on the active centers of the NiO/YSZ catalyst which leads to its rapid poisoning and therefore, to its deactivation as observed in the results shown in fig. 7.22

In order to create free active sites in the catalyst, a previous reduction of the NiO/YSZ will be done. The catalyst sample will be heated at 450°C for 15 min and then it will be treated with 1 l/min N_2 and 2 % H_2 for one minute. Then, NO_x decomposition experiments will be run at 550, 450, 350, 250 and 150°C. The experimental conditions will be, as previously, 1 l/min N_2 and 1000 ppm NO. The results are shown in fig. 7.23

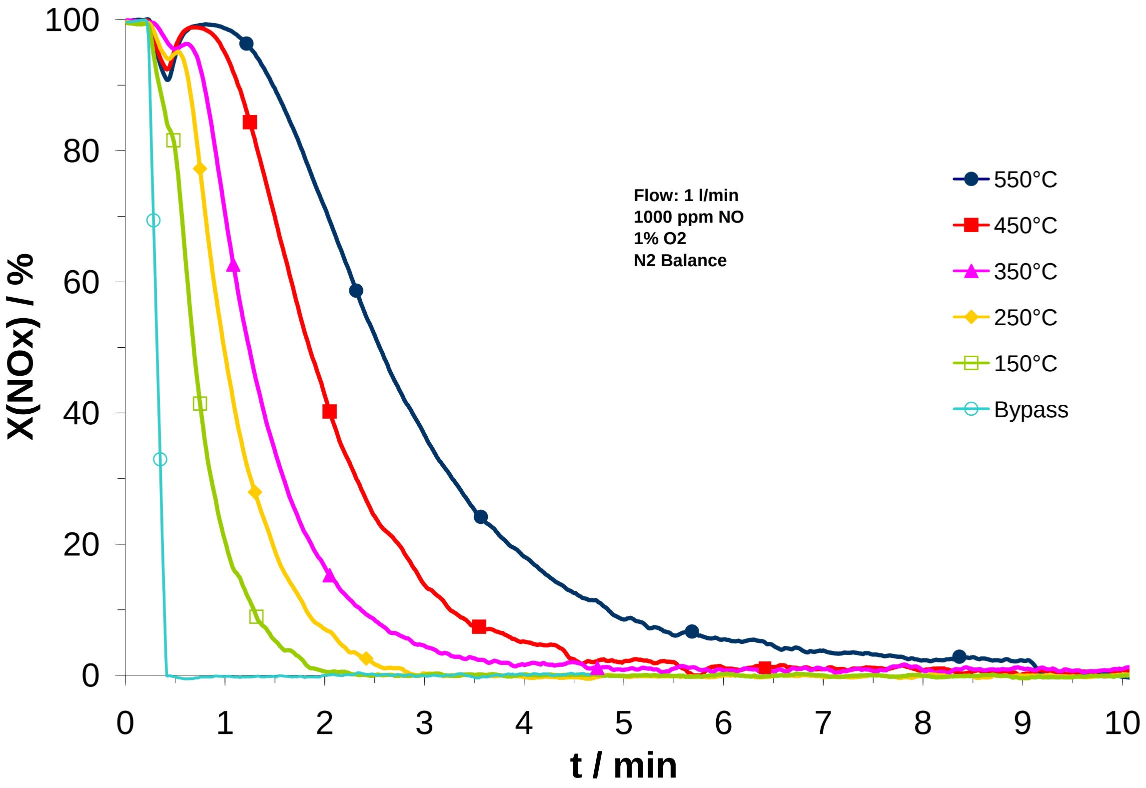

FIGURE 7.22. NOx decomposition activity of the NiO/YSZ powder catalyst as synthesized

As the temperature increases, the NO_x conversion also increases. If we compare the results obtained when the catalyst was not previously reduced and the ones obtained after reducing the catalyst (table 7.3) we can observe that the reduction treatment has clearly increased the amount of NO_x decomposed by the catalyst and therefore the activity of the YSZ/NiO powder.

No NO_2 formation was observed at none of the temperatures studied. The higher NO_x-decomposition activity was achieved at 550°C after reduction with H_2, in which case, 825 μmolNO were decomposed. The catalyst activity decreases as the temperature decreases until finally no significant catalytic activity is obtained at 150°C. Higher conversion rates are achieved after reduction at all temperatures studied but 150°C in which case, the same amount of nitrogen oxides are decomposed when the catalyst was reduced or not.

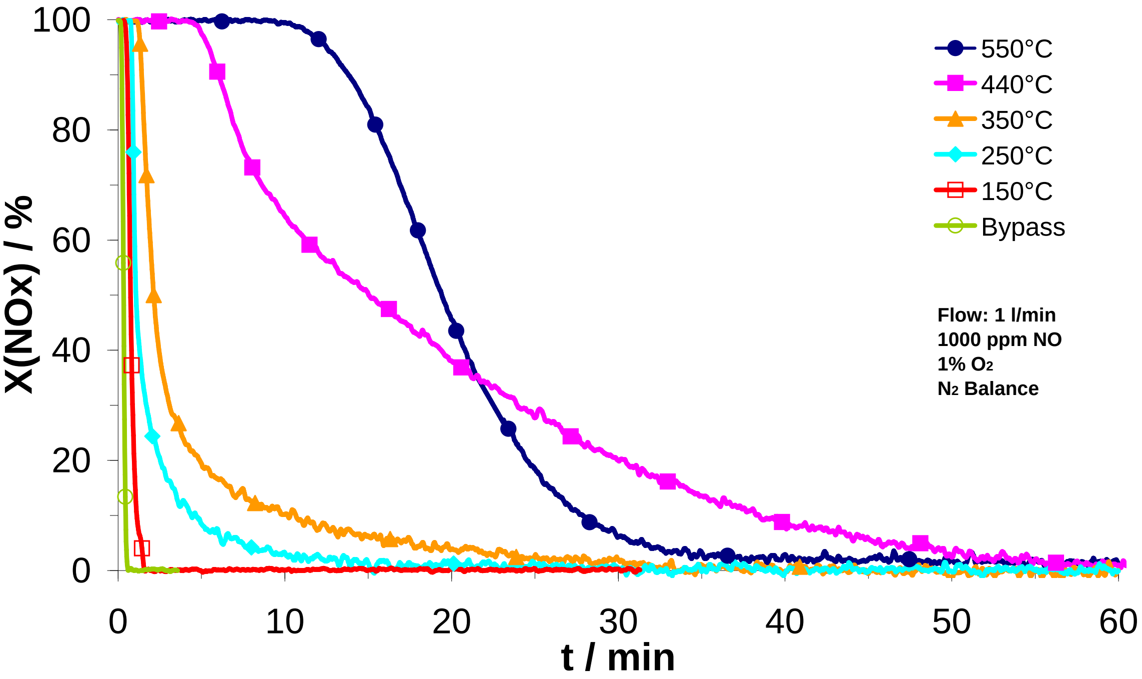

FIGURE 7.23. NOx decomposition activity of the NiO/YSZ powder catalyst after previous reduction at 450°C with 1 l/min N_2 and 2 % H_2

As shown before in equations (7.1) and (7.2), NO can decompose in order to form N_2, N_2O or both of them. In order to determinate which gases are produced as a result of the NO decomposition, the concentrations of N_2, N_2O and NO were simultaneously measured during the catalytic decomposition of NO_x on the YSZ/NiO catalyst. The catalyst was heated at 450°C for 15 min and then a previous reduction was done with a gas mixture composed of 2 % H_2 in Ar balance (1 l/min). The reduction was done during 2 min in order to create more active centers. The experimental conditions were 1000 ppm NO in Ar balance (1 l/min). The temperatures studied were 550, 450, 350, 250 and 150°C. The results are shown in fig. 7.24 - fig. 7.25

At 550°C no NO_2 or N_2O formation was observed. During the first 40 min, only N_2 was produced which indicates that the only reaction that takes place at that temperature is the one shown in equation (7.1). Then, as the NO formation starts, the N_2 concentration decreases until just NO is detected at the end of the experiment. At 150°C, the amount of N_2 formed is much smaller than the one obtained at 550°C. A significant formation of N_2O was observed which indicates that the reaction shown in equation (7.2) competes with the decomposition of NO_x in order to form N_2. The amount of each gas formed during the experiments at the different temperatures studied are summarized in table 7.4 . The nitrogen balance was also calculated as equation (7.8) indicates.

Experiment	$NO/\mu mol$	$NO_2/\mu mol$
without H_2 reduction:		
550 °C	112	0
450 °C	71	0
350 °C	46	0
250 °C	34	0
150 °C	20	0
with H_2 reduction:		
550 °C	825	0
450 °C	775	0
350 °C	162	0
250 °C	86	0
150 °C	21	0

TABLE 7.3. Amount of NO and NO_2 produced during the NO_x decomposition experiments with and without previous reduction

$$B(\%) = \frac{n_{NO}(\mu mol) + n_{NO_2}(\mu mol) + 2\left\{n_{N_2}(\mu mol) + n_{N_2O}(\mu mol)\right\}}{n_{NO}(\mu mol)_0} 100 \tag{7.8}$$

where:

$B(\%)$ is the nitrogen balance in %
$n_{NO}(\mu mol)$ is the amount of NO produced during the experiment in μmol
$n_{NO_2}(\mu mol)$ is the amount of NO_2 produced during the experiment in μmol
$n_{N_2}(\mu mol)$ is the amount of N_2 produced during the experiment in μmol
$n_{N_2O}(\mu mol)$ is the amount of N_2O produced during the experiment in μmol
$n_{NO}(\mu mol)_0$ is the total amount of NO dosed during the experiment in μmol.

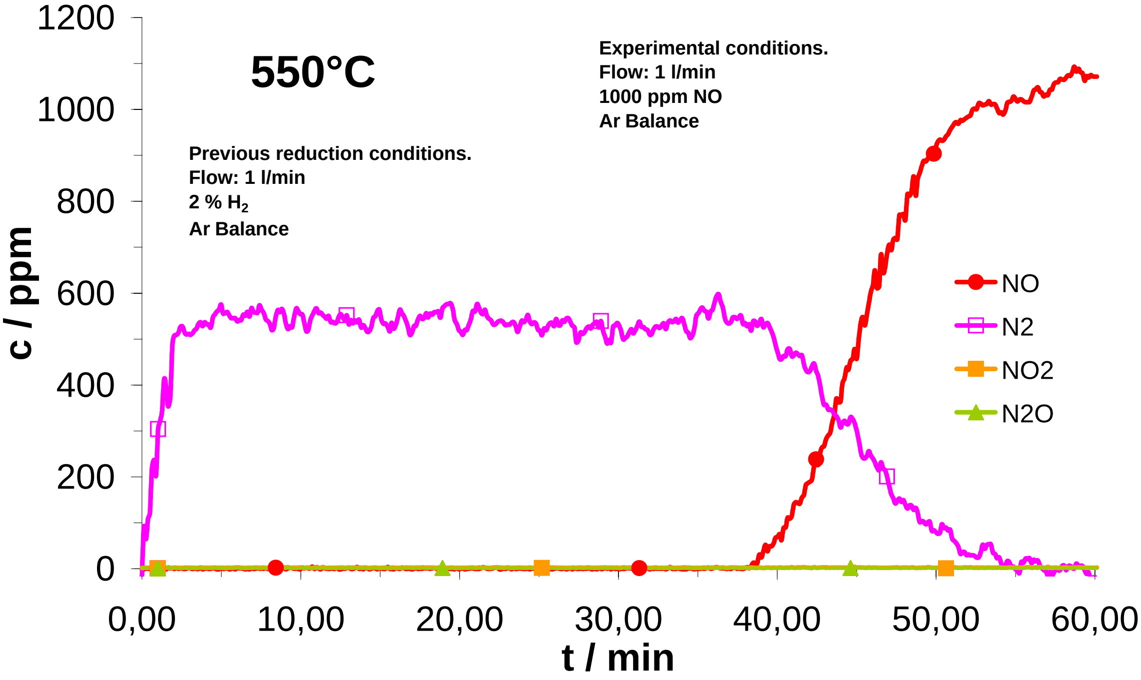

FIGURE 7.24. NO_x decomposition activity of the NiO/YSZ powder catalyst at 550°C after previous reduction at 450°C with 1 l/min N_2 and 2 % H_2

The graphics of the experiment done at 450, 350 and 250°C are shown in the appendix 10.3

In order to study the oxygen effect on the catalyst activity, NO_x decomposition experiments in presence of oxygen were done. The catalyst was heated at 450°C for 15 min and then a previous reduction of the catalyst was done with a gas mixture composed of 2 % H_2 in Ar balance (1 l/min) for 2 min. Then, the catalyst was driven to the temperature to be studied and a mixture composed by 1000 ppm NO and 1 % O_2 in Ar balance was dosed (1 l/min). The experimental results are shown in fig. (7.26) and fig. (7.27).

As shown in fig. 7.26, the only gas detected in the first 4 min of the experiment was N_2. After that time, the N_2 concentration decreases as the NO, NO_2 and

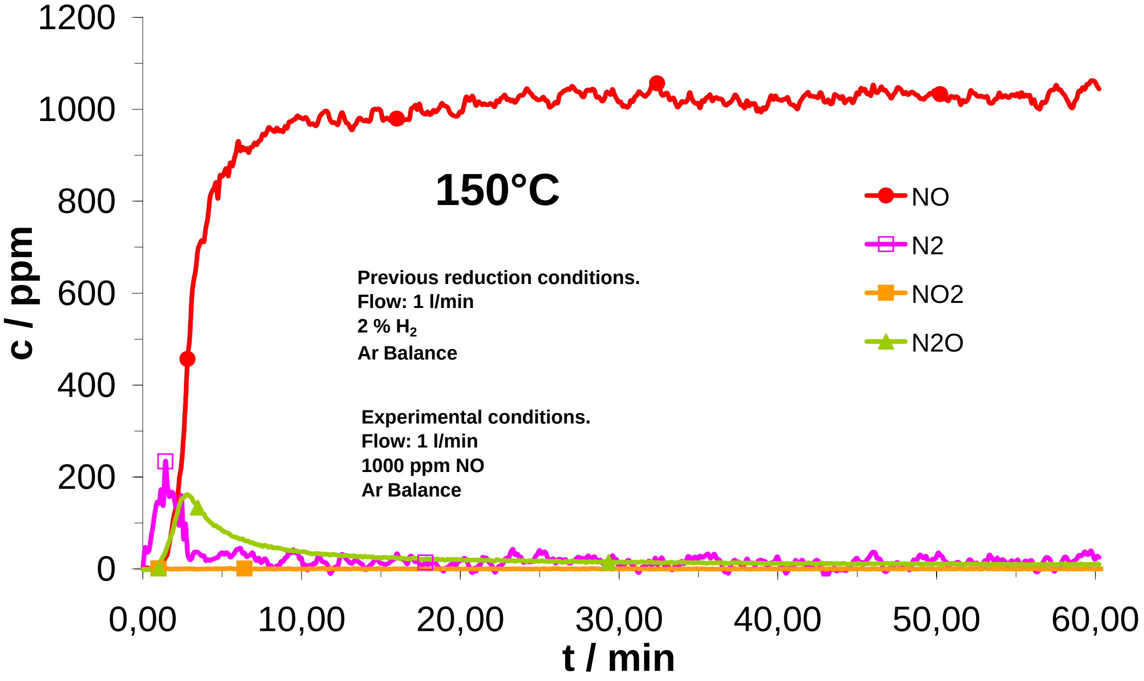

FIGURE 7.25. NOx decomposition activity of the NiO/YSZ powder catalyst at 150°C after previous reduction at 450°C with 1 l/min N_2 and 2 % H_2

O_2 concentration increases until no N_2 was detected and the NO, NO_2 and O_2 concentrations remain stationary. No N_2O was detected during the experiment.

As shown in fig. 7.27, the only gas detected in the first 2 min of the experiment was N_2. After that time, the N_2 concentration decreases as the NO, NO_2 and O_2 concentration increases until no N_2 was detected and the NO, NO_2 and O_2 concentrations remain stationary. No N_2O was detected during the experiment.

In the table 7.5 the amount of the different gases produced in the NO_x decomposition experiments are summarized.

As we can see in table 7.5, the smaller amount of NO detected during the experiments corresponds to the one done at 450°C and it increases as the temperature decreases. The higher NO_2 detection occurs at 350°C. Under 350°C the NO_2 amount detected decreases very fast as the temperature decreases and up to 350°C, the NO_2 amount detected decreases as the temperature increases. The N_2 production decreases as the temperature decreases and down to 350°C no N_2 is detected. A small amount of N_2O is only detected at 350 and 250°C.

$Temperature/°C$	$NO/\mu mol$	$N_2/\mu mol$	$NO_2/\mu mol$	$N_2O/\mu mol$	$Balance/\%$
550	639	1001	0	0	98.2
450	1458	593	0	0	97.5
350	2327	143	0	16	99.1
250	2401	76	0	48	97.9
150	2400	52	0	61	97.4

TABLE 7.4. Amount of NO, NO_2, N_2 and N_2O produced during the NO_x decomposition experiments

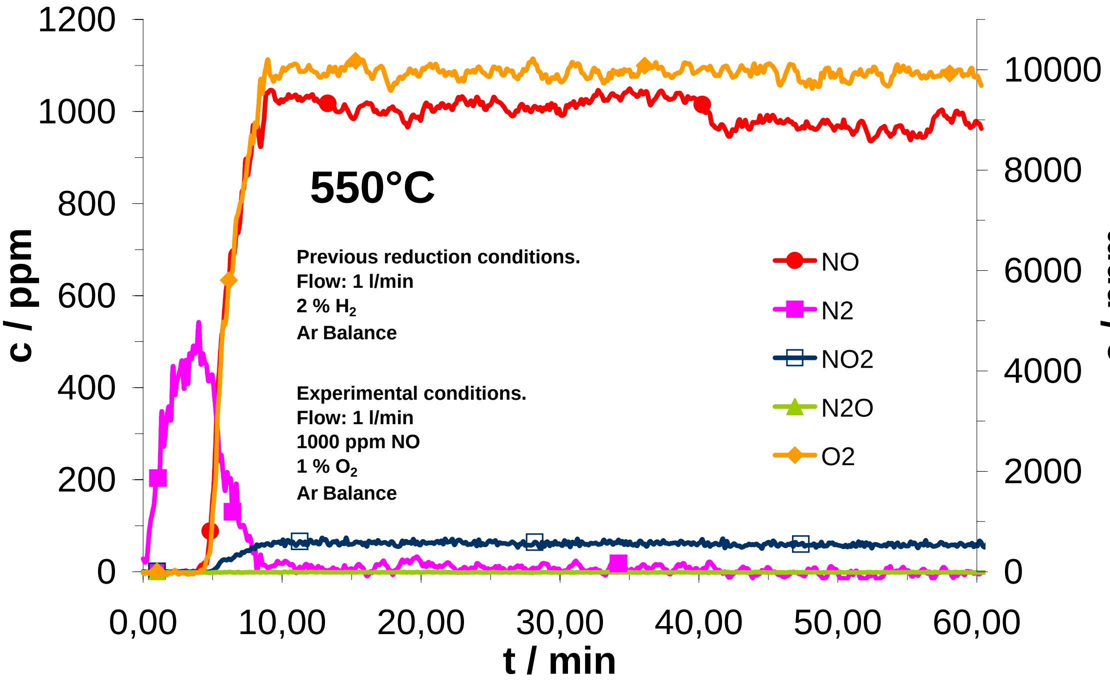

FIGURE 7.26. NOx decomposition activity of the NiO/YSZ catalyst at 550°C after previous reduction at 450°C with 1 l/min N_2 and 2 % H_2

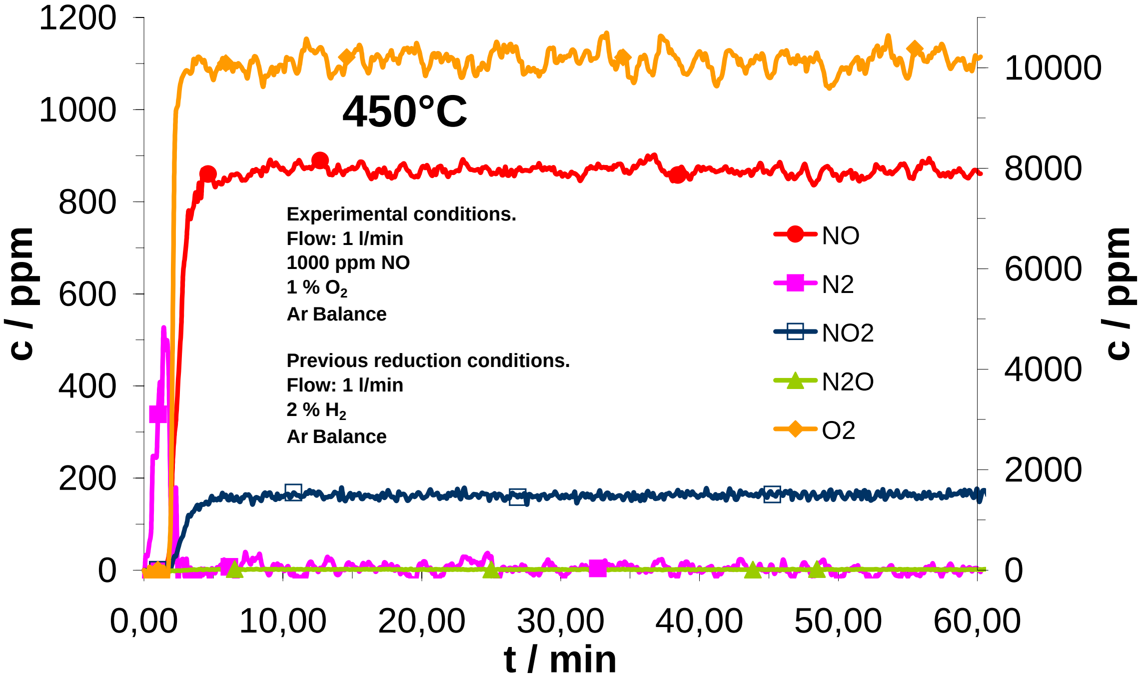

Figure 7.27. NOx decomposition activity of the NiO/YSZ catalyst at 450°C after previous reduction at 450°C with 1 l/min N_2 and 2 % H_2

$Temperature/°C$	$NO/\mu mol$	$N_2/\mu mol$	$NO_2/\mu mol$	$N_2O/\mu mol$	$Balance/\%$
550	2255	105	137	0	99.0
450	2083	30	387	0	98.0
350	2152	0	400	21	97.4
250	2474	0	98	19	95.9

Table 7.5. Amount of NO, NO_2, N_2 and N_2O produced during the NO_x decomposition experiments

7.5.6. NO-decomposition activity of the YSZ powder.

Our catalyst is composed of NiO and YSZ. In order to find out if YSZ contributes to the catalytic activity, a NO_x decomposition experiment with pure YSZ was done. The amount of YSZ used in the experiment should be the same amount present in 1 g of NiO/YSZ catalyst in order to compare both experimental results. 10 g of the NiO/YSZ paste is composed of 4 g NiO and 6 g YSZ paste. The 6 g YSZ Paste is composed of 1.2 g YSZ and 4.8 g terpineol. After calcination, the terpineol is evaporated so the NiO/YSZ powder is composed of 4 g NiO and 1.2 g YSZ. As a result, 1 g NiO/YSZ powder contents 0.231 g YSZ. The YSZ powder was first heated at 450°C for 15min and then, a previous reduction of the catalyst was done with a gas mixture composed of 2 % H_2 in Ar balance (1 l/min). Finally, it was heated to 550°C. The experimental conditions were 1 l/min N_2 and 1000 ppm NO. A comparison of the experimental results obtained with the YSZ and NiO/YSZ powder is shown in fig. 7.28.

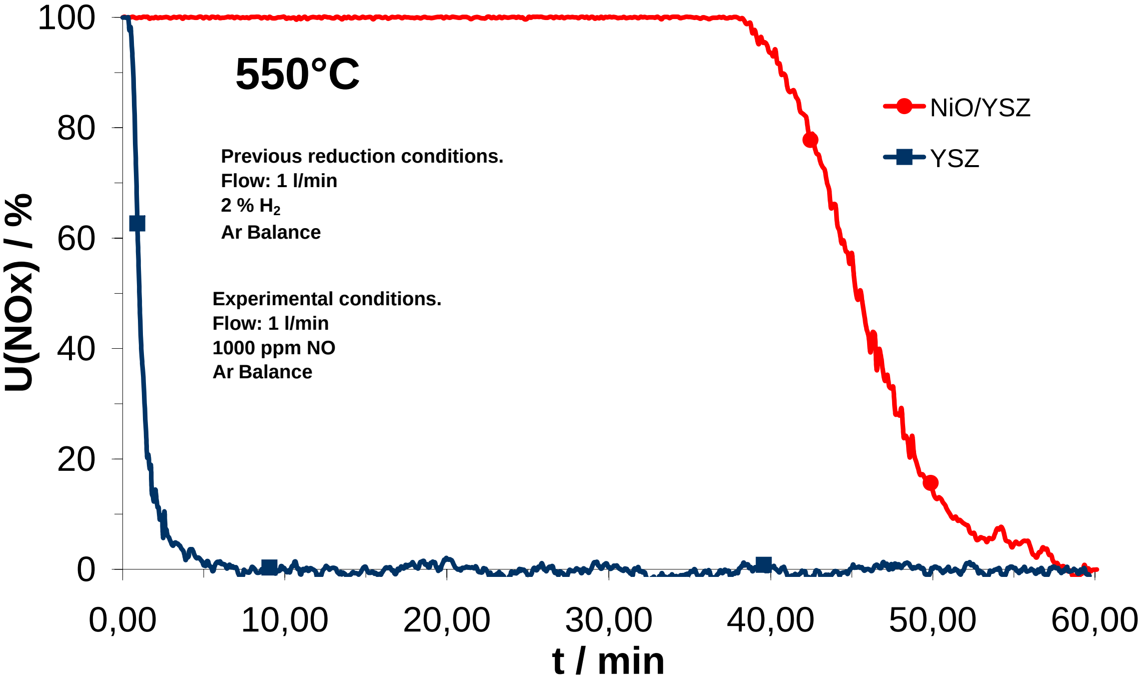

FIGURE 7.28. Comparison between the catalytic activity of the YSZ/NiO and YSZ powder

It can be observed that the conversion rate obtained with the YSZ powder is much smaller than the one obtained with the YSZ/NiO powder.

7.6. NO_x-TPD experiments

7.6.1. NO_x-TPD experiments on the NiO/YSZ powder.

As described in the literature that some catalysts have the capacity of storing NO_x as nitrates and nitrites at low temperatures. In order to find out whether the NiO/YSZ catalyst can store NO_x or not, TPD experiments with the catalyst powder were done. For all experiments 1 g of NiO/YSZ was used. The saturation conditions were done with and without oxygen.

7.6.1.1. *Saturation conditions: 1000 ppm NO and 1 % O_2 (1 l/min in N_2).*

The NiO/YSZ powder catalyst was first heated at 450°C for 15 min. Then it was cooled down to the temperature at which the saturation was done (150, 250 and 350 °C). The catalyst was treated with a gas mixture composed of 1000 ppm NO and 1 % O_2 (1 l/min in N_2 balance) for 30 min. Then, a flow of 1 l/min N_2 was dosed until no NO_x was detected. Finally, the temperature was increased with a rate of 10 °C/min until a final temperature of 450°C was reached. During the experiment the NO and NO_2 production was detected. The results are shown in fig. 7.29. The main storage capacity is observed at 150 and 250°C. At 350°C the storage is much smaller and at temperatures above 450°C no storage was observed.

TPD experiments after previous reduction (2 min 450°C, 1 l/min total flow, 2 % H_2 in N_2 balance) were also performed. No significant differences were observed in comparison with the TPDs without previous reduction.

7.6.1.2. *Saturation conditions: 1000 ppm NO (1 l/min in N_2).*

In order to study the storage capacity of the NiO/YSZ catalyst in absence of oxygen, TPD experiment were done in which the saturation was run with a gas mixture composed of 1000 ppm NO in N_2 balance. The catalyst was heated at 450°C for 15 min and then, a 60 min long saturation at 150, 250 and 350°C was done. The results are shown in fig. 7.30. As we can see, no NO_2 production was observed. The amount of NO desorbed was much smaller than the one obtained when oxygen was present during the saturation.

TPD experiments before previous reduction (2 min 450°C, 1 l/min total flow, 2 % H_2 in N_2 balance) were also performed. No significant differences were observed in comparison with the TPDs without previous reduction.

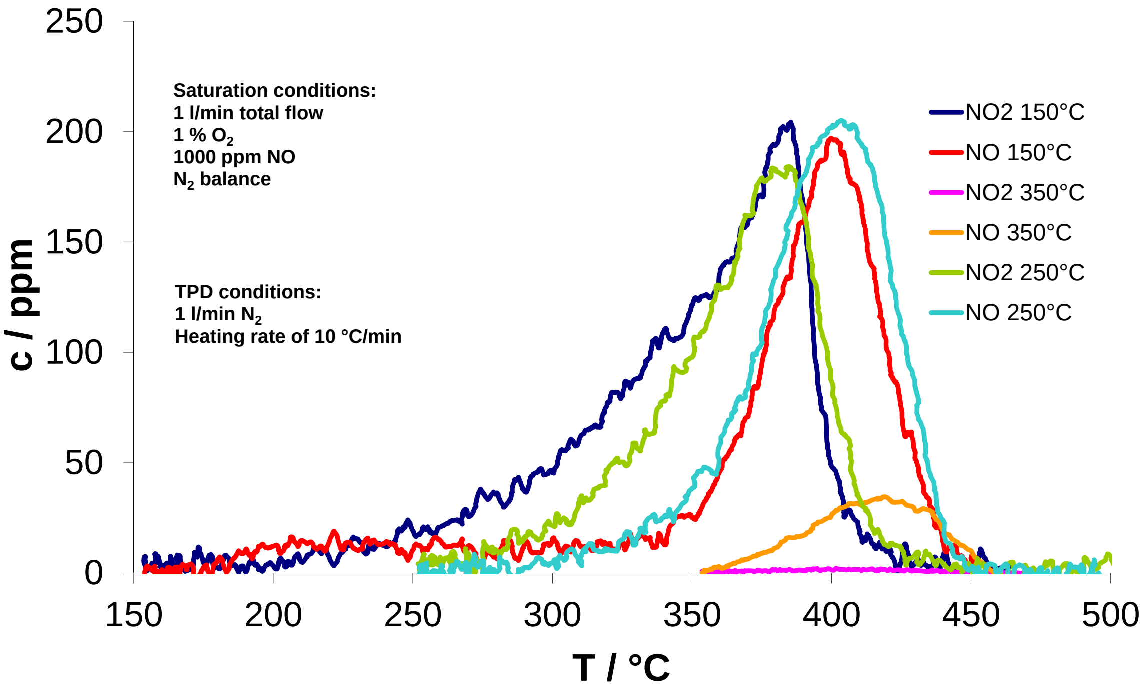

FIGURE 7.29. NO_x-TPD on the YSZ/NiO powder catalyst when the saturation took place at 150, 250 and 350°C in presence of oxygen

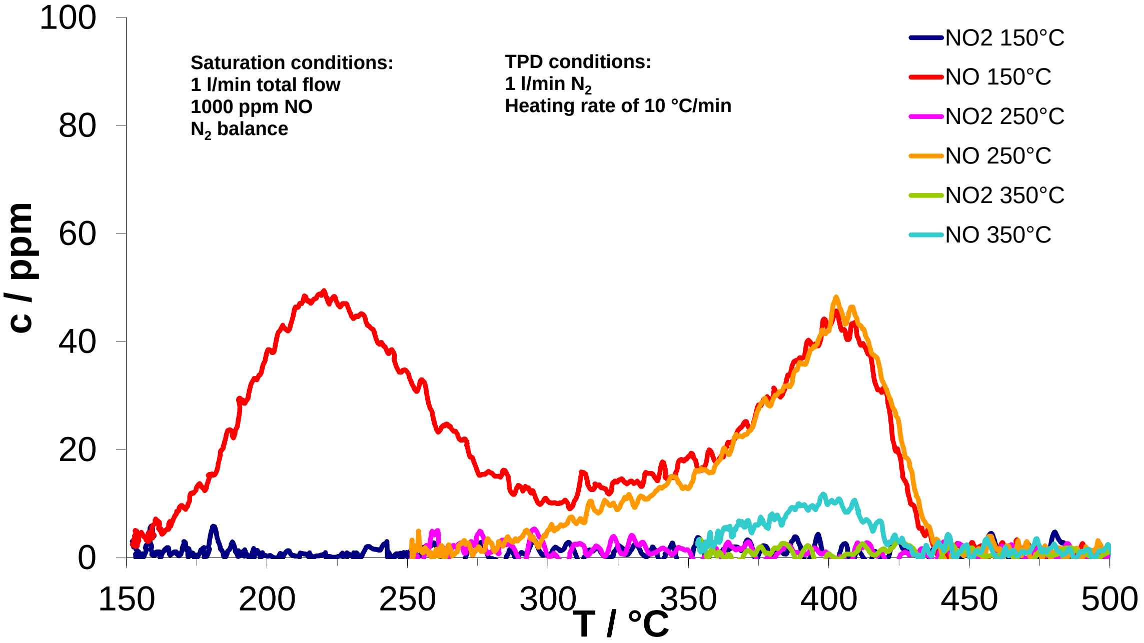

FIGURE 7.30. NO_x-TPD on the YSZ/NiO powder catalyst when the saturation took place at 150, 250 and 350°C

7.6.2. NO_x-TPD experiments on the YSZ powder.

In order to elucidate whether the main storage for NO_x storage is NiO or YSZ, TPD experiments were performed with pure YSZ. The amount of YSZ chosen for the experiments was the one which is contained in one gram of NiO/YSZ powder catalyst. Hence, 0.231 g of YSZ was utilized.

7.6.2.1. *Saturation conditions: 1000 ppm NO and 1 % O_2 (1 l/min in N_2).*

The YSZ powder was first heated at 450°C for 15 min. Then it was cooled down to the temperature at which the saturation was done (150, 250 and 350 °C). The catalyst was treated with a gas mixture composed of 1000 ppm NO and 1 % O_2 (1 l/min in N_2 balance) for 30 min. Then, a flow of 1 l/min N_2 was dosed until no NO_x was detected. Finally, the temperature was increased with a rate of 10 °C/min until a final temperature of 450°C was reached. During the experiment the NO and NO_2 production was detected. The results are shown in fig. 7.31. It is possible to observe that the desorption bands obtained are much smaller than the ones achieved with the NiO/YSZ catalyst at the same experimental conditions. The main storage capacity is observed at 150 and 250°C. At 350°C the storage is much smaller and at temperatures above 450°C no storage was observed.

TPD experiments in which a previous reduction (2 min 450°C, 1 l/min total flow, 2 % H_2 in N_2 balance) were performed. No significant differences were observed in relation with the TPDs without previous reduction.

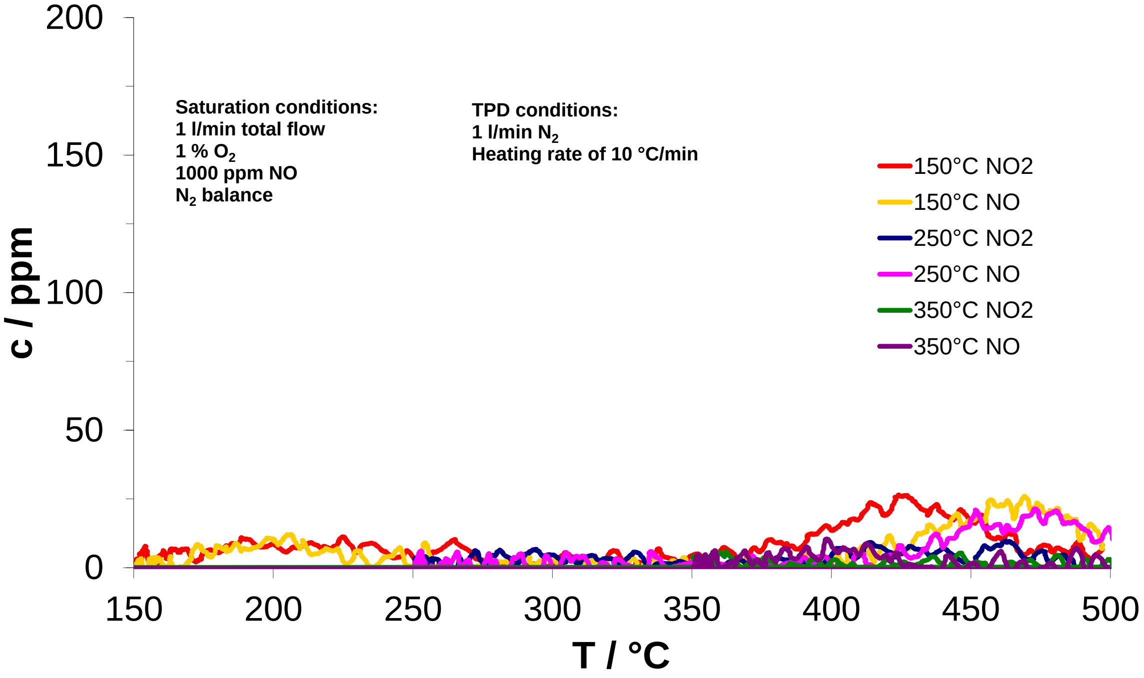

FIGURE 7.31. NO_x-TPD on the YSZ powder when the saturation took place at 150, 250 and 350°C in presence of oxygen

7.6.2.2. *Saturation conditions: 1000 ppm NO (1 l/min in* N_2*).*

In order to study the storage capacity of the YSZ powder in absence of oxygen, TPD experiment were done in which the saturation was run with a gas mixture composed of 1000 ppm NO in N_2 balance. The catalyst was heated at 450°C for 15 min and then, a 60 min long saturation at 150, 250 and 350°C was done. No NO_2 production was observed. No desorption bands were achieved at none of the studied temperatures.

7.7. NO_x-O_2-TPD experiments on the NiO/YSZ catalyst powder

The decomposition of the nitrates and nitrites occurs as shown in equation (7.9) and (7.10) respectively.

$$2\,NO_3^- \rightarrow 2\,NO_2 + \frac{1}{2}O_2 + O^{-2} \tag{7.9}$$

$$2\,NO_2^- \rightarrow 2\,NO + \frac{1}{2}O_2 + O^{-2} \tag{7.10}$$

Taking equation (7.9) and the equilibrium between NO and NO_2 shown in equation (7.3) an oxygen balance of the decomposition of nitrates can be done as follows.

$$n_{O_2}(\mu mol)_d = n_{O_2}(\mu mol)_{NO_2} + n_{O_2}(\mu mol)_{NO_3^-} \tag{7.11}$$

$$n_{O_2}(\mu mol)_d = \frac{1}{2}n_{NO}(\mu mol)_d + \frac{1}{4}n_{NO_2}(\mu mol)_d \tag{7.12}$$

where:

$n_{O_2}(\mu mol)_d$ is the amount of oxygen desorbed during the TPD in μmol.

$n_{O_2}(\mu mol)_{NO_2}$ is the amount of oxygen which comes from the formation of NO starting from NO_2

$n_{NO}(\mu mol)_d$ is the amount of NO desorbed during the TPD in μmol.

$n_{NO_2}(\mu mol)_d$ is the amount of NO_2 desorbed during the TPD in μmol.

Taking equation (7.10) an oxygen balance of the decomposition of nitrites can be done as follows.

$$n_{O_2}(\mu mol)_d = n_{O_2}(\mu mol)_{NO_3^-} \tag{7.13}$$

$$n_{O_2}(\mu mol)_d = \frac{1}{4} n_{NO}(\mu mol)_d \tag{7.14}$$

where:

$n_{O_2}(\mu mol)_d$ is the amount of oxygen desorbed during the TPD in μmol.
$n_{NO}(\mu mol)_d$ is the amount of NO desorbed during the TPD in μmol.

In order to explain the NO_x desorption observed at 150 and 250°C a NO_x-O_2-TPD was performed. The experimental procedure is the same as the one described in the section 7.6.1.1. The results are shown in fig. 7.32 and fig. 7.33.

The TPD results show two desorption zones (zone LT at low temperature and zone HT at high temperature). In zone LT NO and NO_2 peaks but no O_2 peak was observed. In zone HT, NO, NO_2 and O_2 peaks were observed. No N_2O desorption was achieved during the experiment.

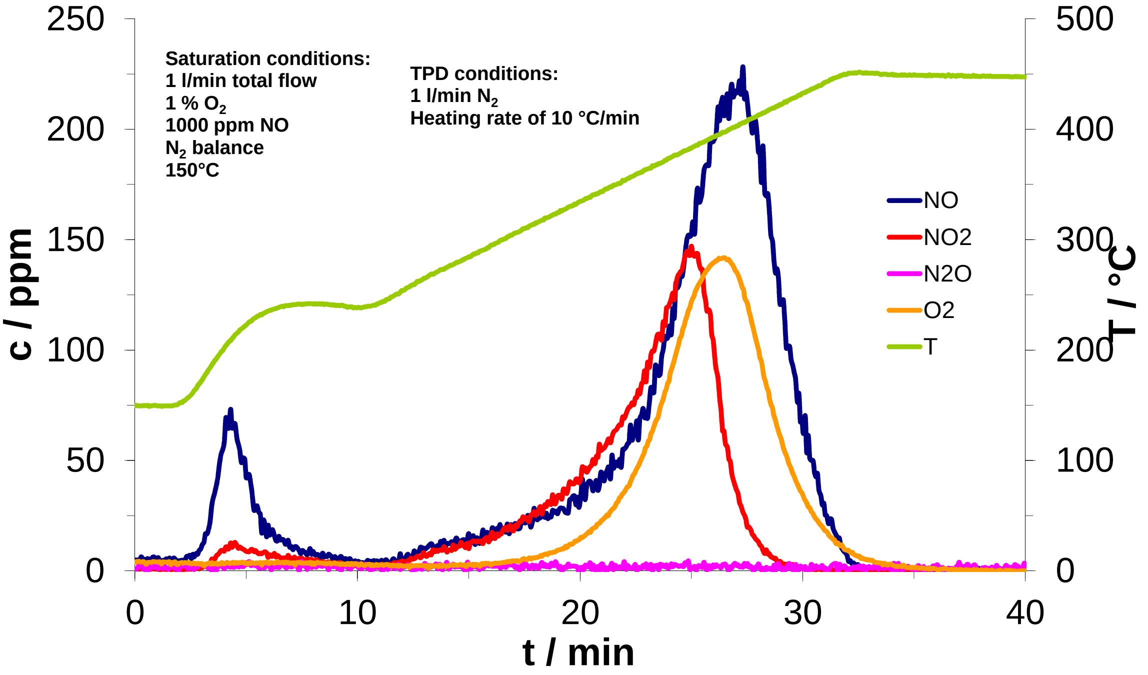

FIGURE 7.32. NO_x-O_2-TPD on the YSZ/NiO powder catalyst when the saturation took place at 150°C in presence of oxygen

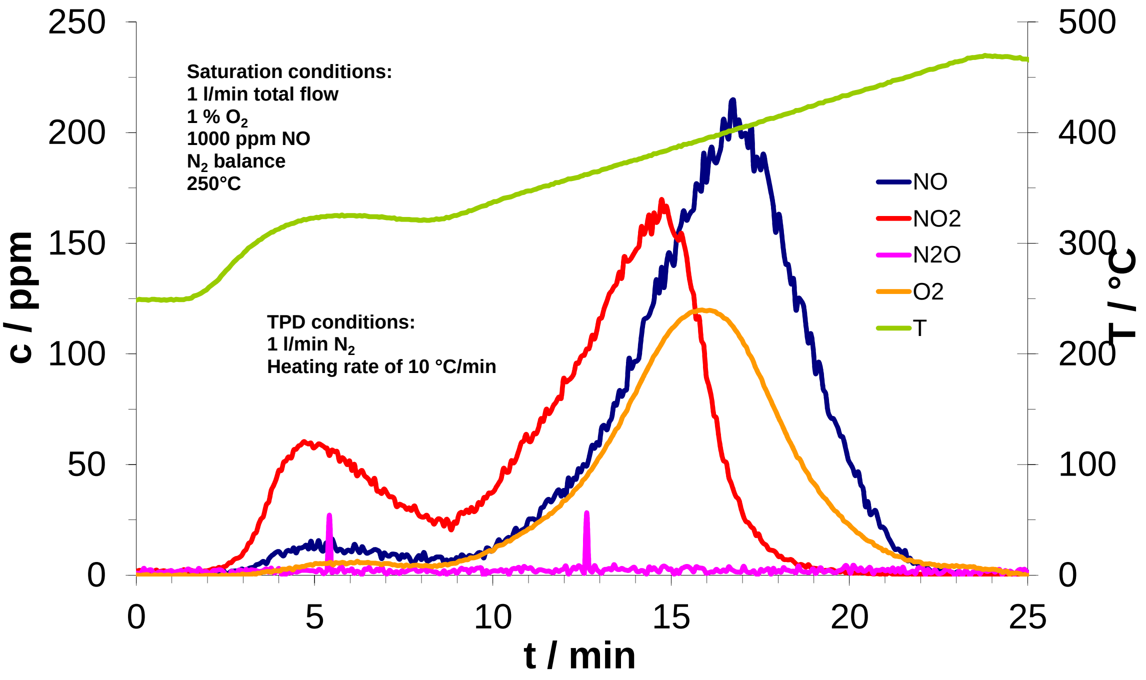

FIGURE 7.33. NO_x-O_2-TPD on the YSZ/NiO powder catalyst when the saturation took place at 250°C in presence of oxygen

7.8. O_2 TPD

In order to determine at which temperature the adsorbed oxygen can be removed from the NiO/YSZ powder catalyst, an oxygen TPD was performed.

1 g of a NiO/YSZ powder catalyst was first heated at 450°C for 15 min in order to eliminate the adsorbed species. Then it was coled down to 150°C. For the saturation, the catalyst was treated for 30 min with a gas total flow of 500 ml/min containing 500 ppm O_2 in N_2 balance. Then, a flow of 1 l/min N_2 was dosed until no O_2 was detected. Finally, the temperature was raised with a heating rate of 10 °C/min until a final temperature of 850°C was reached. During the experiment the O_2 production was detected. The results are shown in fig. 7.34.

Between 200 and 350°C, a very small O_2 desorption band (under 10 ppm) was achieved. That could correspond to the desorption of physisorbed O_2 since a small increase in the temperature was enough to suministrate the energy necessary to break the interaction between NO and the catalyst surface. The main desorption band achieved between 475 and 850°C could correspond to the desorption of the chemisorbed oxygen.

7.9. DRIFT experiments

The $DRIFT$-Spectroscopy will be used in order to study the active molecule IR-vibrations of the different chemical species present on the surface of the NiO/YSZ

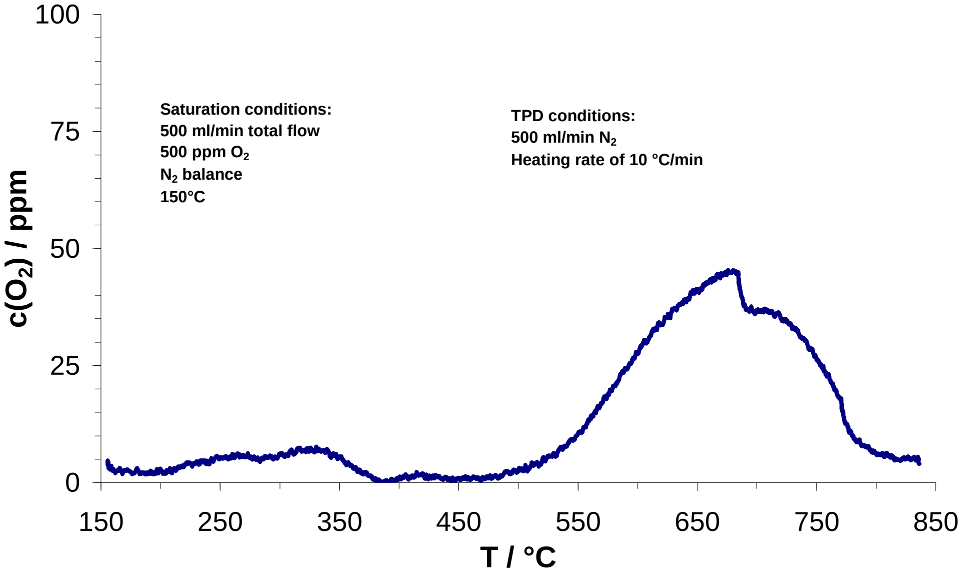

FIGURE 7.34. O_2-TPD performed on 1g of a NiO/YSZ catalyst powder

and pure YSZ powder after saturation and reduction treatment. It can provide some information which would allow us to make some conclusions about the nature of the species adsorbed on the solid surface to be studied and the evolution of such a species when a reduction take place.

In order to obtain more information about what occurs during the saturation and the reduction of the solid surface, the $DRIFT$ experiments were coupled with the mass spectroscopy method in order to detect the gas evolution during the whole experiment. The different nitrite and nitrate surface species discussed in that section are illustrated in fig. 7.35.

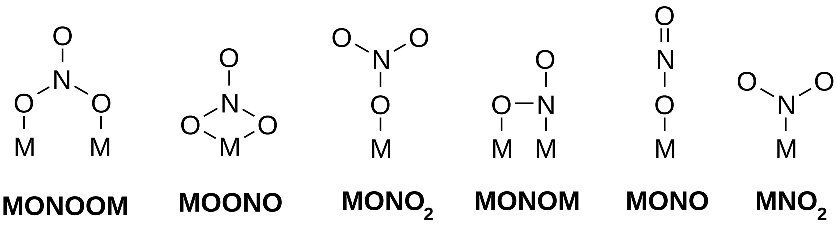

FIGURE 7.35. Surface nitrates and nitrites

7.9.1. NiO/YSZ powder catalyst.

7.9.1.1. *Saturation with NO/N_2.*

NiO/YSZ powder samples were used to make $DRIFT$ experiments. The sample was first heated at 450°C in N_2 atmosphere (500 ml/min) in order to eliminate the nitrogen containing species which could be adsorbed on the catalyst surface. Then, the sample was cooled down to the temperature chosen to make the experiment (150 or 350°C). After 15 min, backgrounds was detected until it remained stationary and then a $DRIFT$ experiment was run. After that a saturation with a 500 ml/min of a gas mixture composed of 1 % NO in N_2 balance was performed for 30 min. Then, the catalyst was treated for 30 min with a 500 ml/min N_2 in order to eliminate the NO from the measurement chamber and a $DRIFT$ experiment was obtained. In order to corroborate if the adsorbed species could be eliminated through a chemical reduction, a 500 ml/min gas mixture composed of 1 % H_2 in N_2 balance was dosed for 5 min. After reduction, another $DRIFT$ spectrum was done.

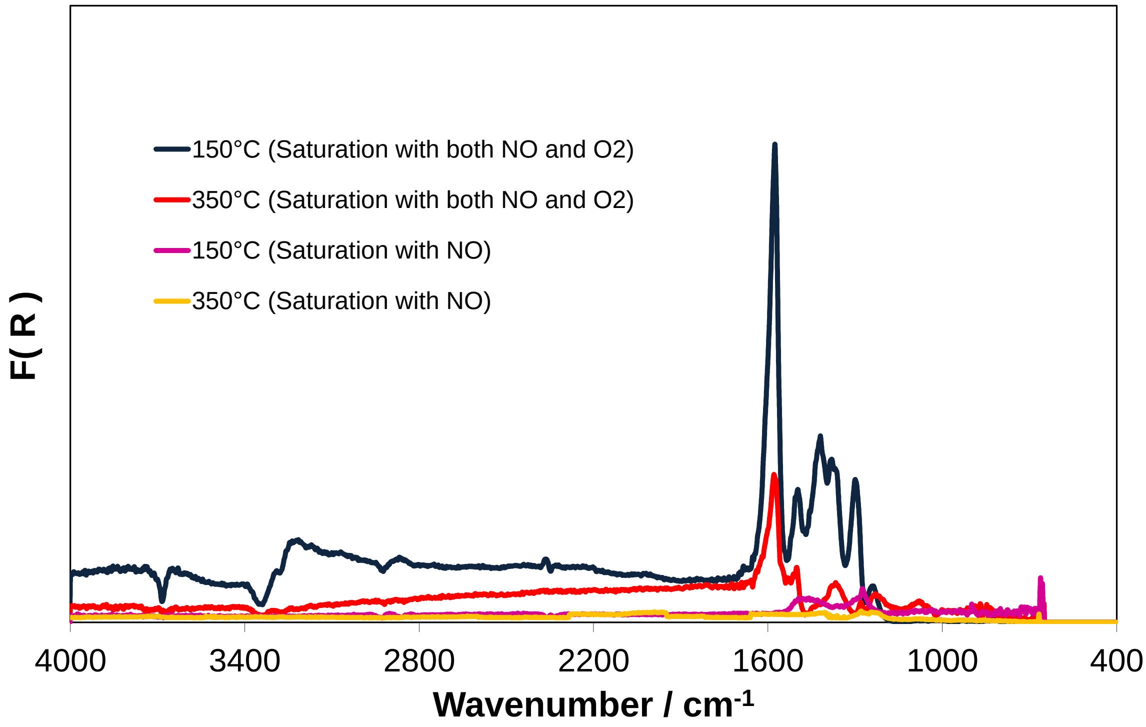

FIGURE 7.36. $DRIFT$ spectra obtained with a NiO/YSZ sample

When the saturation took place at 150°C, two small bands at 1260 and 1480 cm^{-1} appeared in the $DRIFT$ spectrum which can correspond to the surface $MONOM$ nitrite [**112**]. When the saturation took place at 350°C, no $DRIFT$ signals were obtained. A comparison of the results of the $DRIFT$ experiments on the NiO/YSZ catalyst when oxygen was present during saturation and when it was not are shown in fig. 7.36.

7.9.1.2. *Saturation with* $NO/O_2/N_2$ *and coupling of* $DRIFT$ *and mass spectrometry.*

As mentioned before, a coupling of $DRIFT$ and mass spectroscopy was done in order to obtain more information about the nitrogen-species storage and reduction process on the NiO/YSZ powder catalyst. For that purpose, the saturation conditions were $NO/O_2/Ar$ and the temperatures studied were 150 and 350°C.

A sample of the NiO/YSZ powder catalyst was used to make the $DRIFT$ experiment at 150°C. The sample was first heated at 450°C in Ar atmosphere (500 ml/min) in order to eliminate the nitrogen containing species which could be adsorbed on the catalyst surface. Then, the sample was cooled down to 150°C. After 15 min, background was detected until it remained stationary and then a $DRIFT$ experiment was obtained. After that, a saturation with a 500 ml/min of a gas mixture composed of 1 % NO and 10 % O_2 in Ar balance was done for 30 min. During the saturation, the NO, NO_2, N_2, H_2O, H_2 and O_2 productions were measured with a mass spectrometer. The results are shown in fig. 7.37. It can be observed, that only NO, O_2 and NO_2 was detected. Then, the catalyst was treated for 30 min with a 500 ml/min Ar in order to eliminate the NO and O_2 from the measurement chamber and a $DRIFT$ experiment was run.

The bands observed can be assigned as follows [**112**]. The band at 1240 cm^{-1} can correspond to the stretching vibration frequency of the $MONOM$ nitrite and the one at 1300 cm^{-1} can correspond to the stretching vibration frequency of the $MOONO$ nitrate. In both cases, a second peak should appear about 1500 cm^{-1}. As can be seen on the $DRIFT$ spectrum, a wide band about 1500 cm^{-1} is also present. The peaks at 1390 and 1420 cm^{-1} can correspond to the formation of the MNO_2 nitrite. The band at 1380 cm^{-1} can correspond to NO_3^-. If NO_2^- is also present on the catalyst surface, a peak at 1260 cm^{-1} should be observed. Due to the signals overlapping, it is not possible to conclude from the $DRIFT$ results if the storage of inorganic nitrites also takes place or not. The band at 1580 cm^{-1} correspond to the nitro-species which are coordinated to the Zr^{4+} Lewis-acid [**135**].

In order to corroborate if the adsorbed species could be eliminated through a chemical reduction, a 500 ml/min gas mixture composed of 1 % H_2 in Ar balance was dosed for 5 min. During the reduction, the NO, NO_2, N_2, H_2O, H_2 and O_2 production were masured with a mass spectrometer. The results are shown in fig. 7.38. After that, another $DRIFT$ spectrum was obtained. The results obtained from the $DRIFT$ experiments done at 150°C are shown in fig. 7.41.

During the saturation, NO_2 production was detected. During the reduction, no NO, NO_2, N_2, H_2O or O_2 was produced and the characteristic nitrate and nitrite bands remained unchanged.

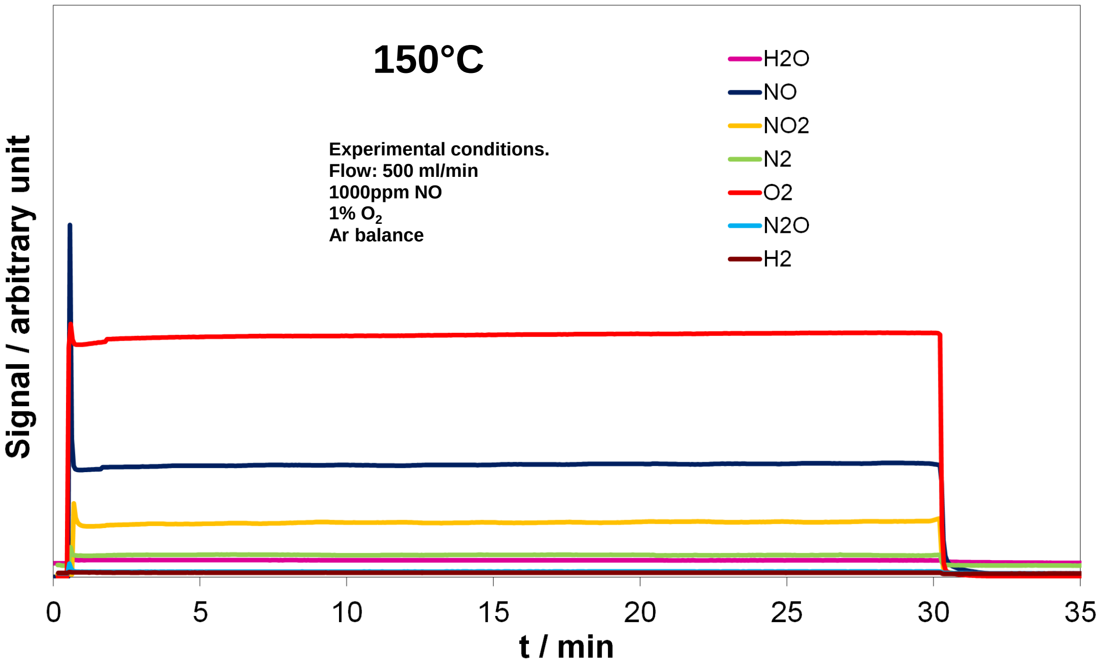

FIGURE 7.37. Gas production during the saturation at 150°C

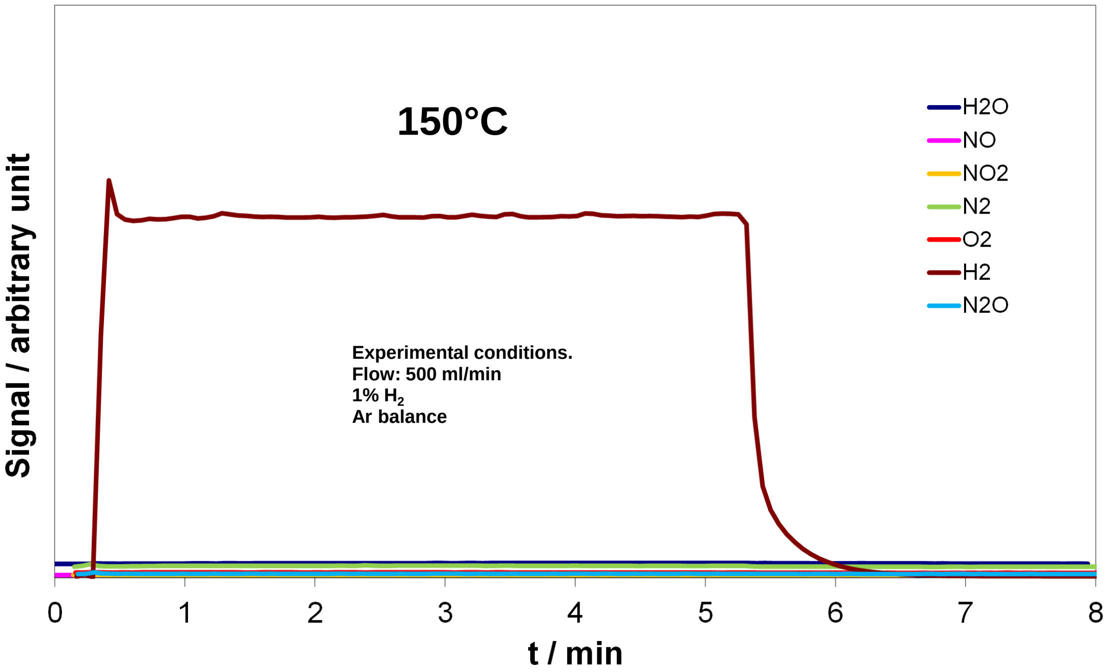

FIGURE 7.38. Gas production during the sample reduction at 150°C

A sample of the NiO/YSZ powder catalyst was used to make the $DRIFT$ experiment at 350°C. The sample was first heated at 450°C in Ar atmosphere (500 ml/min) in order to eliminate the nitrogen containing species which could be adsorbed on the catalyst surface. Then, the sample was cooled down to 350°C. After 15 min, background was detected until it remained stable and then a $DRIFT$ experiment was obtained. After that a saturation with a 500 ml/min of a gas mixture composed of 1 % NO and 10 % O_2 in Ar balance took place for 30 min. During the saturation, the NO, NO_2, N_2, H_2O, H_2 and O_2 production were measured with a mass spectrometer. The results are shown in fig. 7.39. Then, the catalyst was treated for 30 min with a 500 ml/min Ar in order to eliminate the NO and O_2 from the measurement chamber and a $DRIFT$ experiment was done.

The bands could be assigned as follows [**112**]. The band at 1290 cm^{-1} can correspond to the $MONO_2$ or the $MOONO$ nitrates and the band at 1240 cm^{-1} could be assigned to the $MONOM$ nitrite. In the case in which the $MONO_2$ nitrate is stored, a second band in the wavelength interval between 1530 and 1480 cm^{-1} should appear. For the $MOONO$ nitrate another signal between 1565 and 1500 cm^{-1} should be obtained and for the $MONOM$ a signal between 1520-1390 cm^{-1} should be observed. In the $DRIFT$ spectrum a wide band in the wavelength range between 1490 and 1560 cm^{-1} is achieved which may corroborate the storage of the three mentioned nitrogen species. The two bands at 1060 and 1450 cm^{-1} could be assigned to the $MONO$ nitrite. The band observed at 1380 cm^{-1} can correspond to the presence of NO_3^- species. If NO_2^- is also present on the catalyst surface, a peak at 1260 cm^{-1} should be observed. Due to the signals overlapping, it is not possible to conclude from the $DRIFT$ results if the storage of inorganic nitrites also take place or not. The band at 1580 cm^{-1} correspond to the nitro-species which are coordinated to the Zr^{4+} Lewis-acid [**135**].

In order to corroborate if the adsorbed species could be eliminated through a chemical reduction, a 500ml/min gas mixture composed of 1 % H_2 in Ar balance was dosed for 5 min. During the reduction, the NO, NO_2, N_2, H_2O, H_2 and O_2 production were measured with a massenspectromether. The results are shown in fig. 7.40. After that, another $DRIFT$ spectrum was obtained. The results obtained from the $DRIFT$ experiments done at 350°C are shown in fig. 7.42.

During the saturation, NO_2 production was detected. During the reduction, NO and H_2O were detected and the $DRIFT$ experiment run after the reduction treatment showed no signals.

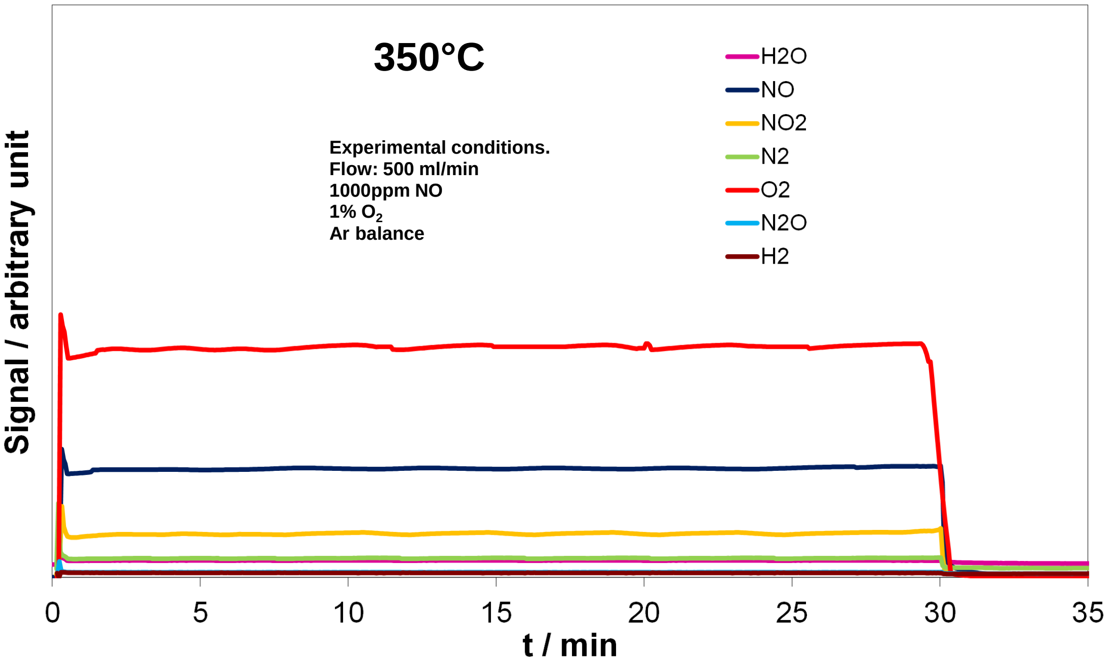

FIGURE 7.39. Gas production during the saturation at 350°C

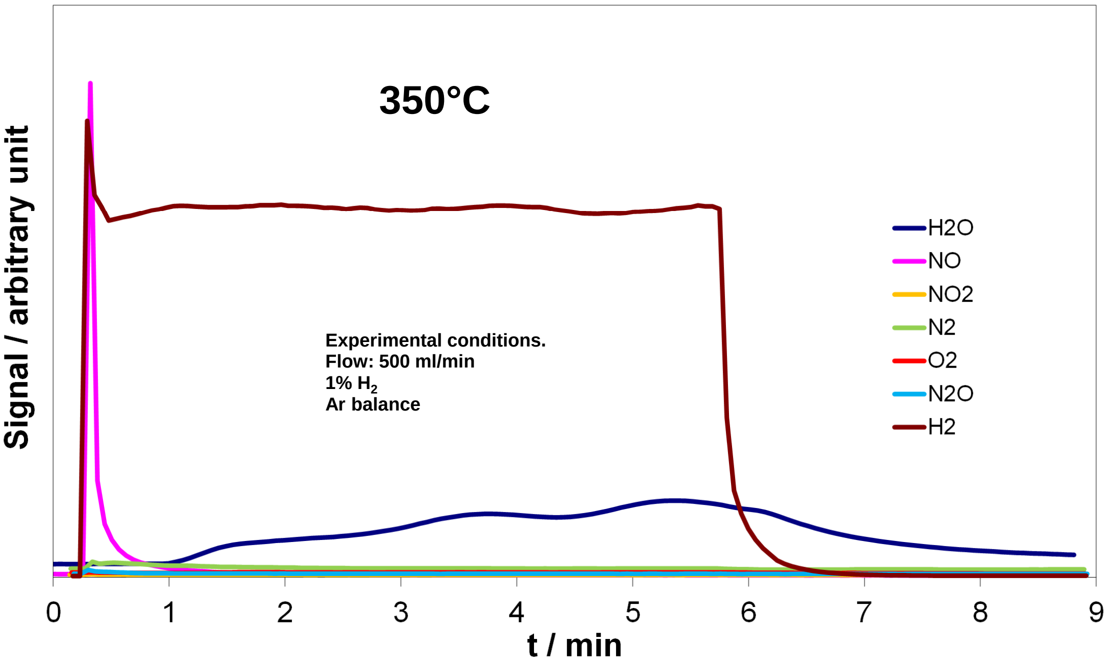

FIGURE 7.40. Gas production during the sample reduction at 350°C

7.9.2. Pure YSZ powder.

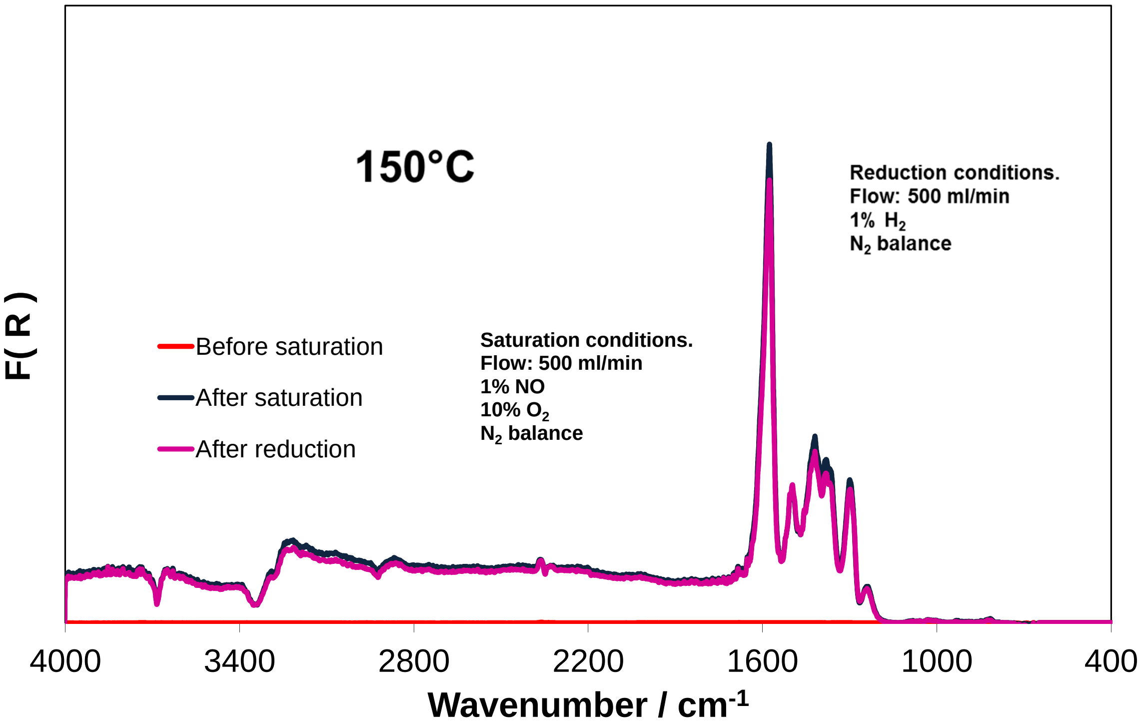

FIGURE 7.41. *DRIFT* spectrum on the NiO/YSZ catalyst at 150°C before and after reduction

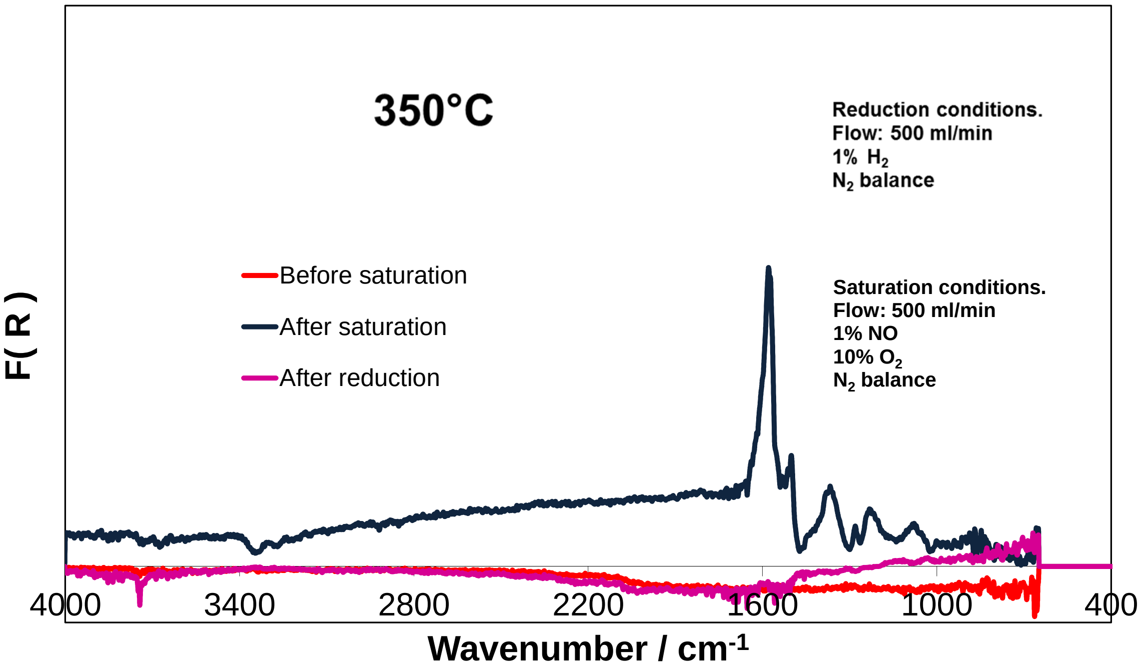

FIGURE 7.42. *DRIFT* spectrum on the NiO/YSZ catalyst at 350°C before and after reduction

7.9.2.1. *Saturation with* $NO/O_2/N_2$. *DRIFT* experiments were also performed with a sample of pure YSZ in order to elucidate whether NiO or YSZ were responsible of the nitrogen-species storage on the NiO/YSZ powder catalyst.

The YSZ powder sample was first heated at 450°C in N_2 atmosphere (500 ml/min) in order to eliminate the nitrogen containing species which could be adsorbed on the catalyst surface. Then, the sample was cooled down to the temperature chosen to make the experiment (150 or 350°C). After 15 min, background was detected until it remained stationary and then a $DRIFT$ experiment was run. After that a saturation with a 500 ml/min of a gas mixture composed of 1 % NO and 10 % O_2 in N_2 balance took place for 30 min. Then, the catalyst was treated for 30 min with a 500 ml/min N_2 in order to eliminate the NO and O_2 from the measurement chamber and a $DRIFT$ experiment was run. The experimental results are illustrated in fig. 7.43. The scale of the YSZ $DRIFT$ spectra is the same than the scala utilized to represent the $DRIFT$ results obtained on the NiO/YSZ powder catalyst.

Very small bands were obtained after saturation at 150°C which can be assigned as follows [**112**]. The bands at 1629 and 1224 cm^{-1} can correspond to the stretching vibration frequency of the $MONOOM$ nitrate. The band at 1294 cm^{-1} can correspond to the $MOONO$ nitrate and the shoulder observed at 1276 cm^{-1} can correspond to the $MONO_2$ nitrate. If both $MONO_2$ and $MOONO$ are stored on the YSZ surface, each species should present another band in the range 1565-1488 cm^{-1}. In the $DRIFT$ spectrum obtained, a wide band at 1517 cm^{-1} is achieved. The wide bands at 1224 and 1517 could also correspond to the stretching vibration frequency of the $MONOM$ nitrite. The bands at 1918 and 1996 cm^{-1} could correspond to the adsorption of NO as $M^{-}NO^{+}$. The two negative signals which appear at 3696 and 3765 cm^{-1} correspond to the OH groups which are bonded to the Zr atoms.

The bands achieved after saturation at 350°C can be assigned as follows [**112**]. The bands at 1631 and 1186 cm^{-1} can correspond to the stretching vibration frequency of the $MONOOM$ nitrate. The bands at 1284 and 1504 cm^{-1} can correspond to the $MONO_2$ or the $MOONO$ nitrate. It is not possible to distinguish between both species since the characteristic frequency region where those compounds should give signals overlap. The same occurs with the nitrites. Since the bands obtained are not narrow enough and the nitrite regions overlap with the nitrate regions, it is not possible to assert or deny the presence of nitrites on the YSZ surface after saturation. The band at 1861 could correspond to the adsorption of NO as M:NO and the signal at 1900 cm^{-1} could correspond to the adsorption of NO as $M^{-}NO^{+}$. The two negative signals which appear at 3698 and 3755 cm^{-1} correspond to the OH groups which are bonded to the Zr atoms.

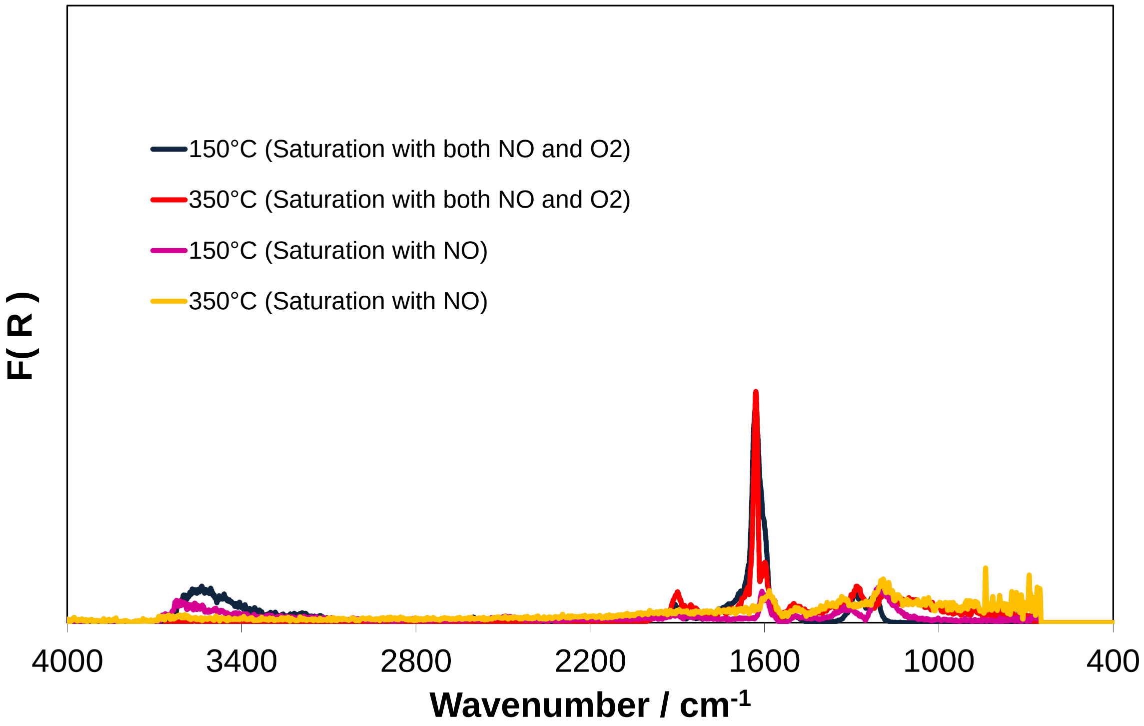

FIGURE 7.43. *DRIFT* spectrum on the *YSZ* powder sample.

7.9.2.2. *Saturation with* NO/N_2.

The *YSZ* powder sample was first heated at 450°C in N_2 atmosphere (500 ml/min) in order to eliminate the nitrogen containing species which could be adsorbed on the catalyst surface. Then, the sample was cooled down to the temperature chosen to make the experiment (150 or 350°C). After 15 min, backgrounds were run until it remained stable and then a *DRIFT* experiment was run. After that a saturation with a 500 ml/min of a gas mixture composed of 1 % *NO* in N_2 balance took place for 30 min. Then, the catalyst was treated for 30 min with a 500 ml/min N_2 in order to eliminate the *NO* from the mesurament chamber and a *DRIFT* experiment was run.

As can be observed in the graphics, no absorption peaks were obtained neither at 150 nor at 350°C after saturation when no oxygen was present in the gas mixture.

CHAPTER 8

Discussion of the experimental results

8.1. Storage of nitrates and nitrites on the NiO/YSZ powder catalyst

For the evaluation of the NO_x decomposition activity, the NO_x conversion rate ($X(NO_x)$) as defined in equation 7.4 was utilized. It indicates the amount of nitrogen oxides which could be removed from the gas phase as a consequence of the catalyst performance. Since such a removal could occur as a consequence of not just the NO_x decomposition in order to build N_2 and O_2 but also as a result of the NO_x storage in form of nitrates and nitrites, the experimental conditions at which the nitrogen oxides are stored should be determined. A NO_x storage on the surface of different catalyst was already reported [**104**].

The NO_x-TPD experiments have shown that nitrogen-containing species storage can mainly be found when the saturation occurs at 150 and 250°C. A very small storage was found when the saturation took place at 350°C and finally no storage was found at temperatures above 450°C since no NO_x desorption band was achieved at temperatures higher than 450°C during the TPD experiments.

NiO may be the responsible for that storage since the amount of stored species on pure YSZ is much smaller than the one achieved on the NiO/YSZ catalyst as the $DRIFT$ and TPD experiments show. In the comparison of the $DRIFT$ results obtained with the NiO/YSZ catalyst and the YSZ powder, the color of both solids should be taken to consideration. The NiO/YSZ powder is a very dark blue (almost black) solid and the pure YSZ powder is completely white. The $DRIFT$ technology measures the radiation which is reflected and diffuse scattered from the sample. The darker a material is, the more radiation it absorbs, the signal expected from a white material should be larger than the one obtained with a dark material when the same amount of adsorbed species are present on the material surface. In conclusion, the difference between the amount of nitrates and nitrites stored on the NiO/YSZ and YSZ powder may be larger than the one that can be observed by comparing directly the intensities of the $DRIFT$ signals obtained in the experimental spectra.

8.1.1. Nature of the stored species.

Information about the nature of the stored nitrogen-containing compounds could be achieved from the $DRIFT$ and the O_2-NO_x-TPD experiments.

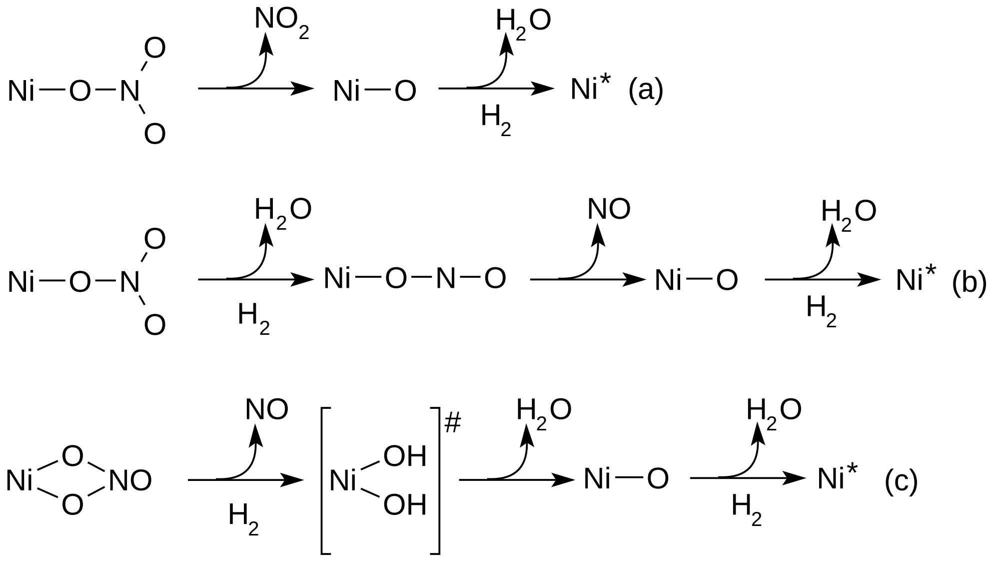

FIGURE 8.1. Reduction of the surface nitrates $MONO_2$ and $MOONO$ with H_2.

Due to the similar symmetry of the nitrato species (C_{2v}), their characteristic signals in the $DRIFT$ spectrum overlap. Hence, their unequivocal assignment in the $DRIFT$ spectrum is not possible. The identification of the stored compounds can just lead us to the conclusion that probably $MONO_2$, $MOONO$, $MONO$, $MONOM$ (these surface nitrates and nitrites are illustrated in fig. 7.35) and NO_3^- are stored on the catalyst surface when the saturation took place at 350°C in presence of oxygen. The presence or absence of another surface and inorganic nitrogen species can not be determined by using $DRIFT$ due to the signal overlapping. The NO, NO_2 and H_2O detection performed during the reduction treatment can add some information which could be helpful in the discussion of that aspect. If we consider that $MONO_2$ nitrates were stored on the catalyst, the surface reduction could occur according to two mechanism which are illustrated in fig. 8.1 (a) and (b). One possible mechanism would involve the elimination of a NO_2 molecule giving rise to the formation of NiO on the catalyst surface. The NiO could then be reduced by the hydrogen and the formation of water should take place. Other possible mechanism could involve first the reduction of the $MONO_2$ nitrate to the $MONO$ nitrite which would give rise to the production of water molecules. Then, the $MONO$ nitrite could be reduced resulting in the elimination of a NO gas molecule and the formation of NiO on the catalyst surface which then could be reduced in order to produce water and Ni atoms. Then, if $MONO_2$ is stored on the catalyst surface, whether a water production should be observed after the NO_2 production has finish or first a water detection is achieved and only after that a NO production occurs.

If $MOONO$ nitrates were stored on the catalyst surface, a reduction mechanism can be proposed as fig. 8.1 (c) illustrates. The first step of the $MOONO$ reduction could be the elimination of a NO molecule and the reduction of the two oxygen atoms which remain adsorbed on the Ni active center giving rise to the formation of the intermediate $Ni(OH)_2$. The dehydration of the $Ni(OH)_2$ intermediate would lead to water elimination and the formation of NiO which then can be reduced by the H_2 giving rise to the formation of water and Ni atoms. Then, if the $MOONO$ nitrate is stored on the catalyst surface, during its reduction, the water production should occur just after the NO elimination has been completed.

The experimental results indicate that no $MONO_2$ but $MOONO$ nitrates may mainly be the adsorbed species on the NiO/YSZ catalyst surface when the saturation takes place at 350°C in presence of oxygen since NO production occurs before a H_2O emission is detected and no NO_2 was achieved during the reduction. The supposition that also $MONO$ and $MONOM$ would be stored on the catalyst surface also fits the experimental results since in that case a NO desorption should first occur and then the oxygen which remains adsorbed may be reduced by the H_2 giving rise to water elimination.

After saturation at 150°C in presence of oxygen, it seems to be clear from the $DRIFT$ experiments that both nitrites and nitrates were stored on the catalyst surface.

These results correlate with the NO_x - O_2 TPD experiments after saturation at 150°C in presence of oxygen which also indicate that both nitrates and nitrites are stored on the catalyst surface. After saturation at 150°C, the first NO desorption band occurs at a temperature at which no O_2 desorption is achieved, which can be mainly due to the decomposition of the $MOONO$ nitrates giving rise to the elimination of NO molecules. The two oxygen atoms may remain adsorbed on the nickel atom as NiO_2 since the $Ni-O$ bond is so strong that it can not be broken at 150°C as could be confirmed by the O_2 TPD experiments which show no significant O_2 desorption at temperatures below 500°C. At the temperature at which the first NO desorption occurs, a very small NO_2 desorption band is achieved which can correspond to the decomposition of the MNO_2 nitrite. The second NO desorption band occurs at a temperature at which also NO_2 and O_2 desorptions are achieved. That can correspond to the thermal decomposition of the inorganic nitrates and nitrites as shown in equation (7.9) and (7.10).

After saturation at 150°C the nitrate decomposition balance done in the second desorption band (section 7.7), which may correspond to the decomposition of the inorganic nitrates or nitrites, shows that the amount of O_2 desorbed (37 μmol) is lower than the amount of O_2 expected to be desorbed if only nitrates were stored on the catalyst surface (38.5 μmol) and the amount of O_2 desorbed (37 μmol) is larger than the amount of O_2 expected to be desorbed if only nitrites were stored on the catalyst surface (32 μmol) which may indicate that both nitrites and nitrates are stored on the catalyst surface when the saturation took place at 150°C in presence of oxygen.

8.1.2. NO_x storage mechanism.

A mechanism for the NO_x storage on the NiO/YSZ surface catalyst could be proposed and it is illustrated in fig. 8.2.

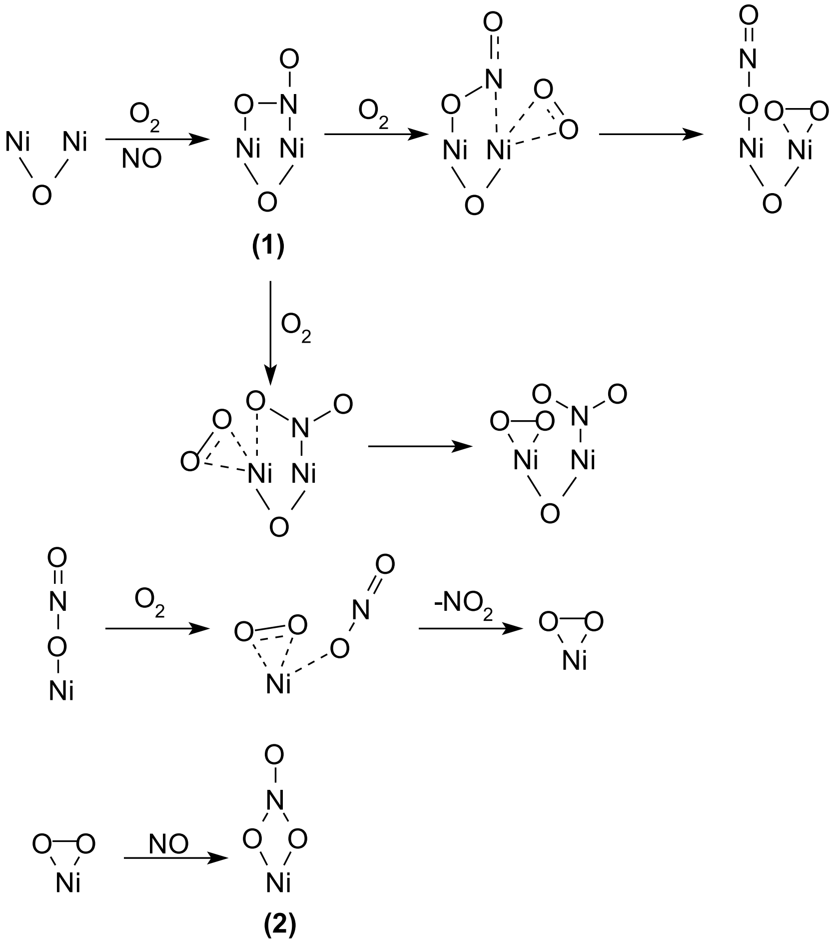

FIGURE 8.2. NO_x storage mechanism on the NiO/YSZ catalyst

The oxygen molecules can dissociatively adsorb on the Ni active centers of the catalyst and the adsorption of NO molecules on the Ni atoms which are close to the NiO could lead to the formation of the $NiONONi$ nitrite (indicated as (1) in fig. 8.2). Then the co-adsorption of oxygen molecules on the $NiONONi$ nitrite could promote the formation of both $NiONO$ and $NiNO_2$ nitrites. The co-adsorption of another oxygen molecule on the Ni atom of the $NiONO$ nitrite followed by the desorption of a NO_2 gas molecule results in the formation of NiO_2 which can then react with a NO molecule giving rise to the formation of $NiOONO$ (indicated as (2) in fig. 8.2). That mechanism correlates with the experimental results achieved by the $DRIFT$ experiments since just the nitrites and nitrates involved in the mechanism could be detected on the $DRIFT$ experiments. Till C. Brüggemann and Frerich J. Keil [**108**] proposed a similar surface mechanism for the oxidation of NO to NO_2 on iron-exchanged $ZSM5$ in which an O_2 co-adsorption also takes place. The mechanism shown in fig 8.2 would explain then, the NO_x storage on the NiO/YSZ surface catalyst and also why the NO_2 formation is observed when O_2 molecules are present in the reactive gas mixture and no NO_2 formation is observed in absence of O_2 even when oxygen is already adsorbed on the catalyst surface (section 8.5).

As the proposed mechanism illustrates (fig. 8.2), only the storage of the $NiONONi$ nitrite does not need the participation of oxygen molecules. As a consequence of that, if the saturation gas mixture does not contain O_2 molecules, the $NiONONi$ nitrite would be the only nitrogen-containing specie stored on the catalyst surface. The experimental results obtained from the $DRIFT$ experiments corroborate the mechanism proposed since just the $NiONONi$ nitrite was detected when no oxygen was present during the saturation.

8.2. Regeneration of the active centers of the catalyst

During the performance of the catalyst, the oxygen resulting from the NO_x decomposition reaction remains strongly adsorbed on the catalyst surface which leads to its poisoning and therefore to its deactivation. In addition, when the catalyst works at 350, 250 and 150°C, nitrates and nitrites are stored on its surface and oxidizes the Ni active centers.

The thermal regeneration of the active centers of the catalyst by heating it at 450°C can remove the nitrates and nitrites which could be adsorbed on the NiO/YSZ surface as the TPD experiments have shown but that thermal treatment can not remove the oxygen adsorbed on the catalyst. In order to do so, the catalyst should be heated at 800°C as the O_2 TPD showed.

$$Ni - (nitrates/nitrites) \overset{450°C}{\rightarrow} Ni - O + NO + NO_2 + O_2 \tag{8.1}$$

$$2\,Ni - O \overset{800°C}{\rightarrow} 2\,Ni^* + O_2 \tag{8.2}$$

The problem in the case of the NiO/YSZ catalyst is that a phase transition occurs when the YSZ is heated at temperatures higher than 600°C which may result in a change of the catalyst structure (fig. 8.4).

Another way of regenerating the active centers of the catalyst is its reduction with hydrogen. As discussed in section 8.1, the reduction of the catalyst surface at 350°C could lead to the elimination of the stored nitrates and nitrites and the reduction of the NiO surface. After reduction with H_2, the Ni active centers of the catalyst are reduced which may originate the enhancement of the catalyst NO_x decomposition activity. That supposition correlates with the experimental results since a higher catalytic activity was achieved after reduction treatment with H_2 at 450°C. The reduction time is also a parameter to be considered. A longer reduction can regenerate more active centers. Therefore, an improvement of the catalytic activity with the reduction time as indicated by the experimental results obtained when the reduction took place for 1 and 2 min can be achieved.

The regeneration of the active centers of the catalyst can also be achieved making use of an electrochemical cell which could pump the oxygen out of the catalytic system as indicated in fig 8.3. That would lead to the continuous regeneration of the catalyst active centers and therefore, the NO_x conversion rate should remain stationary with the cell operating time at a constant voltage value. The results achieved during the electro-catalytic NO_x decomposition experiments corroborates that assertion since no changes in the NO_x conversion rates with time were observed at a fixed voltage value. The nitrogen oxide decompose first in the cathode and the oxygen remains adsorbed on the catalyst surface giving rise to the oxidation of the Ni active centers. Then, the oxygen can diffuse through the lattice of an oxygen ions conductor to the anode where its oxidation and elimination can take place. For that regeneration to work efficiently, the choose of a good O^{2-} conductor is an important matter. Since the 19th century it is known that some solid materials, mainly polycrystalline compounds, can present the requested conduction properties [**97**]. One of the best studied solid electrolytes is the ZrO_2. As observed in the phase diagram in fig. 8.4 [**98**], ZrO_2 is presented in the monoclinic phase at room temperature. The transition to the tetragonal phase occurs around 1100°C and up to 2200°C the cubic phase can be found.

The volume expansion originated by the transition from the tetragonal to the cubic phase and from the monoclinic to the tetragonal modification, leads to high tensions in the ZrO_2 structure which originates the material to break up when it is cooled down from elevated temperatures. In order to stabilize the cubic phase

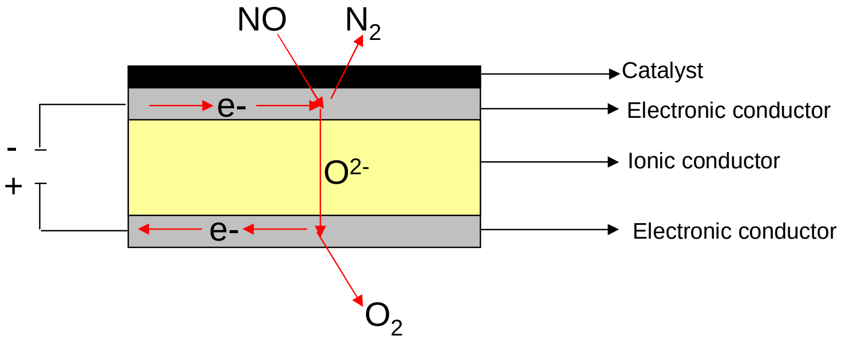

FIGURE 8.3. Electrocatalytic cell

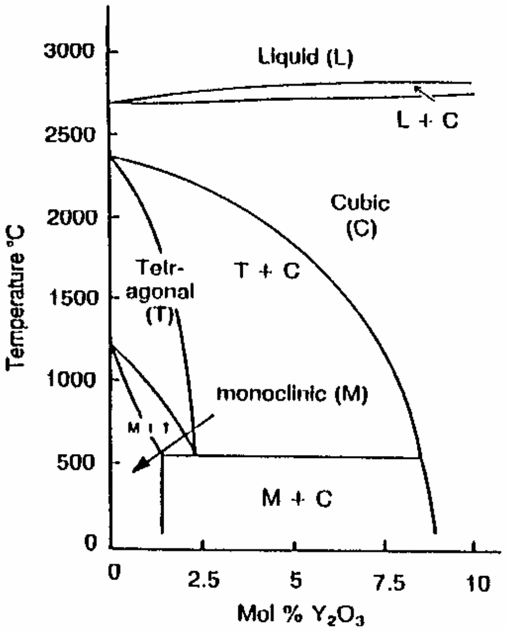

FIGURE 8.4. YSZ phase diagramm

at room temperature, an amount of Zr^{4+} cations can be substituted by M^{2+} (like Ca^{2+} or Mg^{2+}) or M^{3+} cations (like Ce^{3+}, Sc^{3+} or Y^{3+}). In the case in which the substitution is made with Y^{3+}, the resulting compound is represented as YSZ. YSZ is a ceramic oxide in which the cubic phase of the ZrO_2 has been stabilized at room temperature by adding Y_2O_3. That substitution results in the formation of oxygen vacancies since two O^{2-} ions are substituted by four O^{2-} ions and the formation of oxygen vacancies is necessary in order to maintain the crystalline net neutrality. The formation of oxygen vacancies is responsible for the O^{2-} conducting character of the YSZ solid electrolyte. That property increases as the temperature increases and makes the YSZ an adequate material in solid fuel cells applications. When the stabilization is done with Sc^{3+} the best O^{2-} conductivities are obtained due to the greater resemblance of the size of both Sc^{3+} and Zr^{4+} ions which originates a lower destabilization of the crystalline structure. However, for economical reasons, the most used doping agent is the Y^{3+}.

The external voltage applied between the cathode and the anode originates a polarization of the YSZ solid electrolyte which lead to a O^{2-} flow from the YSZ region which is close to the cathode to the YSZ region close to the anode. That process is promoted by the presence of oxygen vacancies in the YSZ solid electrolyte. The O^{2-} diffusion of oxygen ions through the YSZ lattice gives rise to a high concentration of oxygen vacancies in the near cathode region and as a consequence of that, the adsorbed oxygen resulting from the NO_x decomposition reaction on the catalyst active centers can be removed as equation (8.3) indicates.

$$2\,NO \;+\; 4\,e^- \;+\; V_0(ZrO_2) \;\rightarrow\; N_2 \;+\; 2\,O^{2-}(ZrO_2) \tag{8.3}$$

Once the O^{2-} ions reach the anode, they oxidize and the elimination of oxygen molecules take place as indicated in equation (8.4)

$$2\,O^{2-}(ZrO_2) \;\rightarrow\; O_2 \;+\; V_0(ZrO_2) \;+\; 4\,e^- \tag{8.4}$$

8.3. Activity of the NiO/YSZ powder catalyst

The exothermic decomposition of the NO_x compounds is so strongly kinetically hindered so that it only occurs at high temperatures (1100-1200°C). The temperature needed for that reaction to take place can be decreased by using a catalyst.

The active element of the catalyst studied in this work chosen for the NO_x decomposition reaction was Ni since previous studies have proved its high catalytic activity. Y. Yokoi and H. Uchida [**73**] compared the catalytic activity in the decomposition of NO presented by different mixed lanthanum transition metal oxides (perovskite like structures) with the chemical composition $LaMO_3$ where M is a transition metal of the first period and they found that the conversion of NO to N_2 and to O_2 at 700 and 600°C is clearly higher when the transition metal is Ni. The NO reduction on a Ni catalyst has been reported in the literature. According to these works, the nitrogen oxide molecules first adsorbs on the Ni active centers and then, the recombination of the nitrogen atoms of two adsorbed NO molecules take place giving rise to the formation of gas N_2 molecules as described in equations (8.5) and (8.6)

$$2\,NO\,+\,2\,Ni^{*}\,\rightarrow\,2\,Ni-NO \tag{8.5}$$

$$2\,Ni-NO\,\rightarrow\,N_2\,+\,2\,Ni-O \tag{8.6}$$

Two mechanism could be proposed for the NO adsorption and decomposition in order to form N_2. They can involve whether the vertically NO adsorption or the dissociative NO adsorption on the catalyst surface.

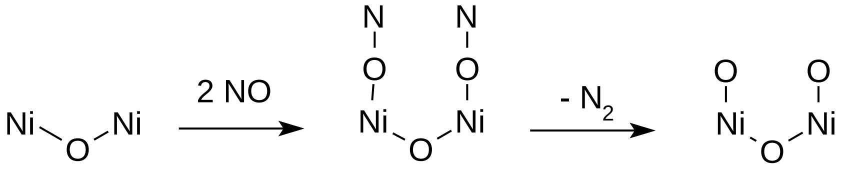

FIGURE 8.5. NO decomposition mechanism

The first mechanism illustrated in fig. 8.5 proposes that the NO molecules are first vertically adsorbed through the oxygen atom. The nitrogen atom of two adsorbed NO molecules could then recombine giving rise to the formation of N_2. The NO molecule has an isolated electron pair (5σ), which is characterized by a higher energy than that on the oxygen atom. Hence, coordination and adsorption are expected to occur from the nitrogen atom [**112**]. Previous studies done with near-edge x-ray adsorption fine structure (NEXAFS) [**116**], photoelectron diffraction (PED) experiments [**117**] - [**118**] and DFT and DFT+U calculations [**121**] have demonstrated that NO adsorbs through the nitrogen atom on the Ni atoms. Therefore, a different mechanism in which the NO adsorption does not take place vertically should operate. The NO molecules could also dissociatively adsorb on the catalyst surface and then the recombination of two adsorbed nitrogen atoms could lead to the formation of N_2.

The dissociative adsorption of the gas NO molecules could occur on two Ni atoms. Another possibility would be that the nitrogen atom would adsorb on a Ni atom and the oxygen atom on a YSZ oxygen vacancy. Then the recombination of the adsorbed nitrogen atoms could occur in order to form nitrogen molecules as shown in equations 8.7 and 8.8 where $*$ indicates an oxygen adsorption site (Ni or oxygen vacancy).

$$NO\,+\,*\,+\,Ni\,\rightarrow\,Ni-N\,+\,*-O \tag{8.7}$$

$$2\,Ni - N \rightarrow N_2 + 2\,Ni \tag{8.8}$$

Both the NO dissociation and the recombination reaction of the adsorbed nitrogen atoms have an activation energy which must be supplied for the N_2 formation to occur. As the experimental temperature increases, more NO molecules would be able to adsorb dissociatively on the catalyst surface and also more adsorbed nitrogen atoms will have the necessary energy to allow its recombination and as a consequence, more gas nitrogen molecules will be formed. Hence, an increase in the catalytic activity of the NiO/YSZ catalyst in the formation of N_2 with the temperature is expected. That tendency is observed in the experimental results but the catalytic activity achieved was very low even at 550°C. The reason for that behavior is that the species which are adsorbed on the NiO/YSZ powder catalyst during its performance occupy the Ni active centers giving rise to its poisoning. Therefore, no stationary state can be reached during the activity experiments since a continuous NO_x decomposition can not be achieved as observed in the experimental results even when no oxygen was present in the gas mixture. The experimental results show a 100 % conversion rate just during the first seconds of the experiments and its rapid decrease with the operating time so after one or two minutes no NO_x conversion at all is achieved. In order to enhance the catalyst activity, a regeneration of the Ni active centers of the catalyst must be performed. The experimental results show that the catalytic activity of the NiO/YSZ in the decomposition of the nitrogen oxides could be clearly improved after reduction treatment with H_2. The catalytic activity also depends on the reduction time. The catalyst was more active when the reduction took place during 2 min than when the reduction was performed for 1 min since more active centers could be regenerated.

At 550, 450 and 350°C and in absence of O_2, the only reaction that occurs is the decomposition of NO_x in order to build N_2 which indicates that the selectivity of the NiO/YSZ catalyst in the N_2 formation is 100 %. At 250 and 150°C, the selectivity of the catalyst in the formation of N_2 drops since N_2O formation (see section 8.4) is also observed. No NO_2 production is observed at any temperature studied when the experiments took place in oxygen absence (see section 8.5)

When O_2 was also dosed during the NO_x decomposition experiments, the catalytic activity strongly decreases if it is compared to the activity achieved when no oxygen was present in the gas mixture during the decomposition experiments. The reason for that is that the active component of the catalyst (Ni) has a very high affinity for the oxygen which compete with NO in the adsorption process on the catalyst surface and since the $Ni - O$ bond is very strong and can not be broken at the experimental temperatures, the catalyst deactivation occurs very fast. That adsorption of both O_2 and NO on the catalyst surface can be observed on the experimental results as during the first moments of the NO_x decomposition reaction at 450 and 550°C, when N_2 formation occurs, no O_2 and NO detection is achieved. Then, when the N_2 production decreases, the O_2 and NO detection starts since the active centers of the catalyst are already oxidized and the catalyst is no longer active. The catalyst selectivity in the formation of N_2 is lower than 100 % for all temperatures studied since a NO_2 formation take place (see 8.5).

8.4. N_2O formation on NiO/YSZ

The thermodynamic products of the NO decomposition reaction are N_2 and O_2 but the nitrogen oxide can also exist in equilibrium with N_2O as equation (7.2) indicates. HSC program calculations [**115**] have shown that as the temperature increases the equilibrium between NO and N_2O shifts to the NO formation. N_2O is also the kinetic product of the NO decomposition reaction.

When NO comes in contact with the NiO/YSZ catalyst surface, the adsorption of the nitrogen oxide molecules can occur both with and without dissociation. Then, there are two principal ways in which nitrogen atoms can be removed from the catalyst surface. Two nitrogen atoms can recombine in order to build N_2 or an adsorbed NO can recombine with a nitrogen atom giving rise to N_2O formation (fig. 8.6). Since the dissociative adsorption of the nitrogen oxide has an activation energy, the number of molecules which dissociatively adsorb on the catalyst surface would increase as the temperature increases. At low temperatures, there are less NO molecules which can dissociate and therefore, the probability of the recombination of two nitrogen atoms would be lower than the probability of the recombination of a NO molecule with a nitrogen atom. As the temperature rises, a larger number of NO molecules dissociate and the probability of the recombination of two nitrogen atoms increases. Hence, the majority product produced as a consequence of the NO decomposition at low temperatures should be N_2O and at higher temperatures the N_2. The experimental results corroborate that supposition since the majority product detected during the NO_x decomposition experiments when no oxygen was present in the gas mixture at low temperatures was N_2O and the majority product at high temperatures was N_2.

8.5. NO_2 formation on NiO/YSZ

The NO oxidation by oxygen on supported particles in order to build NO_2 has been previously studied. According to Mulla et al. [**106**], the O_2 molecule dissociates into two oxygen atoms as it adsorbs on the Pt surface. The NO molecules then, recombine with the oxygen atoms in order to build NO_2 as reactions 8.9 and 8.10

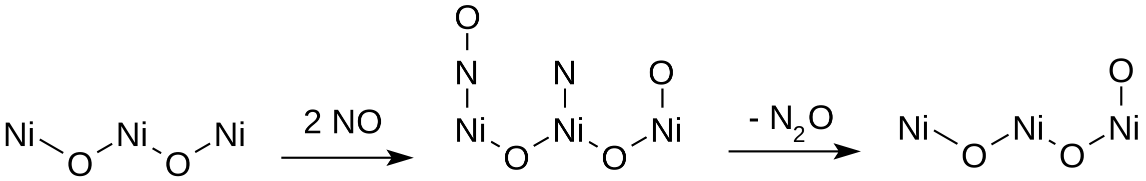

FIGURE 8.6. Formation of N_2O on the NiO/YSZ catalyst surface

show.

$$O_2 + 2* \rightarrow 2\,O^* \tag{8.9}$$

$$NO + O^* \rightarrow NO_2 + * \tag{8.10}$$

When NO and O_2 are present in the gas mixture during the NO_x decomposition experiments, NO_2 is produced but when just NO is present, no NO_2 formation was achieved at any of the temperatures studied. The experiments done at 550°C show that the decomposition of the NO molecules in order to produce N_2 and oxygen (which remains strongly adsorbed on the catalyst surface as $Ni - O$) takes place for about 40min, after that, the catalyst activity drops dramatically and after some minutes, no catalytic activity is no longer achieved since the saturation of the active centers with oxygen take place. Then, if the NO oxidation occurs according to the mechanism described by Mulla et al., NO_2 formation should be expected at some moment of the NO_x decomposition reaction since oxygen atoms are adsorbed on the catalyst surface even when no O_2 is dosed. For that NO oxidation to occur, the catalyst must bind oxygen strongly enough to promote O_2 dissociation but weakly enough to allow $O - NO$ bond formation. The first step of the oxidation is the dissociation of the O_2 molecule and the formation of the $Ni - O$ bond. For that to occur, the half of the bond energy of the O_2 (2.6 eV) has to be smaller than the $Ni - O$ bond energy and the $Ni - O$ bond energy has to be smaller than the $O - NO$ bond energy (3,2 eV). The second constraint is not met at all since the $Ni - O$ bond energy is much higher than 3.2 eV [**122**]. Thats the reason why the dosed NO molecules can not combine with the adsorbed oxygen atoms and no NO_2 production is observed during the NO_x decomposition experiments when no O_2 is present in the experimental gas mixture. The studies done by Mulla et al. are performed on a Pt based catalyst. In that case, the $Pt - O$ bond energy at some coverage values is high enough to promote the O_2 dissociation and low enough to allow the $O - NO$ bond formation [**107**].

When the gas mixture NO/O_2 was dosed in the NO_x decomposition experiments, NO_2 was produced. As discussed before, the $Ni - O$ bond is too strong to allow the recombination of the NO molecules with the adsorbed oxygen atoms and the mechanism of the NO oxidation by oxygen may not occur as described in the mechanism proposed by Mulla et al..

Till C. Brüggemann and Frerich J. Keil [**108**] proposed a surface mechanism for the oxidation of NO to NO_2 on iron-exchanged $ZSM5$ in which O_2 co-adsorption must take place. The mechanism is also consistent with the fact that the NO_2 production starts when the O_2 detection has already begun. When active Ni sites are still present on the catalyst, the oxygen and NO is then adsorbed there and no O_2 or NO is detected. At a certain moment of the experiment, no more active centers are free and then, O_2 detection is observed. Then, the oxygen start co-adsorbing on the $NiONO$ and the NO_2 formation takes place. A mechanism which explain the NO_2 formation and the NO_x storage on the catalyst surface could be proposed (fig. 8.2).

The NO_2 production increases as the temperature increases from 250 to 350°C since the oxidation reaction of NO with O_2 has an activation energy which has to be provided in order to occur. Ab 450°C, the NO_2 formation decreases as the temperature increases since at those temperatures the NO_2 formation is thermodynamically no longer favorable.

8.6. Electrocatalytic NO_x decomposition experiments

8.6.1. NO_x decomposition activity on a tubular reactor. The NO_x electrocatalytic decomposition occurs, as discussed in section 8.2, according to equations 8.3 and 8.4.

For that concept to work, the catalyst should be able to allow the O^{2-} ions to diffuse from its surface, where NO is adsorbed to the cathode and it should also permit that electrons make their way from the cathode to the catalyst surface in order to allow the reduction reaction to take place. Those two processes would be easier if the catalyst layer has a not too wide width and if it present pores which could also increase the contact surface between catalyst and gas phase. The composite NiO/YSZ, employing oxygen ion conducting yttria-stabilized zirconia (YSZ) and NiO, is an example of ionic-electronic conductivity. YSZ is a conductor of O^{2-} ions (section 8.2) and NiO is a typical metal deficient p-type semiconductor with cation vacancies and electron holes as primary defects. Pure stoichiometric NiO is an insulator [**87**]. The best NO_x decomposition activity is expected with the $Pt/YSZ/Pt/NiO - YSZ$ system since the electronic and the ionic conductor which compose the catalyst are mixed and the ionic and electronic conductivity of the catalyst should be higher than the one presented in the other tested systems.

The experimental results corroborate that supposition since the higher conversion rates were achieved with the $Pt/YSZ/Pt/NiO-YSZ$ system. When the post-impregnation was used to deposit the NiO layer on the YSZ coverage, the results were not so good since the achieved contact between NiO and YSZ was lower than the one obtained when the NiO powder and the YSZ paste were first mixed and then together calcinated.

The important role of the YSZ in the good performance of the electro-catalytic cell can be clearly appreciated if the results obtained with the $Pt/YSZ/Pt/NiO-YSZ$ and $Pt/YSZ/Pt-NiO$ systems are compared. The $Pt-NiO$ layer works as both catalyst and conductor of oxygen ions. The electronic conductivity of the $Pt-NiO$ catalyst is higher than the one presented by the $NiO-YSZ$ catalyst and since a reduction reaction should take place in order to regenerate the Ni active centers of the catalyst, that increase in the catalyst electronic conductivity should be advantageous. However, the catalytic activity achieved with the $Pt/YSZ/Pt-NiO$ system is insignificant. The reason for that is that even when the electronic conducting properties are high, the platinum cathode do not contain oxygen vacancies which could allow the adsorbed oxygen to diffuse to the YSZ ionic conductor. Hence the NO_x decomposition reaction is limited to the cases in which the gas molecules can diffuse through the catalyst pores to the catalyst regions which are located near to the Pt cathode.

The system $Pt/YSZ/Pt/YSZ/NiO$ synthesized by means of a post-impregnation presented a lower activity than the $Pt/YSZ/Pt/NiO-YSZ$ but its activity is higher than the one achieved with the $Pt/YSZ/Pt-NiO$ system. In both the $Pt/YSZ/Pt-YSZ$ and the $Pt/YSZ/Pt/YSZ/NiO$ (synthesized by means of a post-impregnation) systems, a lower electronic conducting capacity is obtained if it is compared with the $Pt/YSZ/Pt/NiO-YSZ$ system but the NiO layer obtained with the post-impregnation is thinner than the one in the $Pt/YSZ/Pt-NiO$ system which would lead to an easier NO diffusion through the pores from the catalyst surface to the cathode-near catalyst region where the NO_x decomposition reaction could take place. Hence, the post-impregnation system should present a better performance than the $Pt/YSZ/Pt-NiO$ but worse than the $Pt/YSZ/Pt/NiO-YSZ$ system as can be observed in the experimental results.

The only difference between the $Pt/YSZ/Pt/NiO-YSZ$, $Pt/YSZ/Pt/LaNiO_3-YSZ$ and $Pt/YSZ/Pt/La_2NiO_4-YSZ$ systems is the catalyst. For a good decomposition activity, the contact between the NO gas molecules and the $catalyst/YSZ$ border has to be as large as possible. For that to happen, a large catalyst specific surface area and a large catalyst total pore volume is advantageous. As the BET experiments have shown, the greater specific surface area and total pore volume is achieved with NiO which may make the $Pt/YSZ/Pt/NiO-YSZ$ system the most active of all. The specific surface area of La_2NiO_4 (12,174 m^2g^{-1}) is smaller than the one of $LaNiO_3$ (16,24 m^2g^{-1}) but the $LaNiO_3$ total pore volume is approximately double than the one of the La_2NiO_4. That may be the reason why the $Pt/YSZ/Pt/La_2NiO_4 - YSZ$ system is more active than the $Pt/YSZ/Pt/LaNiO_3 - YSZ$ system.

8.6.2. NO_x decomposition activity on a planar reactor. The reproducible preparation of the catalytic system has a crucial importance for the investigation and understanding of the electro-catalytic NO_x decomposition. In order to make the catalyst preparation easier and more reproducible, a planar reactor was prepared and tested. The preparation of the planar substrates is much easier than the preparation of the tubular reaction since the homogeneity of the catalyst layer can be better controlled. That should originate a better reproducibility in the experimental preparation of the system which should lead to a better reproducibility of the results. The results achieved when two different planar substrates were tested separately show the same NO_x conversion rates at the same voltage and current values. When one planar substrate was placed in the reactor as fig. 6.4 shows, a part of the mixture gas containing NO has no contact with the catalyst surface ("dead gas volume"). Hence, lower NO_x conversion rates should be achieved if they are compared with the results obtained with the tubular reactor. The experimental results are in accordance with that since a lower conversion rate is achieved with the planar reactor. In order to enhance the maximal conversion rated obtained with the planar reactor, the "dead gas volume" must be minimized. The use of two planar substrates in a "sandwich" conformation should decrease the volume of gas which has no contact with the catalyst surface. The electrochemical cell with one and two planar substrate can be described as shown in fig. 8.7.

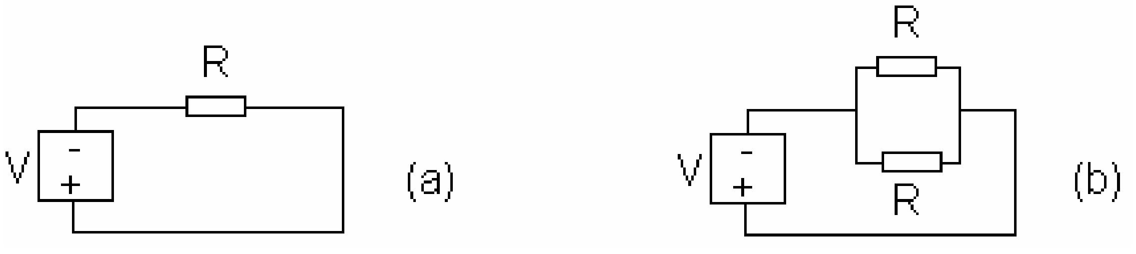

FIGURE 8.7. (a) Electrochemical cell with one planar substrate. (b) Electrochemical cell with two planar substrates.

Since both of the two planar substrate present the current value at each voltage, it is possible to assert that both substrates have the same resistance value indicated as R in the fig. 8.7. The resistance R_s of the electrochemical cell in which the two planar substrates are used can be calculated according to the equation 8.11.

$$\frac{1}{R_s} = \frac{1}{R} + \frac{1}{R} \tag{8.11}$$

Therefore, the resistance of the electrochemical cell in which two planar substrates are used in a "sandwich" conformation should be the half of the resistance of the electrochemical cell which uses just one planar substrate. According to the Ohm law (equation (8.12)), the voltage needed in order to obtain a current value with the cell which uses two planar substrates should be twice lower than the voltage needed to achieve the same current value with the one-substrate reactor. Since the current obtained in the experimental results is a consequence of the NO_x decomposition reaction which occurs in the cathode, the use of the "sandwich" configuration should allow us to achieve the same conversion rates and current values than in the case in which just one substrate is placed in the reactor but at lower voltage values. A higher maximal conversion rate should also be expected if the same voltage values are applied. As a conclusion, an improvement in the cell performance may be observed when two planar substrates in a "sandwich" configuration instead just one planar substrate are used. That can be observed in the experimental results.

$$V = I\,R \tag{8.12}$$

8.6.3. Selectivity of the electro-catalytic system. The theoretical current expected when NO is decomposed on the cathode for a NO decomposition rate value is calculated in appendix 10.4 and it is supposed to be around 67 mA in the case than 100 % NO_x conversion rate would be achieved. The current value obtained in the first experiments is much higer (about 850 mA) and that indicates that not just the reduction of the nitrogen oxides occur in the cathode. The oxygen molecules contained in the experimental gas mixture can also be reduced in the cathode (8.13) giving rise to an increase of the current obtained during the electrocatalytic decomposition of the nitrogen oxides and a decrease of the cell selectivity since less NO_x molecules can be decomposed on the cathode. That decrease of the cell selectivity in the NO_x decomposition when O_2 is also present in the gas mixture can be observed in the experimental results since an increase in the O_2 concentration leads to a decrease of the NO_x conversion rate at a fix curren value.

$$O_2 + 4\,e^- + V_0(YSZ) \rightarrow 2\,O^{2-}(YSZ) \tag{8.13}$$

Another process which could result in the decrease of the cell selectivity is the electrochemical decomposition of the ZrO_2 solid electrolyte [**109**]. As a consequence of both undesired reactions, the selectivity of the $Pt/YSZ/Pt/NiO-YSZ$ cell in the reduction of the nitrogen oxide when it operates in oxygen excess was very low.

8.7. Color change of the NiO/YSZ catalyst during the NO_x decomposition experiments

During the NO_x decomposition experiments a color change in the catalyst from dark-blue to pale-green with the cell operating time was achieved. The XRD and UV/Vis spectra show no change in the NiO structure. The color change may be originated by the transition from a non-stoichiometric NiO to a higher stoichiometric NiO. The dark blue NiO presents a non-stoichiometric structure with Ni defects which can be originated by nickel vacancies or the presence of interstitial oxygen and shows a p-type semiconductor behavior. The presence of interstitial oxygen in the NiO lattice should originate a lattice expansion which should lead to higher d_{hkl} values in the XRD spectrum compared with the ones obtained for the stoichiometric green NiO as can be deduced from equation (8.14).

$$\frac{1}{d_{hkl}^2} = \frac{h^2 + k^2 + l^2}{a^2} \tag{8.14}$$

Where:

d_{hkl} is the distance between two lattice planes

a is the distance between atoms in a cubic lattice

h, k, l are the Miller indices

Then, according to Bragg law (equation (5.6), an increase of the distance between two lattice planes would give rise to a decrease in the sinus of the Θ angle. Since the Θ angle measured in the XRD experiments appears in the range interval between 0 and 180°, the sinus of Θ must increase as Θ increases. As a consequence of that, the transition from a non-stoichiometric NiO to a stoichiometric NiO should originate a shift of the XRD signals to lower Θ values. That supposition is corroborated by Jiin-Long Yang et al. [**110**] who concluded that the non-stoichiometry may be originated by the presence of interstitial oxygen since a shift in the XRD peaks to a lower 2Θ values as the calcination temperature increases points to a lattice expansion originated by the inclusion of interstitial oxygen. The thermal treatment should originate the elimination of the interstitial oxygen giving rise to the formation of a higher stoichiometric NiO which presents a pale-green color. Those results are coherent with the work done by Nikolay N. Kotsev and Luba I. Ilieva [**111**] in which it was found that the higher the calcination temperature of the NiO, the closer to the stoichiometry its composition is. In conclusion, the heating of the NiO/YSZ samples during the experiments should lead to the elimination of the interstitial oxygen and the color change from dark blue to pale green.

8.8. Improvement of the cell selectivity with time

The cell selectivity in the decomposition of the nitrogen oxides is very low but it was observed that it increased with the cell operating time. In the literature, a change in the structure of the catalyst with the cell operating time was observed and the authors asserted that such a change may be the responsible of the improvement of the electro-catalytic performance of the cell. An increase in the YSZ grains and a decrease in the size of the NiO grains was observed. That would lead to the formation of a high concentration of three phase boundaries (YSZ, NiO and gas) which are an advantageous in the NO_x decomposition [**119**] [**120**].

The first process which occurs is the adsorption of the NO and O_2 molecules and then, the diffusion of the oxygen ions through the cell take place. An improvement of the oxygen ions diffusion capacity of the electrochemical cell must not improve the selectivity of the cell since both the NO and the O_2 adsorption give rise to the formation of $Ni-O$. The improvement of the selective adsorption of NO molecules may be responsible for the selectivity increase. It can be possible than the adsorption of the NO and O_2 molecules take place in two different active sites in the catalyst and the change in the catalyst structure create more of the NO adsorption sites.

CHAPTER 9

Conclusions

The present work has contributed to evaluate the performance of the NiO/YSZ catalyst on a electrochemical system. The $Pt/YSZ/Pt/NiO-YSZ$ cell is a promising catalyst for the elimination of the nitrogen oxides since a very good activity and selectivity could be achieved.

Nitrogen-containing species storage on a NiO/YSZ catalyst was mainly found when the saturation occured at 150 and 250°C and both NO and O_2 were present in the gas mixture. NiO was found to be responsible for that storage. The nature of the stored nitrogen-containing species was also studied. A significant storage was observed neither at 350°C nor at 450°C. When the saturation took place in absence of oxygen, no significant amount of nitrogen-containing species could be found on the catalyst surface at any of the temperatures studied. Both nitrates and nitrites were stored on the catalyst surface at 150 and 350°C. It could be concluded that, after saturation at 350°C, the surface nitrates and nitrites MOONO, MONO and MONOM may be present on the NiO catalyst surface. A mechanism for the nitrites and nitrates storage on the catalyst is also proposed. That mechanism is also consistent with the NO_2 production observed during the catalytic experiments when O_2 was both present and absent in the gas mixture.

The catalytic activity of the NiO/YSZ catalyst was also studied. The NO molecules may first adsorb dissociatively on the catalyst surface and then, a recombination of the nitrogen atoms in order to form nitrogen molecules may take place. The oxygen atoms remained adsorbed on the active sites which lead to the catalyst deactivation. For the thermal regeneration of the catalyst, a temperature above 800°C should be needed since the oxygen atoms adsorb strongly on the active centers. At such a high temperature, changes on the YSZ structure may occurs. Therefore, a chemical and electrochemical regeneration of the catalyst were studied. The reduction of the catalyst surface at 450°C with a gas mixture containing H_2 could regenerate the active sites of the catalyst and an enhancement of the catalytic activity was then achieved. High catalytic activity could be observed but it dropped continuously with time until the complete deactivation of the catalyst occurred. The NO_x decomposition experiments done with an electrochemical system achieved a stationary activity since the continuous regeneration of the active sites could take place. For the electro-catalytic studies, different catalysts and systems were tested. The best results were achieved with the $Pt/YSZ/Pt/NiO-YSZ$ system.

Two conformations for the electro-catalytic experiments were studied in which a tubular and a planar reactor were used. In both cases, the same high activity rates were achieved but in the planar conformation consisting on two planar substrates set together in a "sandwich" conformation, the voltage required for a specific conversion rate was lower than the one needed on the tubular conformation.

The selectivity of the NO_x decomposition reaction in order to produce nitrogen molecules when oxygen is present in the gas mixture, is low but an important improvement in the selectivity with the operating time of the $Pt/YSZ/Pt/NiO-YSZ$ electrochemical system could be achieved. Such an improvement in the selectivity could be originated by a change in the NiO/YSZ catalyst structure. In the present work, a change in the catalyst color from dark blue to pale green was observed. That change in the catalyst color may be consistent with a change in the catalyst structure.

The reproducibility of the catalytic system preparation still has to be improved in order to be able to control all the experimental parameters. Only then, the complete understanding and optimization of the processes that take place during the catalyst performance would be possible.

For the application of that catalyst in diesel exhaust purification treatments the O_2 concentration at which the catalyst shows a good activity and selectivity has to be increased since the oxygen concentration in the diesel exhaust is much higher than the one utilized in the present work. The influence of other gases (which also are present in the diesel exhaust) on the catalyst performance has to be also studied.

CHAPTER 10

Appendix

10.1. Chemical ionization in mass spectrometry

There are several methods to ionize the sample molecules. In the electron impact ionization, electrons are emitted from a heated tungsten or rhenium filament and accelerated in an electrical field colliding, finally, with the gas molecules of the sample giving rise to its ionization: the molecule loose an electron and in case of heteroatoms like sulfur, oxygen and nitrogen, the lost of a couple of electrons occurs. The so generated electron beam has a typical energy of 70 eV which is clearly higher than the typical ionization energy of a molecule (10-20 eV). If sample molecules are bombarded with that high energetic electron beam, the excess of energy can be transmitted to them in form of vibrational and rotational energy which can cause the molecules to break up. In the analysis of complex organic molecules, that is precisely the desired effect as the information just about the molecule mass is not enough to identify it. A clarifying example is the identification of the acetone and propanal molecule.

The molecular mass of both molecules is 58.0419 u, so it would not be possible to distinguish between both of them with just that information. As a result of the different structures they present and therefore, its different fragmentation patterns, it is possible to identify each of them when the electron impact ionization is used. In case that the molecules do not present typical fragmentation patterns, the electron impact ionization is only adequate when a previous separation step (through for example gas or liquid chromatography) is done. That is effective but it requires a lot of time.

The exhaust gases are composed of simple molecules like N_2, CO_2, CO, H_2O, O_2, NO, NO_2 and N_2O and such a composition can change drastically in very short time periods (in seconds or even faster). Those simple molecules can not break up giving typical fragmentation patterns so, the ionization through electron impact would lead to a species mixture which can not result in a reliable identification. For example, the N_2O molecule can fragment to give N_2 and O, NO_2 can give N and O_2 or NO and O, CO_2 can give CO and O and so long. If a previous separation step is run, the rapid changes occurred in the gas composition would not be determined.

That is the reason why the chemical ionization is used in such an application. In that method, the high energetic electron beam collides with the molecules of a reagent gas in order to ionize them. The ionization energy of those molecules are much lower than the one of the electron beam and due to the lack of an energy excess, the samples molecules will be ionized without a fragmentation to occur. For example, the ionization of the oxygen molecule will happens as follows.

$$O_2 + Xe^+ \rightarrow O_2^+ \tag{10.1}$$

Gas	Ionization energy [eV]
Mercury, Hg	10.4
Xenon, Xe	13.4
Krypton, Kr	14.4
Mercury, Hg^*	18.8

TABLE 10.1. bla bla.

Molecule to be analyzed	Ionization energy [eV]	Gas used for the ionization
N_2	15,58	Hg^*
O_2	12.07	Xe
CO	14.01	Kr
CO_2	13.77	Kr
H_2O	12.61	Xe
NO	9.26	Hg
NO_2	9.75	Hg
N_2O	12.89	Xe

TABLE 10.2. bla bla.

Table 10.1 shows a resume of the different gases used for the sample ionization. In the table below, some gases found in the exhaust and their ionization energy together with the gas use for its ionization are presented.

10.2. Nitrogen-physisorption experiments

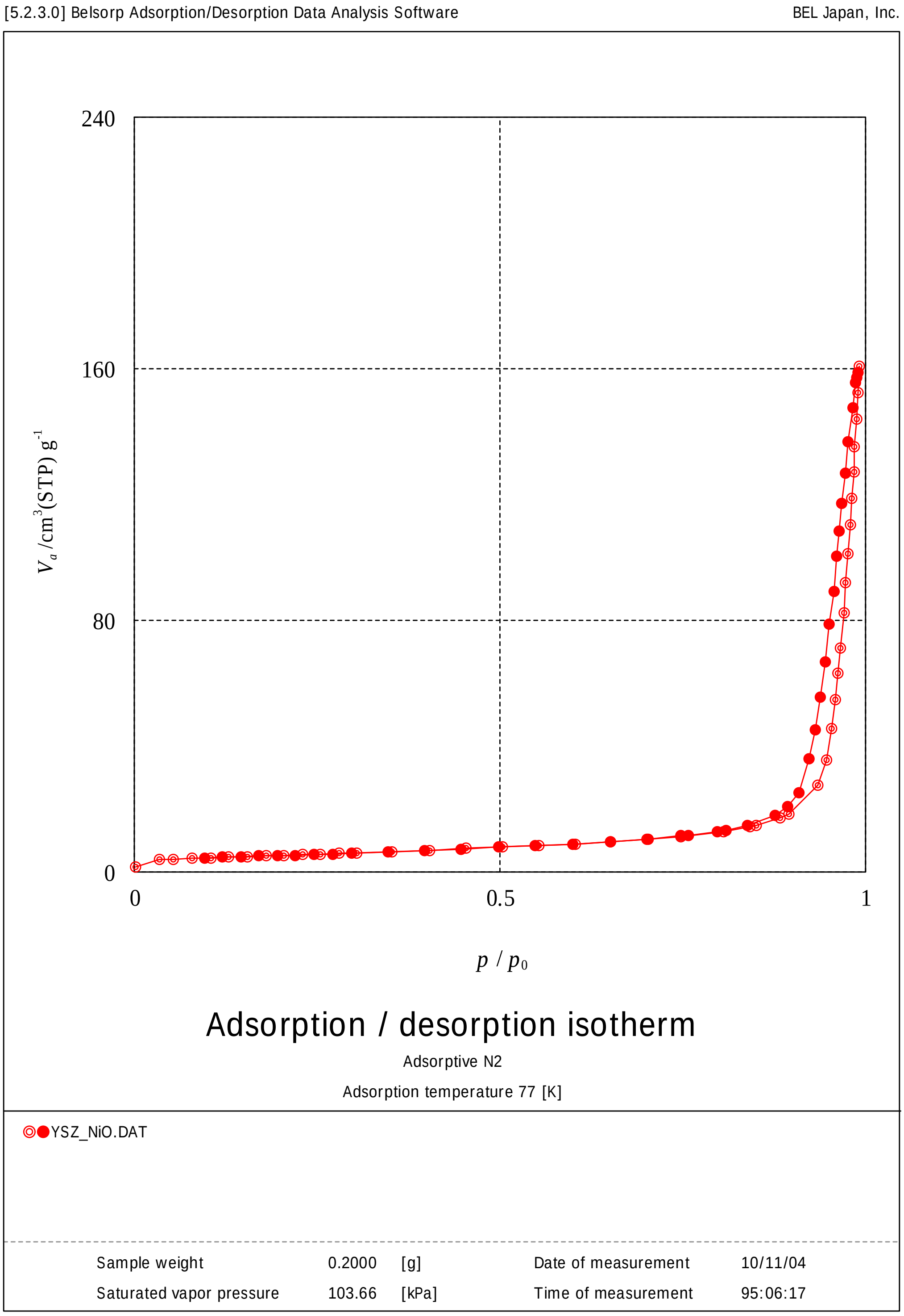

[5.2.3.0] Belsorp Adsorption/Desorption Data Analysis Software BEL Japan, Inc.

Adsorption / desorption isotherm

Adsorptive N2

Adsorption temperature 77 [K]

◎●YSZ_NiO.DAT

Sample weight	0.2000	[g]	Date of measurement	10/11/04
Saturated vapor pressure	103.66	[kPa]	Time of measurement	95:06:17

FIGURE 10.1. Adsorption-desorption isotherm obtained from the nitrogen-physisorption experiment performed on NiO/YSZ

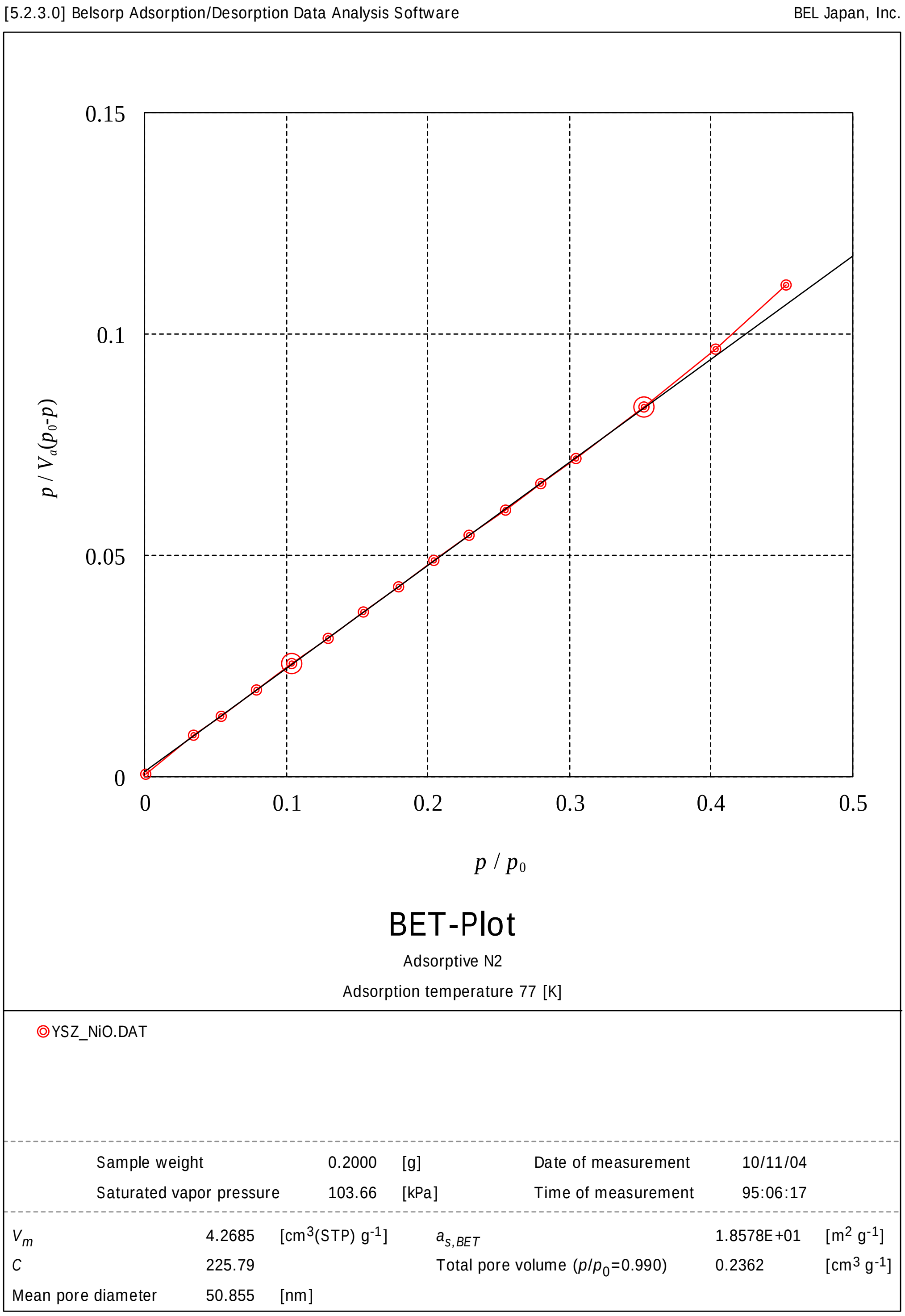

[5.2.3.0] Belsorp Adsorption/Desorption Data Analysis Software

BEL Japan, Inc.

BET-Plot

Adsorptive N2

Adsorption temperature 77 [K]

◎YSZ_NiO.DAT

Sample weight	0.2000	[g]	Date of measurement	10/11/04
Saturated vapor pressure	103.66	[kPa]	Time of measurement	95:06:17

V_m	4.2685	[cm^3(STP) g^{-1}]	$a_{s,BET}$	1.8578E+01	[m^2 g^{-1}]
C	225.79		Total pore volume (p/p_0=0.990)	0.2362	[cm^3 g^{-1}]
Mean pore diameter	50.855	[nm]			

FIGURE 10.2. *BET*-plot obtained from the nitrogen-physisorption experiment performed on NiO/YSZ

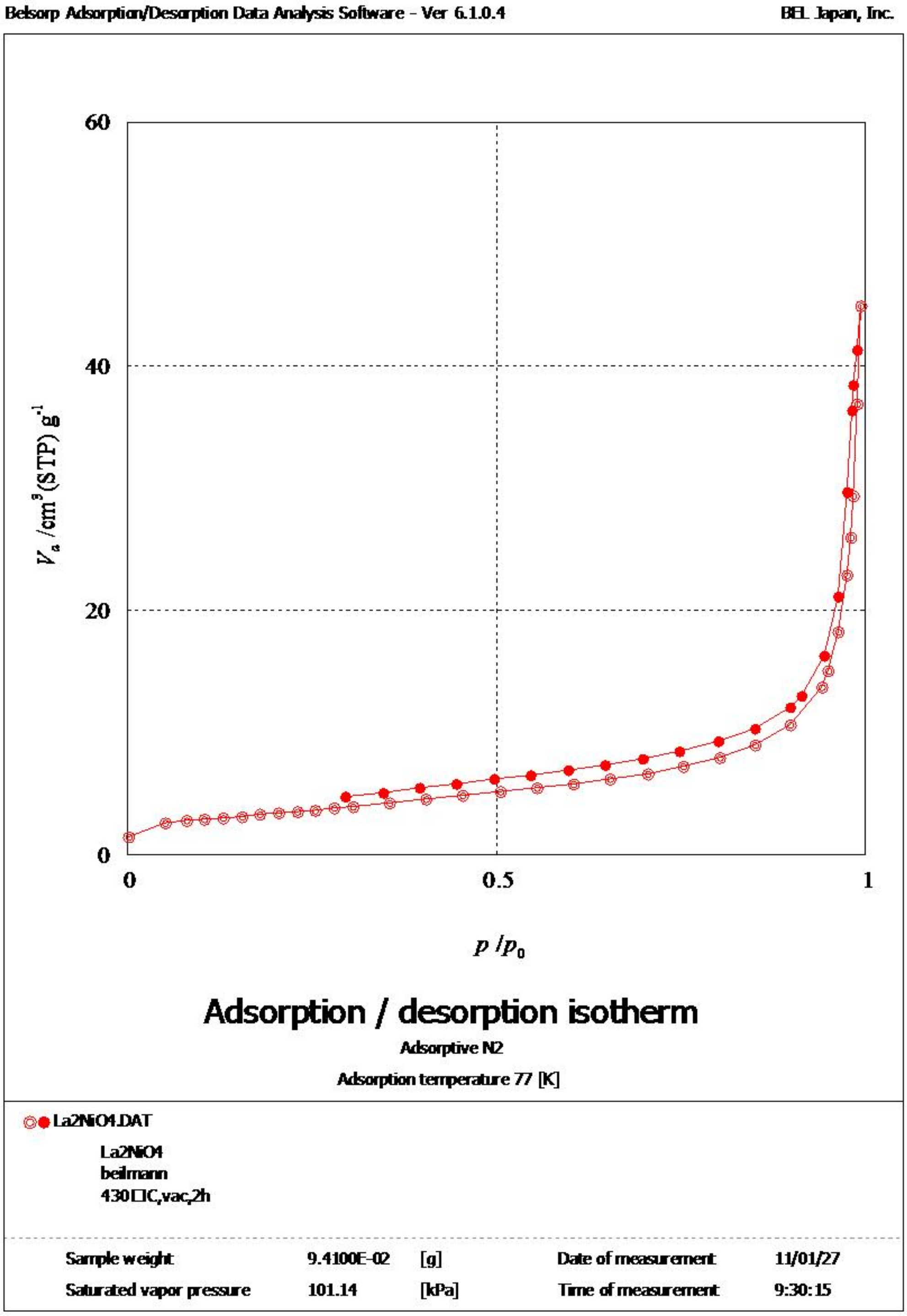

Belsorp Adsorption/Desorption Data Analysis Software - Ver 6.1.0.4 BEL Japan, Inc.

Adsorption / desorption isotherm

Adsorptive N2

Adsorption temperature 77 [K]

◎● La2NiO4.DAT

La2NiO4
beilmann
430□C,vac,2h

Sample weight	9.4100E-02	[g]	Date of measurement	11/01/27
Saturated vapor pressure	101.14	[kPa]	Time of measurement	9:30:15

FIGURE 10.3. Adsorption-desorption isotherm obtained from the nitrogen-physisorption experiment performed on La_2NiO_4

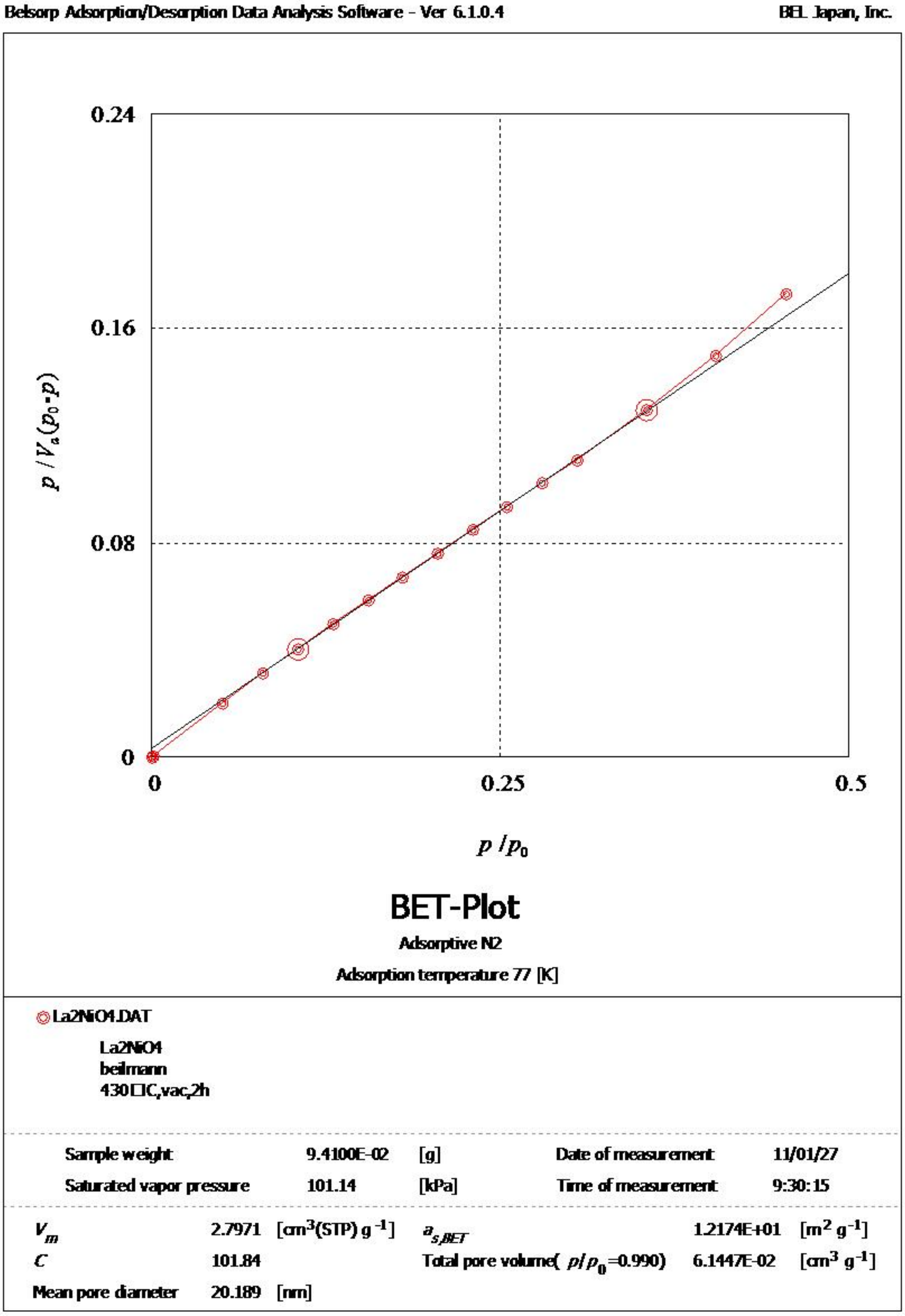

Belsorp Adsorption/Desorption Data Analysis Software - Ver 6.1.0.4 **BEL Japan, Inc.**

BET-Plot

Adsorptive N2

Adsorption temperature 77 [K]

◎ **La2NiO4.DAT**

La2NiO4
beilmann
430□C,vac,2h

Sample weight	9.4100E-02	[g]	Date of measurement	11/01/27
Saturated vapor pressure	101.14	[kPa]	Time of measurement	9:30:15

V_m	2.7971	[cm^3(STP) g^{-1}]	$a_{s,BET}$	1.2174E+01	[m^2 g^{-1}]
C	101.84		Total pore volume(p/p_0=0.990)	6.1447E-02	[cm^3 g^{-1}]
Mean pore diameter	20.189	[nm]			

FIGURE 10.4. *BET*-plot obtained from the nitrogen-physisorption experiment performed on La_2NiO_4

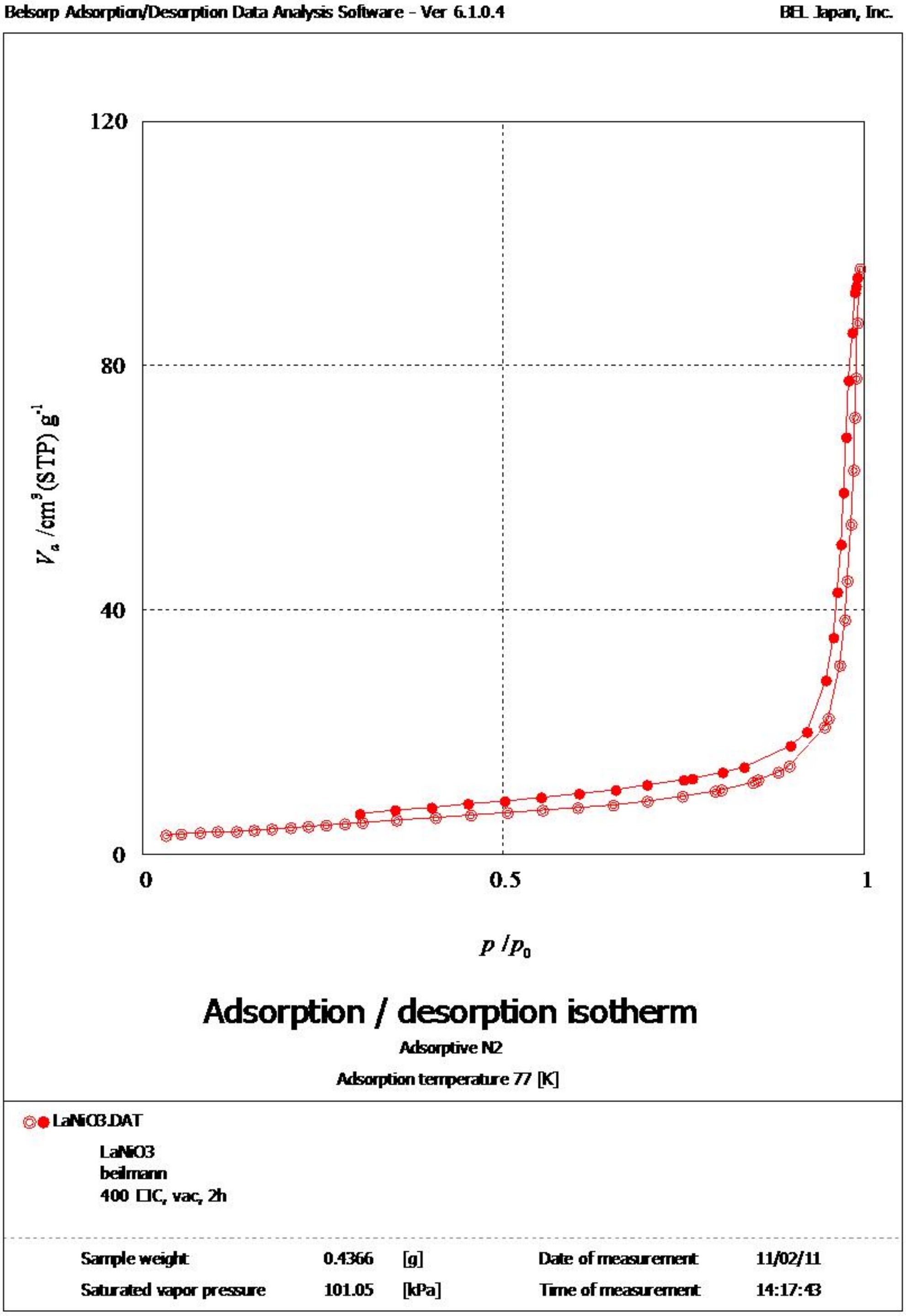

Belsorp Adsorption/Desorption Data Analysis Software - Ver 6.1.0.4 BEL Japan, Inc.

Adsorption / desorption isotherm
Adsorptive N2
Adsorption temperature 77 [K]

LaNiO3
beilmann
400 □C, vac, 2h

Sample weight	0.4366	[g]	Date of measurement	11/02/11
Saturated vapor pressure	101.05	[kPa]	Time of measurement	14:17:43

FIGURE 10.5. Adsorption-desorption isotherm obtained from the nitrogen-physisorption experiment performed on $LaNiO_3$

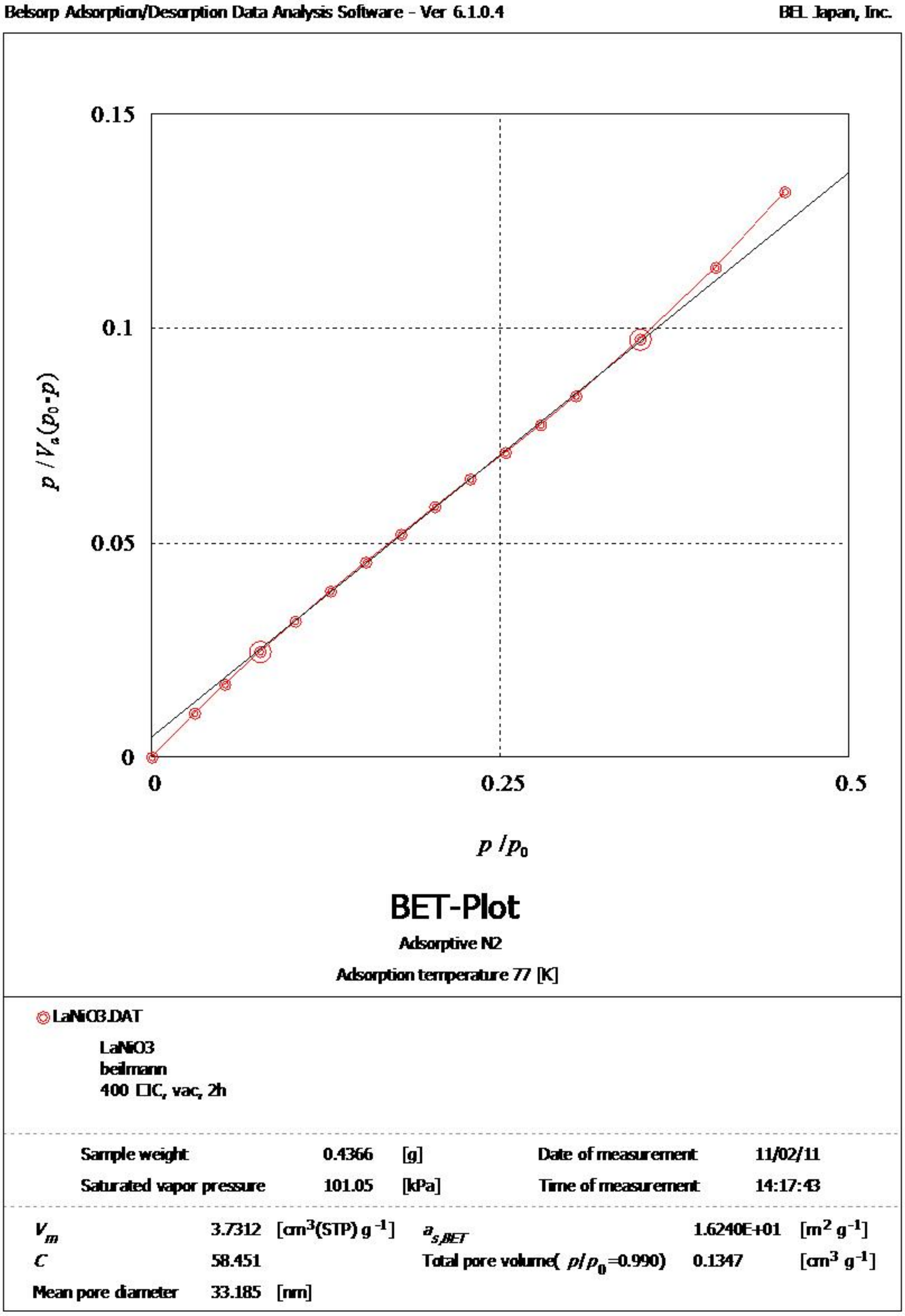

Belsorp Adsorption/Desorption Data Analysis Software - Ver 6.1.0.4 **BEL Japan, Inc.**

BET-Plot

Adsorptive N2

Adsorption temperature 77 [K]

◎ **LaNiO3.DAT**

LaNiO3
beilmann
400 □C, vac, 2h

Sample weight	0.4366	[g]	Date of measurement	11/02/11
Saturated vapor pressure	101.05	[kPa]	Time of measurement	14:17:43

V_m	3.7312	[cm^3(STP) g^{-1}]	$a_{s,BET}$	1.6240E+01	[m^2 g^{-1}]
C	58.451		Total pore volume(p/p_0=0.990)	0.1347	[cm^3 g^{-1}]
Mean pore diameter	33.185	[nm]			

FIGURE 10.6. *BET*-plot obtained from the nitrogen-physisorption experiment performed on $LaNiO_3$

10.3. NO_x decomposition experiments on YSZ/NiO catalyst

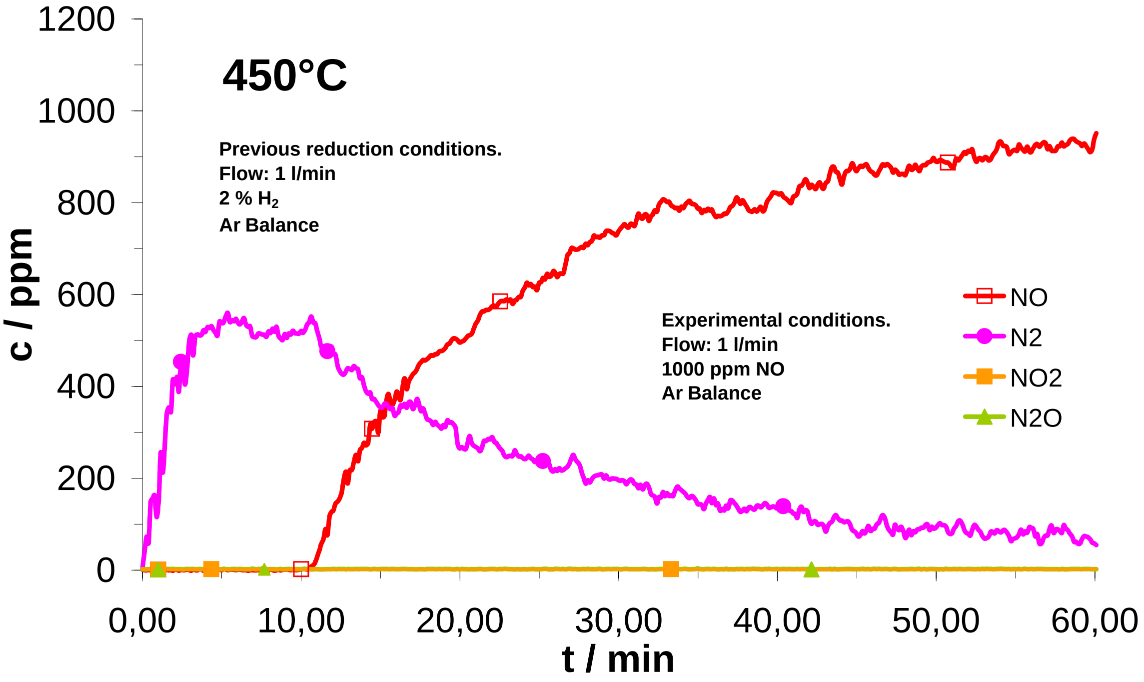

FIGURE 10.7. NO_x decomposition activity of the NiO/YSZ powder catalyst at 450°C after previous reduction at 450°C with 1 l/min N_2 and 2 % H_2

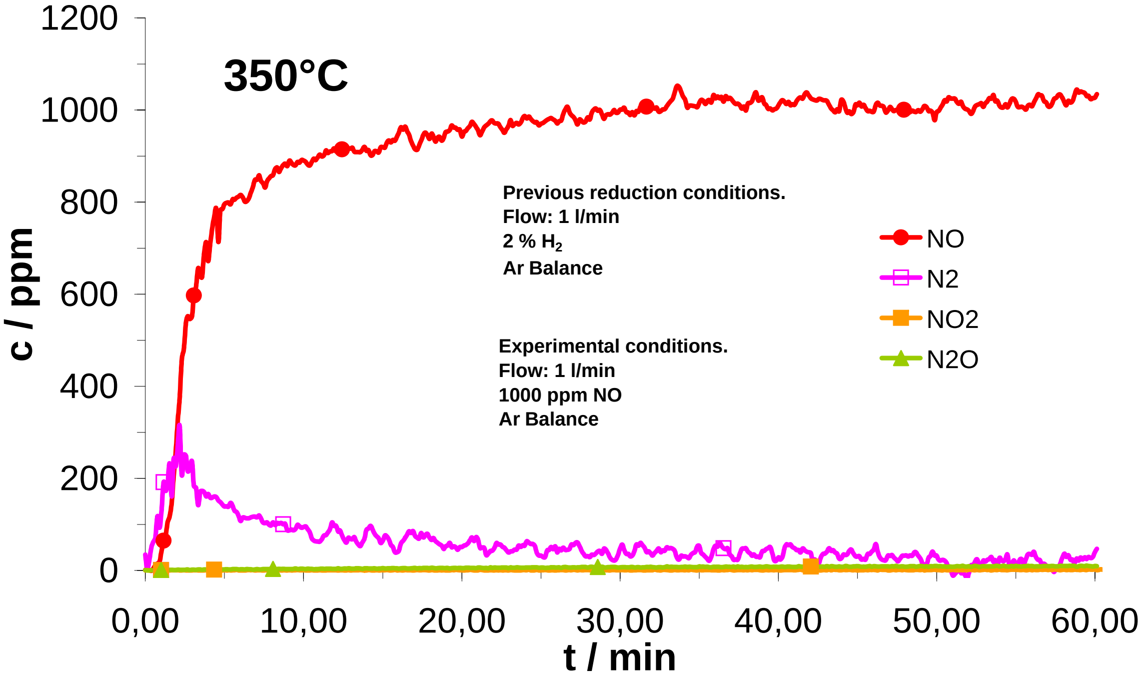

FIGURE 10.8. NO_x decomposition activity of the NiO/YSZ powder catalyst at 350°C after previous reduction at 450°C with 1 l/min N_2 and 2 % H_2

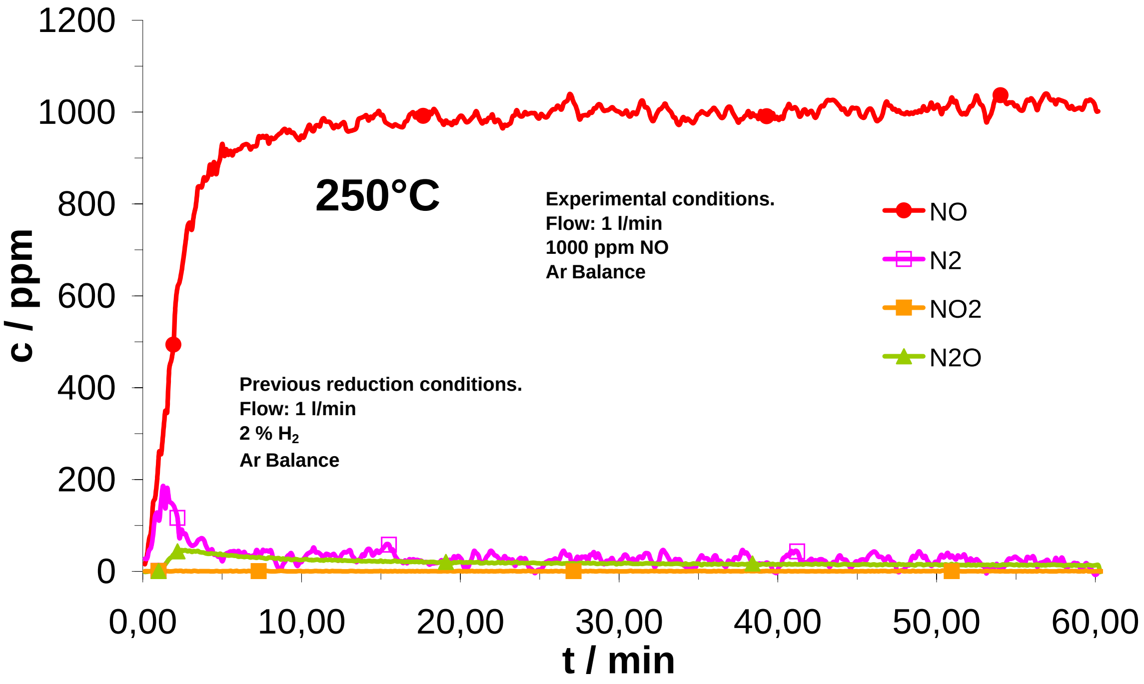

FIGURE 10.9. NO_x decomposition activity of the NiO/YSZ powder catalyst at 250°C after previous reduction at 450°C with 1 l/min N_2 and 2 % H_2

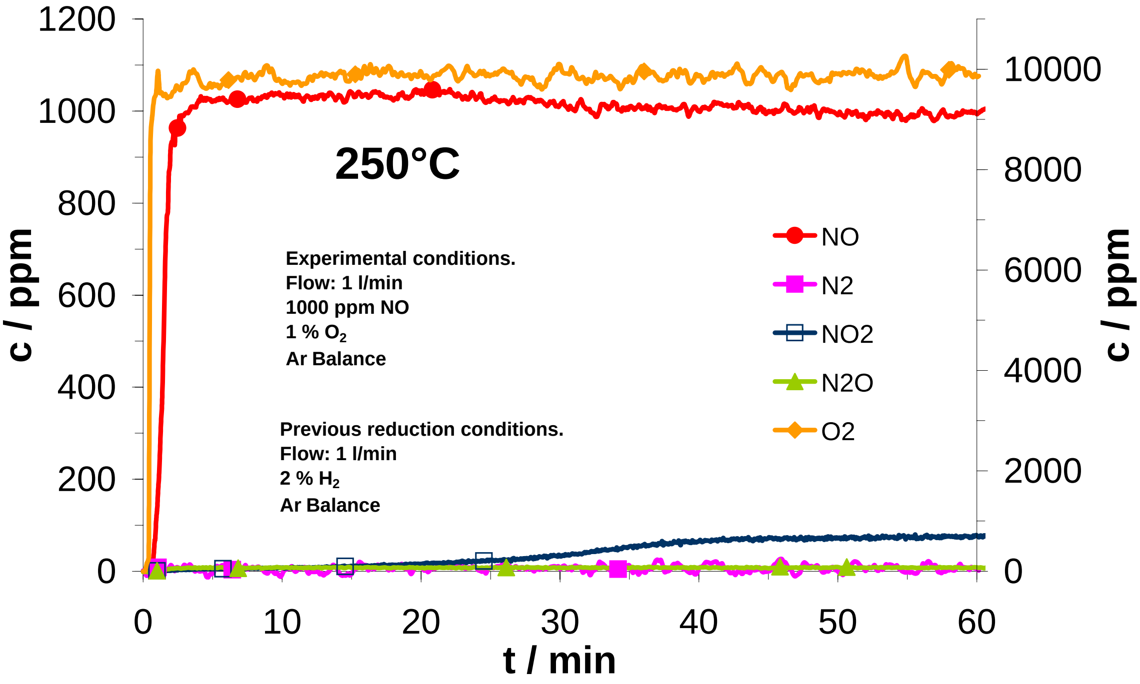

FIGURE 10.10. NO_x decomposition activity of the NiO/YSZ powder catalyst at 250°C (when O_2 was present in the experimental gas mixture) after previous reduction at 450°C with 1 l/min N_2 and 2 % H_2

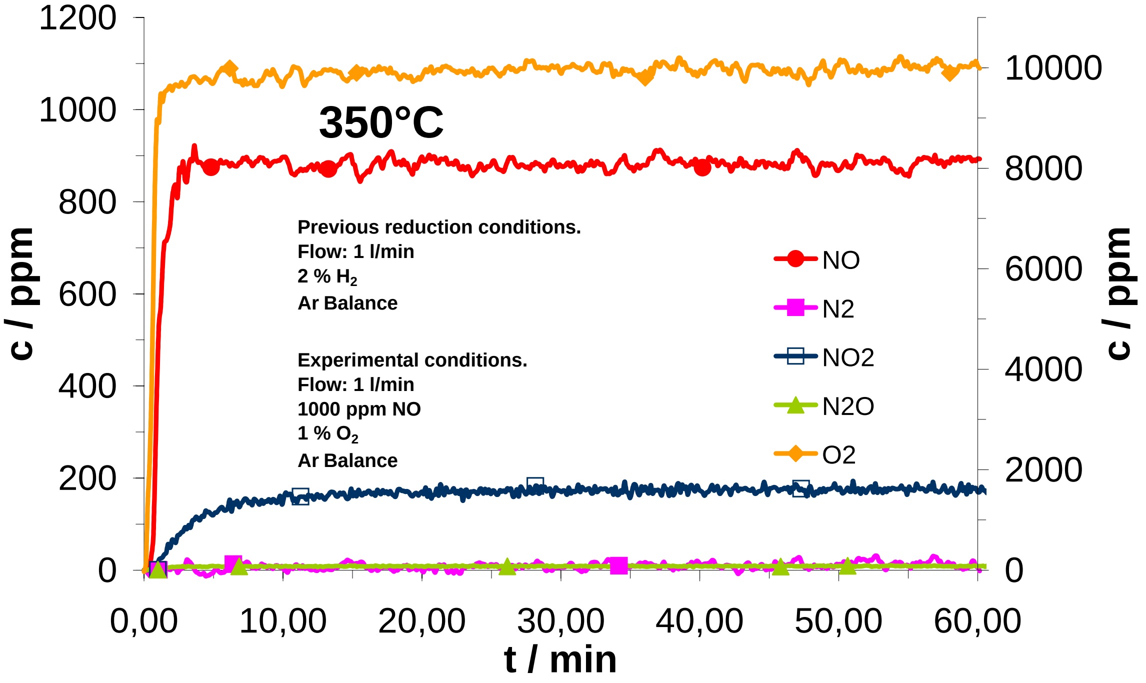

FIGURE 10.11. NO_x decomposition activity of the NiO/YSZ powder catalyst at 350°C (when O_2 was present in the experimental gas mixture) after previous reduction at 450°C with 1 l/min N_2 and 2 % H_2

10.4. Calculation of the theoretical current expected when NO, NO_2 or O_2 is decomposed on the cathode

The amount of NO in mol which is decomposed in the cathode (equation (10.2)) per second ($n(NO)$) can be calculated as equation (10.3) indicates. The experimental conditions are: 500 ml/min of a gas mixture composed of 1000 ppm NO and 1 % O_2 in N_2 balance. $X(NO)$ is the NO conversion rate in %

$$2\,NO\;+\;4\,e^-\;\rightarrow\;N_2\;+\;2\,O^{2-} \tag{10.2}$$

$$n(NO)\;=\;\frac{X(NO)\,0,5}{100\;24\;60\;10^3}\;\frac{mol\;NO}{s} \tag{10.3}$$

Then, the current (I) obtained when the amount of NO described by $n(NO)$ is decomposed can be calculated with equation (10.4).

$$I\;=\;\frac{n(NO)\,6,02\;10^{23}\;4}{6,2\;10^{18}} \tag{10.4}$$

The amount of NO_2 in mol which is decomposed in the cathode (equation (10.5)) per second ($n(NO_2)$) can be calculated as equation (10.6) indicates. The experimental conditions are: 500 ml/min of a gas mixture composed of 1000 ppm NO_2 and 1 % O_2 in N_2 balance. $X(NO_2)$ is the NO_2 conversion rate in %

$$2\,NO_2\;+\;8\,e^-\;\rightarrow\;N_2\;+\;4\,O^{2-} \tag{10.5}$$

$$n(NO_2)\;=\;\frac{X(NO_2)\,0,5}{100\;24\;60\;10^3}\;\frac{mol\;NO_2}{s} \tag{10.6}$$

Then, the current (I) obtained when the amount of NO_2 described by $n(NO)$ is decomposed can be calculated with equation (10.7).

$$I\;=\;\frac{n(NO)\,6,02\;10^{23}\;8}{6,2\;10^{18}} \tag{10.7}$$

The amount of O_2 in mol which is decomposed in the cathode (equation (10.8)) per second ($n(O_2)$) can be calculated as equation (10.9) indicates. The experimental conditions are: 500 ml/min of a gas mixture composed of 1000 ppm NO and 1 % O_2 in N_2 balance. $X(O_2)$ is the O_2 conversion rate in %

$$O_2 \; + \; 4\, e^- \; \rightarrow \; 2\, O^{2-} \tag{10.8}$$

$$n(O_2) \; = \; \frac{X(O_2)\, 5}{100\; 24\; 60\; 10^3}\, \frac{mol\, O_2}{s} \tag{10.9}$$

Then, the current (I) obtained when the amount of O_2 described by $n(O_2)$ is decomposed can be calculated with equation (10.10).

$$I \; = \; \frac{n(O_2)\; 6,02\; 10^{23}\; 4}{6,2\; 10^{18}} \tag{10.10}$$

10.5. Calculation of the amount of substance from the experimental results

The volume fraction (v_i) of a gas component i in the total volume flow V_{ges} can be calculated as the integral of $c_i^d(T)$ with respect to T divided by the temperature interval (ΔT) as equation (10.11) indicates.

$$v_i = \frac{\displaystyle\int_{T_A}^{T_B} c_i^d(T)\, dT}{\Delta T} \tag{10.11}$$

Where:

T_A is the temperature in K at the beginning of the TPD experiment

T_B is the temperature in K at the end of the TPD experiment

ΔT is the temperature difference T_B-T_A in K

$c_i^d(T)$ is the fraction of the desorbed gas component i (c_i^d) in the gas mixture in ppm

The total volume V_{total} which has passed through the catalyst during the experiment can be calculated as indicated in equation (10.12).

$$V_{total} = \frac{\dot{V}\, \Delta T}{\beta} \tag{10.12}$$

Where:

$\dot{V}$ is the volume flow in h^{-1}

β is the temperature rate in $°C/h$

The total volume of the desorbed gas specie i ($V_{total,i}$) can be calculated as follows

$$V_{total,i} = V_{total}\, v_i\, 10^{-6} \tag{10.13}$$

Using the ideal gas law the total amount of desorbed substance i in mol (n_i) can be calculated according to equation (10.14).

$$n_i = \frac{V_{total,i}\, p}{R\, T} \tag{10.14}$$

The substitution of equations (10.11)-(10.13) in (10.14) leads to the obtaining of equation (10.15)

$$n_i \;=\; \frac{\dot{V}\,10^{-6}\,p}{R\,T\,\beta}\int_{T_A}^{T_B} c_i^d(T)\,dT \tag{10.15}$$

Where T is the temperature in K at which c_i^d is measured.

The application of the ideal gas law makes equation (10.15) an approximation for the evaluation of the amount of substance of the specie i desorbed during the TPD experiments (n_i). However, it can be used since it will be utilized for comparing different results.

The calculation of n_i during the time-experiments is analog to the one utilized in the TPD experiments. The equation (10.16) can be used to calculate $V_{total,i}$.

$$V_{total,i} \;=\; \int_{t_A}^{t_B} c_i^d\,dt\,\dot{V}\,10^{-6} \tag{10.16}$$

Bibliography

[1] E. Rotter, VDA. *Entwicklung der internationalen Automobilmärkte*, Innovations-Report, www.innovations-report.de

[2] A. Bedwell *The global diesel sales forecast*, J. D. Power-LMC, 2003, Global Markets for Diesel Powered Light Vehicles to 2015 Study (SM), www.jdpower.com

[3] *DCL International Inc*, http://www.dcl-inc.com/dieseloxidationcatalyst

[4] Klaus Bliefert *Umweltchemie*, Wiley-VCH, (2002)

[5] Seinfeld, John H. Pandis, Spyros N. *Atmospheric Chemistry and Physics - From Air Pollution to Climate Change*, John Wiley & Sons, (2006)

[6] John Wright *Environmental chemistry*, Routledge (2003)

[7] Gary W. vanLoon y Stephen J. Duffy *Environmental chemistry*, Oxford University Press (2005)

[8] Martyn V. Twigg *Progress and future challenges in controlling automotive exhaust gas emissions*, Applied Catalysis B: Environmental (2007), 70, 2-15

[9] *Emission standards. European Union*, http://www.dieselnet.com/standards/eu/

[10] Jacques Barbier Jr. and Daniel Duprez *Steam effects in three-way catalysis*, Applied Catalysis B: Environmental 4 (1994) 105-140

[11] Hussam Abdulhamid, Erik Fridell y Magnus Skoglundh *Influence of the type of reducting agent (H_2, CO, C_3H_6 and C_3H_8) on the reduction of stored NO_x in a $Pt/BaO/Al_2O_3$ model catalyst*, Topics in Catalysis (2004), 30-31, 1-4, 161-168

[12] Guido Busca, Luca Lietti, Gianguido Ramis y Francesco Berti *Chemical and mechanistic aspects of the selective catalytic reduction of NO_x by amonia over oxide catalysts. A review*, Applied Catalysis B: Environmental (1998), 18, 1-2, 1-36

[13] Frans J. J. G. Janssen, Frans M. G. van den Kerkhof, Hans Bosch y Julian R. H. Ross *Mechanism of the reaction of nitric oxide, amonia and oxygen over vanadia catalyst. 1. The role of oxygen studied by way of isotopic transients Ander dilute conditions*, Journal of Physical Chemistry (1987), 91, 23, 5921-5927

[14] M. Schneider , PhD, Universität Karlsruhe 1999

[15] F. Buchholz , PhD, Universität Karlsruhe 2000

[16] Louise Olsson, Bjoern Werterberg, Hans Persson, Eric Fridell, Magnus Skoglundh y Bengt Andersson *A kinetic study of oxygen adsorption/desorption and NO oxidation over Pt/Al_2O_3 catalysis*, Journal of Physical Chemistry B (1999), 103, 47, 10433-10439

[17] Oliver Krocher y Martin Elsener *Combination of V_2O_5/WO_3-TiO_2, $Fe-ZSM5$ and $Cu-ZSM5$ Catalysts for the selective catalytic reduction of nitric oxide with ammonia*, Industrial & Engineering Chemistry Research (2008), 47, 22, 8588-8593

[18] Akira Miyamoto, Bunkei Inoue y Yuchi Murakami *Automotive exhaust emissions control using the three-way catalyst system. 1. Computer simulation of the nitric oxide-hydrogen-oxygen reaction on platinum/aluminium oxide catalyst*, Industrial & Engineering Chemistry Product Research Development (1979), 18, 2, 104-109

[19] Mordecai Shelef, James H. Jones, Joseph T. Kummer, Klaus Otto y E. Eugene Weaver *Selective catalytic reaction of hydrogen with nitric oxide inthe presence of oxygen*, Environmental Science and Technology (1971), 5, 9, 790-798

[20] Florian Schott , Diplomarbeit, Universität Karlsruhe (2003).

[21] A. Wildermann , PhD, Universität Erlangen (1994).

[22] G. Heil , PhD, Universität Karlsruhe (1995)

[23] Eric Frank, H. Oguz y Werner Weiweiler *Modeling of kinetic expressions for the reduction of* NO_x *by hydrogen in oxygen-rich exhausts using a gradient-free loop reactor*, Chemical Engineering & Technology (2003), 26, 6, 679-683

[24] R. Burch, P. J. Millington y A. P. Walker *Mechanism of the selective reduction of nitrogen monoxide on platinum-based catalysts in the presence of exceso oxygen*, Applied Catalysis B: Environmental (1994), 4, 1, 65-94

[25] M. Machida, S. Ikeda, D. Kurogi y T. Pijama *Low temperatura catalytic* $NO_x - H_2$ *reductions over* $PtTiO_2 - ZrO_2$ *in an exceso oxygen*, Applied Catalysis B: Environmental (2001), 35, 2, 107-116

[26] R. Burch y M. D. Coleman *An investigation of the* $NO/H_2/O_2$ *reaction on noble-metal catalysts at low temperaturas Ander lean-burn conditions*, Applied Catalysis B: Environmental (1999), 23, 2-3, 115-121

[27] Brigitte Frank, Ragnar Luebke, Gerhard Emig y Albert *Investigation of the reduction of nitric oxides by CO and* H_2 *on* $Pt - Mo$ *catalysts ander oxidizing conditions*, Chemical Engineering & Technology (1998), 21, 6, 498-502

[28] K. Yolota, M. Fukui y T. Tanaka *Catalytical renoval of nitric oxide with hydrogen and carbon monoxide in the presence of exceso oxygen*, Applied Surface Science (1997), 121/122, 273-277

[29] Young-Whan Lee y Erdogan Gulari *Improved performance of* NO_x *reduction by* H_2 *and CO over* Pd/Al_2O_3 *catalyst at low temperaturas ander lean-burn condition*, Catalysis Communications (2004), 5, 9, 499-503

[30] B. Wichterlova, P. Samaza, J. P. Breen, R. Burch, C. J. Hill, L. Capek y Z. Sobalik *An in situ UV-vis and FTIR spectroscopy study on the effect of* H_2 *and CO during the selective catalytic reduction of nitrogen oxides over a silver alumina catalyst*, Journal of Catalysis (2005), 235, 1, 195-200

[31] John P. Breen, Robbie Burch, Christopher Hardacre y Chris J. Hill *Structural investigation of the promotional effect of hydrogen during the selective catalytic reduction of* NO_x *with hidrocarbons over* Ag/Al_2O_3 *catalysts*, Journal of Physical Chemistry B (2005), 109, 11, 4805-4807

[32] Brigitta Frank, Gerhard Emig y Albert Renten *Kinetics and mechanism of the reduction of nitric oxides by* H_2 *under lean-burn conditions on a* $Pt - Mo - Co/\alpha - Al_2O_3$ *catalyst*, Applied Catalysis B: Environmental (1998), 19, 1, 45-57

[33] C. N. Costa, P. G. Sawa, C. Andronikou, P. S. Lambrou, K. Polychronopoulou, V. C. Veléis, V. N. Stathopoulos, P. J. Pomonis y A. M. Efstathiou *An investigation of the* $NO/H_2/O_2$ *(lean de-*NO_x*) reaction on a highly active and selective* $Pt/La_{0,7}Sr_{0,2}Ce_{0,1}FeO_3$ *catalyst at low temperature*, Journal of Catalysis (2002), 209, 2, 456-471

[34] Scott R. Segal, Ken B. Anderson, Kathleen A. Carrado y Christopher L. Marschall *Low temperatura steam reforming of methanolover layered double hydroxide-derived catalyst*, Applied Catalysis A: General (2002), 231, 1-2, 215-226

[35] Brant A. Peppley, John C. Amphlett, Lyn M. Kearns y Ronald F. Mann *Methanol-steam reforming on* $Cu/ZnO/Al_2O_3$ *catalysts. Part 2. A comprehensive kinetic model*, Applied Catalysis A: General (1999), 179, 1-2, 31-49

[36] B. J. Dreyer, I. C. Lee, J. J. Krummenacher y L. D. Schmidt *Autothermal steam reforming of higher hydrocarbons: n-Decane, n-hexadecane and JP-8*, Applied Catalysis A: General (2006), 307, 2, 184-194

[37] Qi Aidu, Wang Shudong, Ni Changjun y Wu Diyong *Autothermal reforming of gasoline on Rh-based monolithic catalysts*, *I*nternational Journal of Hydrogen Energy (2007), 32, 8, 981-991

[38] R. P. O´Connor, E. J. Klein y L. D. Schmidt *High yields of synthesis gas by milisecond partial oxidation of higher hydrocarbons*, *C*atalysis Letters (2000), 70, 3-4, 99-107

[39] R. Burch, P. J. Millington y A. P. Walker *Mechanism of the selective reduction of nitrogen monoxide on platinum-based catalysts in the pressence of excess oxygen*, Applied Catalysis B: Environmental (1994), 4, 1, 65-94

[40] Stefan Kurze y Werner Weisweiler *Catalytic cracking of n-dodecane and diesel fuel to improve the selective catalytic reduction of* NO_x *in automotive exhaust containing excess oxygen*, *C*hemical Engineering & Technology (1999), 22, 10, 855-858

[41] S. Kureti , *D*iplomarbeit. Institut für Chemische Technik, Universität Karlsruhe (1996)

[42] Isabella Nova, Lidia Castoldi, Luca Lietti, Enrico Tronconi, Pio Forzatti, Federica Prinetto y Giovanna Ghiotti NO_x *adsorption study over* $Pt - Ba/alumina$ *catalysts: FT-IR and pulse experiments*, *J*ournal of Catalysis (2004), 222, 2, 377-388

[43] F. Rohr, S. D. Peter, E. Lox, M. Koegel, A. Sassi, L. Juste, C. Rigaudeau, G. Belot, P. Gelin y M. Primet *On the mechanism of sulfur poisoning and regeneration of a commercial gasoline* NO_x*-storage catalyst*, Applied Catalysis B: Environmental (2005), 56, 3, 201-212

[44] Louisse Olsson, Hans Persson, Erik Fridell, Magnus Skoglundh y Bengt Andersson *A kinetic study of NO oxidation and* NO_x *storage on* Pt/Al_2O_3 *and* $Pt/BaO/Al_2O_3$, Journal of Physical Chemistry B (2001), 105, 29, 6895-6906

[45] Andrea Scotti, Isabella Nova, Enrico Tronconi, Lidia Castoldi, Luca Lietti y Pio Forzatti *Kinetic study of lean* NO_x *storage over the* $Pt - Ba/Al_2O_3$ *system*, *I*ndustrial & Engineering Chemistry Research (2004), 43, 16, 4522-4534

[46] H. Mahzoul, J. F. Brilhac y P. Gilot *Experimental and mechanistic study of* NO_x *adsorption over NOx trap catalysts*, Applied Cataysis B: Environmental (1999), 20, 1, 47-55

[47] Luca Lietti, Pio Forzatti, Isabella Nova y Enrico Tronconi NO_x *storage reduction over* $Pt - Ba/\gamma - Al_2O_3$ *catalyst*, *J*ournal of Catalysis (2001), 204, 1, 175-191

[48] Isabella Nova, Lidia Castoldi, Luca Lietti, Enrico Tronconi, Pio Forzatti, Federica Prinetto y Giovanna Ghiotti NO_x *adsorption study over* $Pt/Ba/alumina$ *catalysts: FT-IR and pulse experiments*, *J*ournal of Catalysis (2004), 222, 2, 377-388

[49] I. Nova, L. Castoldi, F. Prinetto, V. Dal Santo, L. Lietti, E. Tronconi, P. Forzatti, G. Ghiotti, R. Psaro y S. Rechia NO_x *adsorption study over Pt-Ba/alumina catalysts: FT-IR and reactivity study*, *T*opics in Catalysis (2004), 30/31, 1-4, 181-186

[50] Erik Fridell, Hans Persson, Bjorn Westerberg, Louisse Olsson y Magnus Skoglundh *The mechanism for* NO_x *storage*, *C*atalysis Letters (2000), 66, 1-2, 71-74

[51] S. B. Xie, G. Mestl, M. P. Rosynek y J. H. Lunsford , J. Am. Chem. Soc. (1997), 119, 10186

[52] Bjorn Westerberg y Eric Fridell *A transient FTIR study of species formed during* NO_x *storage in the* $Pt/BaO/Al_2O_3$ *system*, Journal of Molecular Catalysis A: Chemical (2001), 165, 1-2, 249-263

[53] Peter J. Schmitz y Ronald J. Baird *NO and* NO_2 *adsorption on barium oxide: Model study of the trapping stage of* NO_x *conversión via lean* NO_x *traps*, Journal of Physical Chemistry B (2002), 106, 16, 4172-4180

[54] B.-H. Jang, T.-H. Yeon, H.-S. Han, Y.-K. Park y J.-E. Yie *Deterioration Mode of Barium-Containing* NO_x *Storage Catalyst*, Catalysis Letters. (2001), 77, 1-3, 21-28

[55] G. Mestl, M. P. Rosynek, J. H. Lundsford , J. Phys. Chem. (1997), 101, 9321

[56] Christian Hess y Jack H. Lunsford *Mechanism for* NO_2 *storage in barium oxide supported on magnesium oxide studied by in situ Raman spectroscopy*, Journal of Physical Chemistry B (2002), 106, 25, 6358-6360

[57] Yaying Ji, Courtney Fisk, Vencon Easterling, Uschi Graham, Adam Poole, Mark Crocker, Jae-Soon Choi, William Partridge y Karen Wilson NO_x *storage-reduction characteristics of Ba-based lean* NO_x *trap catalysts subjected to simulated road aging*, Catalysis Today (2010), 151, 3-4, 362-375

[58] H. Y. Huang, R. Q. Long y R. T. Yang *The promoting role of nobel metals on* NO_x *storage catalyst and mechanistic study of* NO_x *storage under lean-burn conditions*, Energy & Fuels (2001), 15, 1, 205-213

[59] Jianhua Xiao, Xuehui Li, Sha Deng, Furong Wang y Lefu Wang NO_x *storage-reduction over combined catalyst* $Mn/Ba/Al_2O_3 - Pt/Ba/Al_2O$, Catalysis Communications (2008), 9, 5, 563-567

[60] Karl Jellinek *Über Zersetzungsgeschwindigkeit von Stickoxyd und Abhängigkeit derselben von der Temperatur*, Zeitschrift für Anorganische und Allgemeine Chemie (1906), 49, 229-276

[61] Antonella Gervasini, Paolo Carnati and Vittorio Ragaini *Studies of direct Decomposition and Reduction of Nitrogen Oxide with Ethylene by supported noble Metal Catayisis*, Applied Catalisys B: Environmental (1999), 22, 3, 201-213

[62] A. M. Pisanu and C. E. Gigoló *NO Decomposition and NO Reduction by CO over* $Pd/\alpha - Al_2O_3$, Applied Catalisys B: Environmental (1999), 20, 3, 179-189

[63] K. Almusaiteer, R. Krishnamurthy and S. S. C. Chuang *In situ Infrared Study of Catalytic Decomposition of NO on carbon-supported Rh and Pd Catalyst*, Catalisys Today (2000), 55, 3, 291-299

[64] Thomas Edward Green and Cyril Norman Hinshelwood *The catalytic Decomposition of Nitric Oxide at the Surface of Platinum*, Journal of the Chemical Society (1926), 1709-1713

[65] Paul W. Bachman and Guy B. Taylor *Decomposition of Nitric Oxide by Platinum at elevated Temperatures and its Retardation by Oxygen*, Journal of Physical Chemistry (1929), 33, 447-455

[66] Chuang, Steven S. C. Tan and Cher-Dip *Promotion of Oxygen Desorption to Enhance Direct NO Decomposition over* $Tb - Pt/Al_2O_3$, Journal of Physical Chemistry B (1997), 101, 15, 3000-3004

[67] Y. Teraoka, C. Tai, H. Ogawa, H. Furukawa and S. Kagawa *Characterization and NO Decomposition of* $Cu - MFI$ *Zeolite in relation to Redox Behavior*, Applied Catalysis A: General (2000), 200, 1-2, 167-176

[68] Y. Yokomichi, T. Yamabe, T. Kakumoto, O. Okada, H. Ishikawa, Y. Nakamura, H. Kimura and I. Yasuda *Theoretical and Experimental Study on metal-loaded Zeolite Catalysts dor direct NO_x Decomposition*, Applied Catalysis B: Environmental (2000), 28, 1, 1-12

[69] R. J. H. Voorhoeve, J. P. Remeika and L. E. Trimble *Defect Chemistry and Catalysis in Oxidation and Reduction over Perovskite-type Oxides*, Annals of the New York Academy of Sciences (1976), 272, 3-21

[70] Hiromichi Shimada, Susumu Miyama and Haruo Kuroda *Decomposition of Nitric Oxide over $Y - Ba - Cu - O$ mixed Oxide Catalyst*, Chemistry Letters (1988), 10, 1797-1800

[71] Yasutake Teraoka, Tomohiro Harada and Shuchi Kagawa *Reaction Mechanism of direct Decomposition of Nitric Oxide over Co- and Mn-based Perovskite-type Oxides*, Journal of the Chemical Society, Faraday Transactions (1998), 94, 13, 1887-1891

[72] C. Tofan, D. Klvana y J. Kirchnerova *Decomposition of nitric oxide over perovskite axide catalysts: effect of CO_2, H_2O and CH_4*, Applied Catalysis B: Environmental (2002), 36, 4, 311-323

[73] Yasuharu Yokoi y Hiroshi Ushida *Catalytic activity of perovskite-type oxide catalysts for direct decomposition of NO. Correlation between cluster model calculations and temperature programmed desorption experiments*, Catalysis Today (1998), 42, 1-2, 167-174

[74] S. Pancharatnam, R. A. Huggins y D. M. Mason *Catalytic decomposition of nitric oxide on zirconia by electrolytic removal of oxygen*, Journal of the Electrochemical Society (1975), 112, 7, 869-875

[75] T. Hibino, Y. Kuwahara, T. Otsuka, N. Ishida y T. Oshima *NO_x detección using the electrolysis of water vapor in a YSZ [yttria-stabilized zirconio] cell. Part I. NO_x detection*, Solid State Ionics (1998), 107, 3-4, 213-216

[76] S. Bredikhin, K. Maeda y M. Awano *Low current density electrochemical cell for NO decomposition*, Solid State Ionics (2002), 152-153, 727-733

[77] H. Arashi and H. Naito , Solid State Ionics, (1992), 53-56, 431.

[78] T. Kawada, N. Sakai, H. Yokokawa, and M. Dokiya , Solid State Ionics, (1992), 53-56, 418

[79] M. T. Hernandez, J. R. Jurado, and P. Duran , Solid State Ionics, (1992), 51, 417

[80] P. Han and W. L. Worrell , J. Electrochem. Soc., (1995), 142, 4235.

[81] X. J. Huang and W. Weppner , J. Chem. Soc., Faraday Trans., (1996), 92, 2173.

[82] C. C. Liang , J. Electrochem. Soc., (1973), 120, 1289

[83] V. B. Tare and J. B. Wagner , Jr., J. Appl. Phys., (1983), 54, 6459

[84] K. S. Yoo and J. B. Wanger , Jr., Solid State Ionics, (1994), 69, 107.

[85] L. J. Gauckler and K. Sasaki , Solid State Ionics, (1995), 75, 203

[86] V. B. Tare, G. M. Mehrotra, and J. B. Wagner , Jr., Solid State Ionics, (1986), 18-19, 747

[87] Young Min Park y Gyeong Man Choi *Mixed ionic and electronic conduction in $YSZ - NiO$ composite*, Journal of the Electrochemical Society (1999), 146, 3, 883-889

[88] S. Bredikhin, K. Maeda y M. Awano *Electrochemical cell with two layers cathode for NO decomposition*, Ionics (2001), 7, 1-2, 109-115

[89] S. Bredikhin, K. Maeda y M. Awano *Peculiarity of NO decomposition by electrochemical cell with a mixed oxide working electrode*, Journal of the Electrochemical Society (2001), 148, 10, D133-D138

[90] Xueping Xu y D. Wayne Goodman *The effect of particle size on nitric oxide decomposition and reaction with carbon monoxide on palladium catalysts*, Catalysis Letters (1994), 24, 1-2, 31-35

[91] S. Bredikhin, K. Maeda y M. Awano *NO decomposition by an electrochemical cell with mixed oxide working electrode*, Solid State Ionics (2001), 144, 1-2, 1-9

[92] Masanobu Awano, Yoshinobu Fujushiro, Koichi Hamamoto, Shingo Katayama y Sergei Bredikhin *Advances in nano-structured electrochemical reactors for NO_x treatment in the presence of oxygen*, International Journal of Applied Ceramic Technology (2004), 1, 3, 277-286

[93] Koichi Hamamoto, Takuya Hiramatsu, Osamu Shiono, Shingo Katayama, Yoshinobu Fujushiro, Sergei Bredikhin y Masanobu Awano *Microstructure-controlled high selective deNO_x electrochemical reactor*, Journal of the Ceramic Society of Japan (2004), 112, 5, S1071-S1074

[94] Christian Hess y Jack H. LunsforD. Upadhyay, V. Panduri, A. Ghio y D. W. Kampd *Particulate matter induces alveolar ephitelial cell DNA damage and apoptosis*, American Journal of Respiratory Cell and Molecular Biology (2003), 29, 180-187.

[95] J. Strutz, K. P. Schick, S. Stahlhut y R. Blaha *Katalysator zur Herabsetzung der Zündtemperatur von Dieselruß und damit beschichtetes Dieselruß-Filter*, Patente DE 36 23 600 A1 (1988)

[96] B. J. Cooper, H. J. Jung, J. E. Thoss *Treatment of diesel exhaust gases*, Patente US 4902487 (1990)

[97] W. Nernst *Über die elektrolytische Leitung fester Körper bei sehr hohen Temperaturen*, Zeitschrift für Elektrochemie (1899), 6, 2, 41-43)

[98] D. G. Lamas, G. E. Lascalea, R. E. Juérez y N. E. Walsöe de Reca *Caracterización estructural de polvos nanocristalinos de circonia - itria homogéneos en composición*, Jornadas SAM 2000 - IV Coloquio Latinoamericano de Fractura y Fatiga (2000), 925-932

[99] K. Matsuda, S. Bredikhin, K. Maeda y M. Awano *Optimization of an electrochemical cell for NO decomposition by compositional control of the electro-catalytic electrode*, Solid State Ionics (2003), 156, 1-2, 223-231

[100] Zhonglin Wu y Meilin Liu *Modeling of ambipolar transport properties of composite mixed ionic-electronic conductors*, Solid State Ionics (1996), 93, 1-2, 65-84

[101] Thomas Schröder *Katalysierte Zersetzung von NO am Perowskit $LaNiO_3$*, PhD (2006), University Karlsruhe.

[102] S. K. Saha and P. Pramanik *Innovative chemical method for preparation of calcia-stabilized zirconia powders*, British Ceramic Transactions (1995), 94, 3, 123-127

[103] Klaus Beetz *Die geschlossene Fest-elektrolyt-Sauerstoffpumpe*, PhD, University Karlsruhe (1993).

[104] Pio Forzatti, Luca Lietti, Isabella Nova and Enrico Tronconi *Diesel NOx aftertreatment catalytic technologies: Analogies in LNT and SCR catalytic chemistry*, Catalysis Today (2010), 151, 202-211.

[105] Ming L. Yu and Wilhad Reuter *Secondary ion emission from binary alloy systems. Part I: O_2^+ bombardment*, J. Appl. Phys. (1981), 52, 1478-1488

[106] S. S. Mulla, N. Chen, L. Cumaranatunge, G. E. Blau, D. Y. Zemlyanov, W. N. Delgass, W. S. Epling and F. H. Ribeiro *Reaction of NO and O_2 to NO_2 on Pt: Kinetics and catalyst deactivation*, Journal of Catalysis (2006), 241, 389-399.

[107] Rachel B. Getman and William F. Schneider *DFT-Based Coverage-Dependent Model of Pt-Catalyzed NO Oxidation*, Chem. Cat. Chem. (2010), 2, 1450-1460

[108] Till C. Brüggemann and Frerich J. Keil *Theoretical Investigation of the Mechanism of the Oxidation of Nitrogen Oxide on Iron-Form Zeolites in the presence of water*, The Journal of Physical Chemistry (2011), 115, 2114-2133.

[109] Pilar Alfonso Martínez *Eliminacion de NO_x de los gases de escape procedentes de los vehículos diesel con un catalizador electroquímico*, Trabajo de Máster (2010), Universidad de Murcia and Karlsruher Institut of Technology (KIT).

[110] Jiin-Long Yang, Yi-Sheng Lai and J.S. Chen *Effect of heat treatment on the properties of non-stoichiometric p-type nickel oxide films deposited by reactive sputtering*, The Solid Films (2005), 488, 242-246

[111] Nikolay N. Kotsev and Luba I. Ilieva *Determination of non-stoichiometric oxygen in NiO by temperature programmed reduction*, Catalysis Letters (1993), 18, 173-178

[112] Anatoli Davydov *Molecular spectroscopy of oxide catalyst surfaces*, Wiley, 2003

[113] H. Conrad, G. Ertl, J. Küppers and E. E. Latta *Interation of NO with a Ni (111) surface*, Surface Science (1975), 50, 296-310

[114] D. F. Remar, A. M. Turiev, N. I. Tsidaeva and T. T. Magkoev *Adsorption of nitrogen oxide molecules to the surface of nanosized nickel clusters formed on the (111) surface of a magnesium oxide film*, Russian Physics Journal (2010), 53, 5, 480-485

[115] Thomas Scröder *Katalysierte Zersetzung von NO am Perowskit $LaNiO_3$*, PhD (2006), Karlsruhe University

[116] 2H. Kuhlenbeck, G. Odörfer, R. Jaeger, G. Illing, M. Menges, Th. Mull, H. J. Freund, M. Pöhlchen, V. Stämmler, S. Witzel, C. Scharfschwerdt, K. Wennemann, T. Liedtke, and M. Neumann , Phys. Rev. B (1991), 43, 1969-

[117] 3R. Lindsay, P. Baumgärtel, R. Terborg, O. Schaff, A. M. Bradshaw, and D. P. Woodruff , Surface Science (1999) 425, L401.

[118] Y. Yokomichi, T. Yamabe, T. Kakumoto, O. Okada, H. Ishikawa, Y. Nakamura, H. Kimura, I. Yasuda *Theoretical and experimental study on metal-loaded zeolite catalysts for direct NO_x decomposition*, Applied Catalysis B (2000), 28, 1, 1-12

[119] Norio Miura, Geyu Lu, Noboru Yamazoe *High-temperature potentiometric/amperometric NOx sensors combining stabilized zirconia with mixed-metal oxide electrode*, Sensors and Actuators B: Chemical (1998), 52, 169-178

[120] Norio Miura, Hideyuki Kurosawa, Masaharu Hasei, Geyu Lu, Noboru Yamazoe *Stabilized zirconia-based sensor using oxide electrode for detection of NO_x in high-temperature combustion-exhausts*, Solid State Ionics (1996), 86-88, 1069

[121] A. Rohrbach and J. Hafner *Molecular adsorption of NO on NiO(100): DFT and DFT+U calculations*, Physical Review B (2005), 71, 045405

[122] Lyn R. Watson, Terry L. Thiem, Rainer A. Dressler, Richard H. Salter, and Edmond Murad *High Temperature Mass Spectrometric Studies of the Bond Energies of Gas-Phase ZnO, NiO, and CuO*, J. Phys. Chem. (1993), 97, 5577-5580

[123] Stephen Brunauer, Paul Hugh Emmett, and Edward Teller *Bestimmung der spezifischen Oberfläche von Feststoffen durch Gasadsorption nach Brunauer, Emmett und Teller (BET)*, DIN 66131

[124] *Powder Diffraction Files*, 47-1049

[125] *Powder Diffraction Files*, 44-1159

[126] *Powder Diffraction Files*, 37-1484

[127] *Powder Diffraction Files*, 37-31

[128] *Powder Diffraction Files*, 49-1642

[129] *Powder Diffraction Files*, 50-1089

[130] *Powder Diffraction Files*, 34-1181

[131] *Powder Diffraction Files*, 34-314

[132] A. Vadivel Murugan b, S.C. Navale a, V. Ravi a,. *Synthesis of nanocrystalline La2O3 powder at 100 °C*, Materials Letters (2006), 60, 848-849

[133] *Powder Diffraction Files*, 14-481

[134] Syukri, Takayuki Ban, Yutaka Ohya and Yasutaka Takahashi *A simple synthesis of metallic Ni and $Ni-Co$ alloy fine powders from a mixed-metal acetate precursor* , Materials Chemistry and Physics (2003), 78, 645-649

[135] Florian Schott *Untersuchungen zur katalysierten NO_x-Reduktion mittels H_2 an $Pt/WO_3/ZrO_2$-Katalysatoren unter O_2-reichen Bedingungen*, PhD (2009), Karlsruhe Institut of Technology.

[136] Manfred Koebel, Giuseppe Madia, Martin Elsener *Selective catalytic reduction of NO and NO_2 at low temperatures*, Catalysis Today (2002), 73, 239-247

[137] Antonio Grossale, Isabella Nova, Enrico Tronconi *Study of a Fe-zeolite-based system as NH_3-SCR catalyst for diesel exhaust aftertreatment*, Catalysis Today (2008), 136, 18-27

[138] Massimo Colombo, Isabella Nova, Enrico Tronconi *A comparative study of the NH_3 - SCR reactions over a Cu-zeolite and a Fe-zeolite catalyst*, Catalysis Today (2010), 151, 223-230

[139] Masaoki Iwasaki, Hirofumi Shinjoh *A comparative study of "standard", "fast" and "NO_2" SCR reactions over Fe/zeolite catalysts*, Applied Catalysis A: General (2010), 390, 71-77

[140] K. Moradi, C. Depecker, J Corset *Diffuse reflectance infrared spectroscopy: Experimental study of non absorbing materials and comparison with theories*, Applied Spectroscopy (1994), 48, 12, 1491-1497

[141] J. Sirita, S. Phanichphant, F C. Meunier *Quantitative Analysis of Adsorbate Concentrations by Diffuse Reflectance FT-IR*, Anal. Chem. (2007), 79, 3912